Title
Design of Earthquake Resistant Bridges Using Rocking Columns

Author
Barthes, Clement Benjamin

Publication Date
2012

Peer reviewed|Thesis/dissertation

Design of Earthquake Resistant Bridges Using Rocking Columns

by

Clément Benjamin Barthès

A dissertation submitted in partial satisfaction of the
requirements for the degree of
Doctor of Philosophy

in

Engineering- Civil and Environmental Engineering

in the

Graduate Division

of the

University of California, Berkeley

Committee in charge:

Professor Bozidar Stojadinovic, Chair
Professor Filip C. Filippou
Professor John A. Strain

Spring 2012

Design of Earthquake Resistant Bridges Using Rocking Columns

Abstract

Design of Earthquake Resistant Bridges Using Rocking Columns

by

Clément Benjamin Barthès

Doctor of Philosophy in Engineering- Civil and Environmental Engineering

University of California, Berkeley

Professor Bozidar Stojadinovic, Chair

The California Department of Transportation (CalTrans) is urging researchers and contractors to develop the next generation highway bridge design. New design solutions should favor the use of modular construction techniques over conventional cast-in-place reinforced concrete in order to reduce the cost of the projects and the amount of constructions on site. Earthquake resistant bridges are designed such that the columns are monolithically connected to the girder and the foundations. Hence, despite the great improvements recently made in modular bridge construction, a large amount of concrete is still cast in place to properly splice the reinforcements between the segments.

Instead of designing earthquake resistant bridges with monolithic joints, it is proposed to use discontinuous connections in this thesis. The segments may rock at their interface during a severe earthquake and, if rocking rotation is too large, the structure may collapse. However, if a bridge is allowed to rock moderately, it may modify the earthquake response and drastically reduce the resisting forces within the structure.

The research presented in this dissertation focuses on the modeling of rocking connections. First, the behavior of rocking rigid blocks under earthquake excitation is studied. It is proposed to restrain the rigid blocks with an unbonded post-tensioning cable in order to allow rocking but prevent overturning. The findings made on rigid blocks, however, cannot be applied to deformable structures because of the limitations of the model. Therefore, a completely different approach is proposed. Instead of modeling the behavior of an entire block, it is proposed to model only the rocking surface. A zero-length finite element is developed, allowing to represent the in-plane rocking rotation between two frame elements. It allows to investigate the behavior of a deformable column rocking freely on its base as well as the stability of a rocking column restrained with a cable and subjected to a large earthquake excitation. The consequences of a post-tensioning cable failure and yielding of the column are also investigated. It is proposed to add a dissipative fuse between the base of the column

and its footing in order to enhance the stability of the structure. Finally, the behavior of a conventional monolithic bridge is compared with a bridge allowed to rock at the columns joints.

The results obtained with the rigid block model show that, when columns are allowed to rock under earthquake excitation, it is possible to adjust the response and preserve stability with a Post-Tensioning (PT) cable. The implementation of the zero-length rocking element permits to study the behavior of deformable structures that are allowed to rock. At first, this element is used in combination with a very stiff elastic element and the results are consistent with the response of a rigid block. This element shows that the free rocking response of an elastic column may stop rocking and start to oscillate in flexure. The dissipative fuse in combination with a long unbonded PT cable proves to be effective. However, it is shown that, if the dissipative fuse is too large, it may prevent the column from returning to its initial position. At last, it is shown that a bridge structure allowed to rock and restrained with cables can sustain a large earthquake. The resisting moments within the columns are greatly reduced when compared with a conventional bridge while the drift ratio remains moderate.

Several subjects are left for further research. First, the zero-length rocking element represents rocking only in the plane of the frame. The development of a $3D$ rocking element is challenging because the column may rock and roll and may also twist around one corner. The design of the rocking surface is not investigated; a bridge prototype should be designed and tested experimentally to validate the feasibility of the solution proposed in this study.

Contents

List of Figures

List of Tables

Acknowledgments

First and foremost, I would like to thank my advisor Professor Bozidar Stojadinovic for all his help. He always encouraged me to pursue the research field that I was most interested in, yet he always directed me in the right way. Thank you very much for your time and effort spent on my PhD.

I would also like to thank Professor Filippou for his help on the development of my rocking element in FedeasLab as well as Professor Govindjee for sharing his knowledge with me on impact mechanics.

I am very grateful to Professor Ibrahimbegovic from my French University the Ecole Normale Supérieure of Cachan. His support allowed me to join the PhD program here at UC Berkeley.

I would also like to thank Professor Mosalam, who offered me an internship while I was a master student. He introduced me to the field of experimental research and offered me a wonderful experience that thrived me to pursue in this domain.

To my friend Dr. Véronique Le Corvec, I am very thankful for your help and for your support. I have learned a lot from our countless discussions on our respective research.

I am very grateful to my parents Jean-Paul and Franǫise as well as my sister Julie and my brother Charles for always being very supportive, despite the distance.

Last and most of all, I would like to thank my wife Rika and our son Alexis, who was born a year ago in the course of my PhD. Their love and support are essential to me. This dissertation goes to them.

1 Introduction

New construction or repair of bridges in a traffic network causes disturbances that increase the risks to traveling public and often have a major detrimental impact on the economic activity supported by the traffic network. Hence, there is a growing demand for Accelerated Bridge Construction (ABC). ABC entails deployment of engineering and construction techniques with the goal to minimize construction-induced disturbances (closures and/or traffic lane or speed restrictions). Throughout the entire United States Departments of Transportations (DoTs) are using innovative techniques that result in faster construction. Some roadways are so vital to local economies that public administrations are ready to pay the high cost to avoid long time closures. A present example is the construction of the new East Bay Bridge (2013), where the traffic closure is restricted to less than 72 hours per year [1]. The ABC techniques developed for these type of projects are very efficient when used in conventional bridge construction. The Federal Highway Administration (FHWA) highly recommends states administrations to use ABC technologies [15]. On one hand, the industrial processes and equipments developed by the precast industry significantly reduce costs: reinforcement cages can be built quickly by machines despite significant complexity, concrete mixes can cure quickly and attain excellent short-term and long-term mechanical properties, and concrete placement techniques have improved to yield very low rates of poorly executed members. On the other hand, transportation and site preparation costs could be substantial, since large precast elements often require oversized vehicles and cranes. Nevertheless ABC projects are becoming more competitive since prompt constructions are greatly appreciated by the traveling public.

Current philosophy in earthquake engineering of reinforced concrete bridges is to ensure the continuity between the different parts of the structure as shown in Figure 1 and Figure 2. Reinforced concrete columns are strongly tied to the foundations and to the superstructure in order to resist to the large moments induced by earthquakes. Therefore, the latest modular construction techniques are rarely used in seismic areas. Typical modern bridge columns have large amounts of longitudinal and transverse reinforcement, requiring complex splices even if no cold joint or precast segments are used in construction.

The principal hypothesis behind the research presented herein is that a breakthrough in design of segmental earthquake-resistant bridges is needed to enable implementation of ABC in seismic regions. The segmental column design investigated herein comprises of precast segments joined using cold, non-monolithic joints tied together using an axial force produced by a concentric post-tensioning cable. Such column design allows rocking to occur between the column as well as its foundation and between the column and the deck bent-cap. Rocking

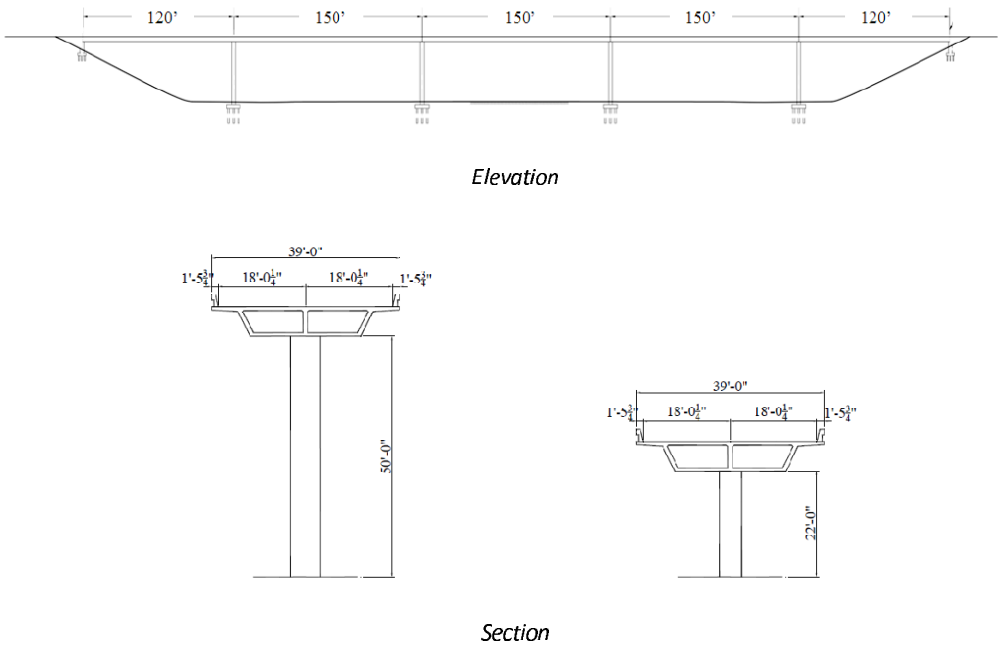

Figure 1: Typical multi-span California standard ordinary bridge

may even occur between the column segments along the column height. Close attention is given to rocking behavior; instead of preventing or limiting it, it is proposed to use rocking behavior as an energy dissipation and seismic isolation mechanism in bridge columns. Such seismic response modification technique is expected to enable ABC as well as to enhance the seismic performance of bridges, ushering in the next generation of earthquake-resistant bridge design.

In Chapter 2, modular construction techniques for seismic resistant bridges are presented. In particular, design solutions allowing monolithic connections between precast elements are discussed. Currently, large parts of the structure are often cast in place in order to ensure the continuity of the concrete reinforcements. So it is propoosed to consider a new design approach, allowing discontinuity between precast elements.

In Chapter 3, a literature review for the behavior of rigid blocks subjected to rocking is presented. It is then proposed to restrain a rigid block with an unbonded post-tensioning cable in order to allow rocking but prevent overturning.

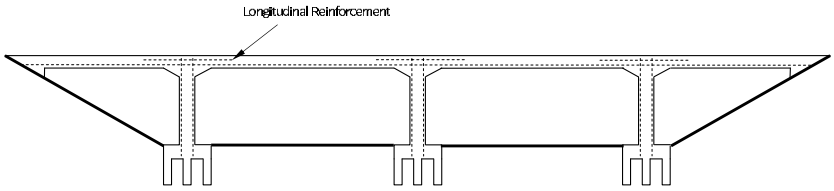

Figure 2: Monolithic design of a standard ordinary bridge

In Chapter 4, the implementation of a finite element capable of representing rocking is presented. This element can be used in combination with existing prismatic elements, allowing it to model very complex deformable structures with multiple rocking surfaces. Specific issues concerning the handling of the discontinuous constraints by the computational algorithm are discussed.

In Chapter 5, the rocking element developed in the previous chapter is used to investigate the interaction between rocking and elastic deformation. Issues concerning the implementation of the viscous damping are discussed and the rocking termination due to column bending is also investigated.

In Chapter 6, the stability of a deformable rocking column subjected to an earthquake ground motion is studied. For a severe earthquake, the restraining cable may fail and lead to collapse. Therefore, it is proposed to use a mild-steel fuse at the base of the column in order to dissipate energy during the earthquake excitation.

In Chapter 7, it is proposed to compare the seismic response of a conventional monolithic bridge with the response of a bridge with columns allowed to rock at both ends. Several bridge configurations are investigated. Notably, the rocking behavior of a multi-span bridge whose columns have a different aspect ratio is investigated. The benefits of a dissipative fuse are also investigated.

At last in Chapter 8, the findings made during this Ph.D. are summarized. Several recommendations for further research, including the implementation of a $3D$ rocking element, are presented.

2 Modular Bridge Construction

2.1 Introduction

Nearly eighty percent of Californian highway bridges are cast-in-place post-tensioned concrete bridges designed and developed using engineering techniques of the 1980's and 1990's. Great effort has been made in the last few decades to increase safety concerning earthquake hazards, in particular. Today, Californian highway bridges are safe. They fulfill strict seismic safety standards prescribed in Caltrans Seismic Design Criteria [3].

Meanwhile, modular bridge construction techniques have greatly improved over the last decades. Many departments of transportation tend to avoid cast-in-place (CIP) concrete as much as possible for several reasons. First of all, it induces larger environmental impact on the construction site and a large quantity of concrete may be wasted due to late delivery or over production. Second, the quality of the precast concrete has greatly improved over the last few decades. A compressive strength 50% higher than CIP concrete can easily be obtained with modern curing process. Modular construction also allows faster and cheaper constructions. Costs can be greatly reduced when segments are built with modern industrial processes during both module construction and module on-site assembly.

The principal advantage is that the modular construction accelerates construction for design and building of the next generation highway overpass bridges. However, ABC is rarely used in seismic areas because of the perceived weakness of the connections between the elements. Typically, a column of a bridge designed to provide high seismic resistance and satisfactory seismic performance is designed with substantial continuous longitudinal and transversal reinforcement. It is strongly anchored in the footing and the bridge deck and particular attention is given to the reinforcement splices. Such reinforcement continuity is not achievable with precast concrete elements unless large amounts of cast-in-place concrete are used. In some cases, these prefabricated elements simply consist of reinforced concrete, steel, glass, carbon fiber, or even polymer shells and are capable of resisting the hydraulic forces of the cast-in-place concrete. However, the DoTs use more and more entirely precast elements and only the connections are cast-in-place.

The purpose of this chapter is to present the review of column construction and connection techniques with respect to their use in ABC and their capability to meet seismic safety standards.

2.2 Existing Precast Elements Connections

Conventional design of segmental bridges comprised of prefabricated elements (steel or concrete) is predicated on the rigidity (ability to transfer moments, shears and axial forces without deformation) or semi-rigidity of column connections to the foundation and the superstructure. The heavy mass of the superstructure generates a lateral force at the top of the column. If the connection between the column and the superstructure behaves as a pin, the column is loaded as a cantilever; as a result, a substantial demand on the foundations. Therefore, it is preferred to clamp the column and the bent-cap together, preventing the top of the column to rotate and reducing the moment at the base, as shown in Figure 3.

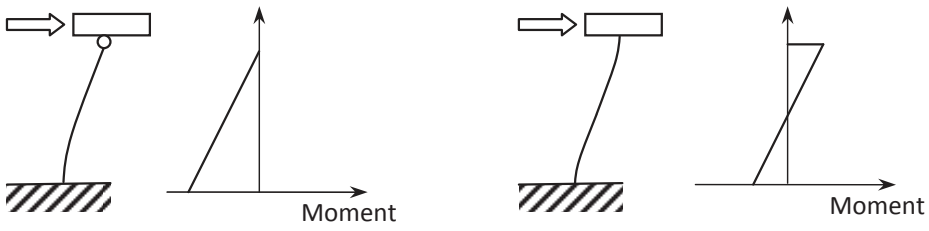

Figure 3: The moment at the base of the column is reduced when the rotation is locked at the top

This rule is easy to apply to cast-in-place structures but specific joints are required for applying it to prefabricated structures. It is difficult to drastically reduce the cast-in-place concrete volume and ensure monolithic junctions. The columns can be delivered with standby reinforcements on both ends, allowing for monolithic connection with the footing and the superstructure. Figure 4 shows an example of the installation of a precast bent-cap over a precast column in Texas. But if the columns exceed $100ft$, it is inconceivable to use full precast columns.

If the column has to be segmented, then the splices between the longitudinal reinforcements become too complicated; therefore, it is more reasonable to go for a permanent formwork system to ensure a correct shear resistance. A new design is now used in Japan called Sumitumo Precast form for Resisting Earthquake and for Rapid construction (SPER) [29], shown in figures 5 and 6. This system is made to use the precast element as both permanent formworks and structural elements. There are two versions of the product, for piers up to $40ft$ the square sections are delivered with cross ties already installed. They are stacked on

Figure 4: Precast Bent-Cap Installed on Site (Texas DOT)

top of each other using epoxy glue along the vertical reinforcements. The concrete is then cast inside the pier to give a solid section. The cross-ties inside the forms give enough lateral resistance to the panels to resist to the pressure while pouring the concrete, so it does not require any temporary shoulder during the construction. The time saved with this technique compared to an entirely cast-in-place system is 50%.

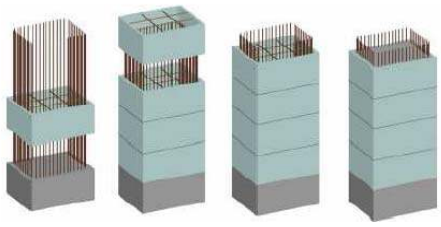

Figure 5: SPER System for Solid Section Columns [29]

The second version of the product is designed for higher piers, up to 160 ft. It is a hollow section where both inner and outer formworks are permanent structural elements. They are segmented in half-sections to reduce size for hauling. They are placed around the vertical reinforcements and then connected using couplers. The cross ties also have to be installed on site, then the concrete is poured. The time saved compared to a traditional technique is 30%.

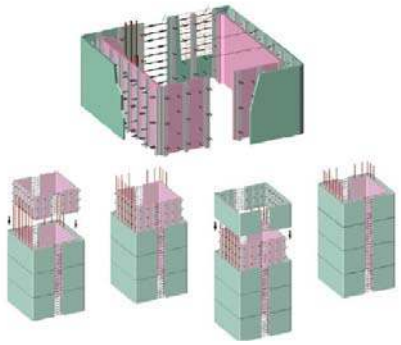

Figure 6: SPER System for Hollow Section Columns [29]

2.2.1 Grouted Pockets

The bent-caps are designed to remain elastic during a large earthquake. The plastic hinges are supposed to form at each end of the column, and the bent-cap should resist that demand. Therefore, the behavior of the connections between the prefabricated elements plays a key role in the seismic behavior of the bridge structure. A couple of connection examples between a column and a bent-cap are given in Figure 7.

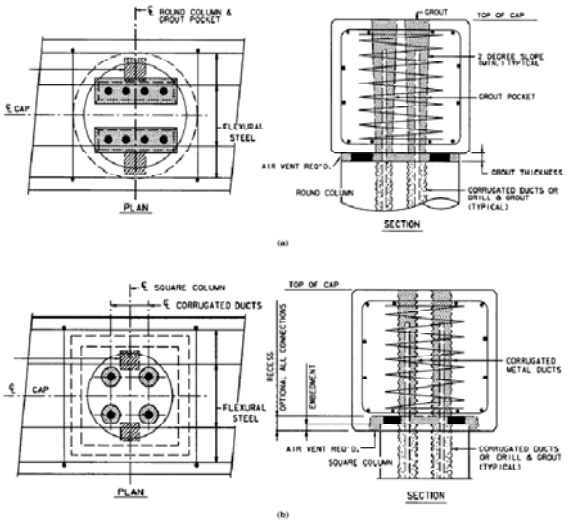

Figure 7: Grouted pocket connections between a precast column and a precast bent-cap [36]

These examples of connections were tested by E. Matsumoto et al. [24]. One connection has through holes with corrugated ducts and the other one has tapered holes. The longitudinal reinforcing bars of the columns are driven into these ducts and then high performance grout is cast in place. Such connections should provide sufficient bond to allow the reinforcements to yield in tension. If the bridge substructure is composed of a single column, instead of a trestle as shown in Figure 8, the longitudinal reinforcing bars will have a larger diameter and grouted pockets will not withstand their yielding strength.

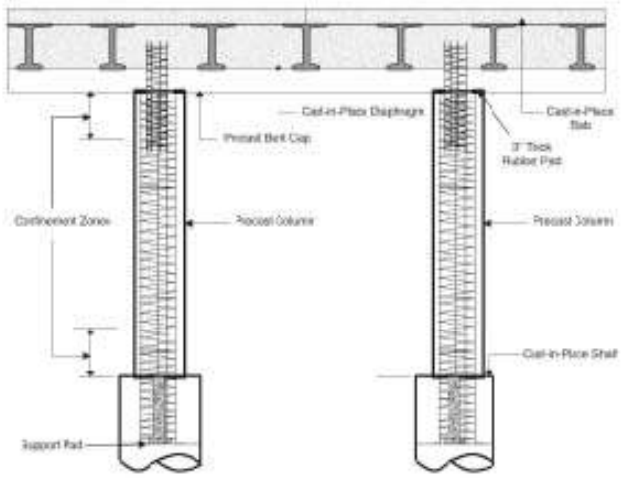

Figure 8: Trestle Type Prefabricated Concrete Columns [36]

2.2.2 Self-Compacting Concrete

The mechanical properties of Self-Compacting Concrete (SCC) are the same as conventional concrete. However, SCC is less sensitive to the casting process, so if the concrete is correctly tested when it is delivered, its strength and its compaction are almost insensitive to human errors such as over vibration. For conventional concrete, the flowing ability is increased by adding water, but this reduces the mechanical properties. But for SCC, the flowing ability is given by superplasticisers. The cohesiveness is usually insured by high powder contents such as ground granulated blast furnace slag, fly ash and other fine inert materials. At similar water/cement ratios, the strength of SCC is equal or slightly better than conventional concrete. Compressive strength between 5 and 10 ksi can easily be achieved. When delivered, the SCC requires more tests than a conventional concrete, so the foremen need to be trained to use this new material. Since the SCC can be pumped to the formworks and simply poured, little or no vibration is required, so the task for the workers is easier. SCC is used to reduce costs in various projects. It is because the process is faster but also because the surface does not need any other treatment or finish. Because it is mainly constituted of fine granulates, it is easy, for example to incorporate an esthetic pattern in the formworks. SCC is used for urban construction to reduce noises. It is a key element to run a quiet construction and allows night work. For example, it is now common to prepare formworks during daytime, and then schedule most of the casting during night time. In addition to saving time, it also avoids concrete trucks blocking the area near the construction site.

Figure 9: Self-Compacting Concrete being cast

The principal use of SCC in ABC is to implement the monolithic (pocket-type or other types) connections between pre-cast segments. Since all the reinforcements have to be spliced,

it requires a high density of reinforcements at the connection as shown in Figure 10. Due to its flowing ability, SCC allows to cast in place integral connections between two prefabricated elements.

Figure 10: Congested Reinforcements

2.3 Bridge Columns With Unbonded Segments

Segmental construction of bridge columns in seismic areas constituted the main incentive for the research presented below. Current practice consists of bonding the different elements with adequate reinforcement splicing. But these splices limit the use of precast elements. The column reinforcements can be bonded to the bent-cap with grouted pockets as shown in Figure 7 but, even with properly designed corrugated grouted pockets, slipping is observed at ultimate capacity.

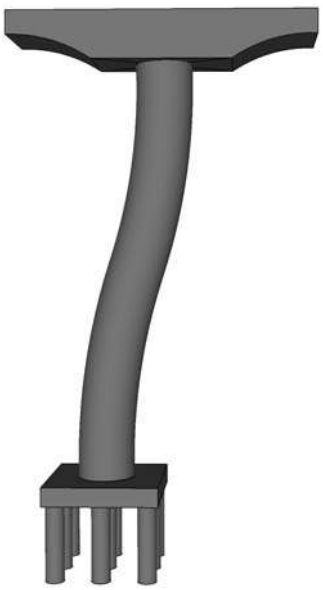

Figure 11: Monolithic Bridge Substructure Assembly Subjected to Earthquake Motion

Figure 11 shows the behavior of a Californian bridge substructure subjected to earthquake motion. It consists of a continuous structure with column connections capable of transferring shear and moment to the footing and the superstructure. On the contrary, segmental bridge construction technique simply consists of stacking the column elements with a cold, grouted or ungrouted, joint. Such simple design would lead to rocking and slipping between the elements when subjected to a severe earthquake. However, it is believed that a post-tensioning cable may be able to prevent slipping and limit rocking to reasonable rotations. Furthermore, the rocking between the different elements may be beneficial for the bridge. Rocking dissipates energy through shock wave radiation and it also modifies the response of the structure, making it less sensitive to earthquake excitations in some cases.

Figure 12 shows the expected behavior of an unbonded segmented column.

Figure 12: Unbonded Segmented Bridge Substructure Subjected to Earthquake Motion

The behavior of rigid blocks rocking on their base is inherently unstable, so designers have been trying to prevent it. It was only after Housner [16], who observed that some water tanks resisted a major earthquake in Chile, likely due to their rocking behavior, that research was led on this subject. Recently, a lot of studies were done on rocking shear walls. M.R. Eatherton et al. [8] tested a rocking shear wall with a special fuse on the E-Defense shake table in Japan. Some structures allowing a frame to rock were even recently built, such as the Orinda City Hall [23].

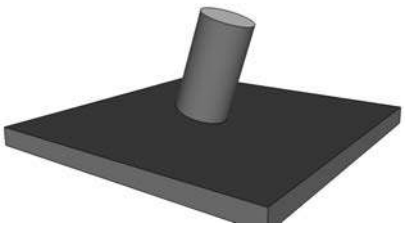

Figure 13: Cylinder Rocking

In order to use rocking in earthquake resistant bridge design, the fundamentals of rocking rigid body have to be well understood. The dynamic behavior of rocking blocks induces shock

waves, so the quasi-static approach often used in civil engineering may not be sufficient. Chapter 3 covers the dynamics of rocking rigid blocks, required to assess the integrity of segmented columns. A particular attention will be given to the instability issue and a solution will be proposed using post-tensioning cable.

2.4 Repairability of Modular Bridges

During a severe earthquake, structural damage cannot be avoided. The formation of plastic hinges plays a key role in energy dissipation. However, it will induce large concrete cracks, the reinforcements will yield and will have to be replaced. Even though existing bridges will guarantee life safety if an earthquake occurs, they may not be repairable. But the next generation bridge design should anticipate the cost and the feasibility of the repairs. Modular bridge construction seems to meet this requirement. Most of the bridge elements are designed to remain elastic using capacity design principles. However, it is possible to replace prefabricated elements only if their connections with the neighboring elements are not permanent. For instance the connections presented in Section 2.2 are not designed to allow repair. Current design philosophy consist of assembling prefabricated elements on site such that the structure built is monolithic. But efforts should be made to preserve modularity, even after their construction.

The bridge elements are designed to be repaired or replaced. The replace option requires non-permanent connections between the prefabricated elements. If the prefabricated modules are made out of steel, then bolted connections will be preferred to welded ones. However if the elements are made out of reinforced concrete, they have to be bonded with cast-in-place concrete, according to conventional design philosophy. The elements become permanently connected, hence the repair option will be preferred. One solution proposed by Cheng and al. [4] is to use bolted fuse elements instead of conventional longitudinal reinforcements, as shown in Figure 14. After a severe earthquake, the cracked concrete can be removed, then the fuses are replaced by new ones and concrete is cast-in-place. The column can be repaired locally, without being replaced.

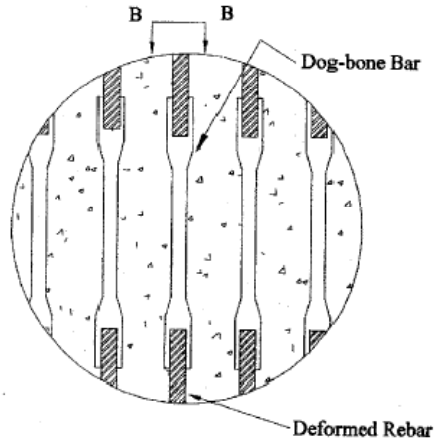

Figure 14: Bolted Longitudinal Reinforcements [4]

The prefabricated column elements studied in this thesis have discontinuous reinforcements. They are assembled on site with a simple joint of grout and the flexural resistance of the column comes from the post-tensioning cables. Such design may allow DoTs to replace damaged elements after a severe earthquake if the post-tensioning cable remains unbonded. But such structure will behave differently than current standard ordinary bridges under earthquake loading. The grouted joints will fail, allowing rocking between the elements. New design guidelines have to be made, and the cables must allow the substructure to remain stable.

3 Rigid Blocks Subjected to Rocking

In this chapter, it is proposed to focus on the rocking behavior of rigid blocks (RB). This subject was first discussed by Housner in 1963 [16]. He showed that the rocking oscillations of a RB are dissipative and non-linear. So a RB must be inelastic in order to rock; otherwise, it will bounce. The rocking behavior of two stacked rigid blocks is also discussed. The analytical solution of such system is extremely complex due to the large amount of rocking modes and impact modes. This challenging problem was solved by Psycharis [28].
Secondly, the behavior of a rocking RB allowed to rock in 3D (in-plane and out-of-plane) is discussed. The shape of the rocking surface is essential. A new mode of instability can occur for rectangular surfaces, and circular surfaces may not rock at all but simply roll.
At last, it is proposed to model the behavior of a rocking RB restrained with an unbonded post-tensioning cable. The intent is to allow rocking but prevent overturning.

3.1 Single Block Rocking Behavior

A rigid block under rocking motion acts as a non-linear dissipative oscillating system. This dissipation mechanism can be used to attenuate earthquake response, but there is a risk of instability that is hard to predict. During impact, a shock wave will radiate in the RB and dissipate, but it may overturn under certain excitations.

3.1.1 Assumptions

The dynamic behavior of a RB has been studied by several researchers. Equation 1 describes the free vibration of a RB. It was first presented by Housner [16]. The system is shown in Figure 15. It is assumed that the RB is not rocking out of plane. The friction between the RB and the base is considered sufficient to prevent sliding.

$$I_0\ddot{\theta} = -mgR\sin(\alpha sgn(\theta) - \theta) \tag{1}$$

In equation (1), $\theta(t)$ is the rotation angle, I_0 the moment of inertia with respect to the point of rotation, m the mass, R the block dimension and α the slenderness angle, as shown in 15. Housner linearized the system for slender blocks subjected to small angle of rotations assuming that $\sin(\alpha - \theta) \approx \alpha - \theta$.

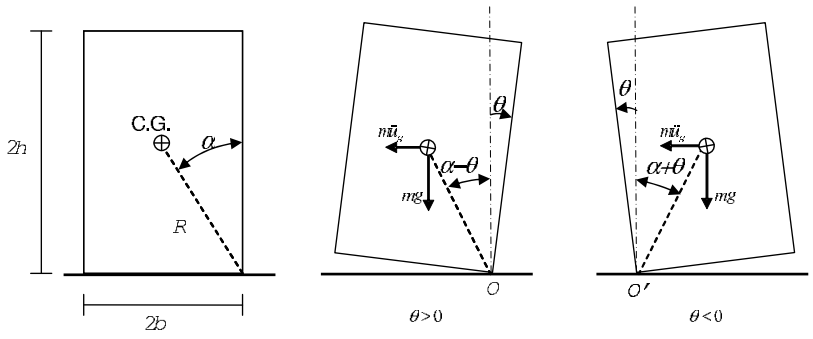

Figure 15: Description of the Rocking Block

The RB behavior can be described with only two parameters p and α, leading to equation (2), where $p[1/sec]$ represents the frequency parameter of the system. This parameter can be compared to the natural frequency parameter describing harmonic oscillator, ω_n. As p gets larger, the free rocking oscillations frequency of a RB will be higher. Free harmonic oscillations periods can be quickly computed with ω_n , but there is no simple interpretation of p to determinate the behavior of a rocking RB. For the case of a rectangular block, the frequency parameter is $p = \sqrt{3g/4R}$.

$$\ddot{\theta} = -p^2\{\sin(\alpha sgn(\theta(t)) - \theta(t)) + \frac{\ddot{u}_g(t)}{g}\cos(\alpha sgn(\theta(t)) - \theta(t))\} \tag{2}$$

α plays a major role in the energy dissipation of the system as described below. To incorporate the energy dissipation at the impact, Housner [16] assumed that the rotation continues smoothly from point O to O' (no sliding) and that the angular momentum during the impact is conserved (see Figure 15). The relationship between the angular velocities is obtained by applying the conservation of angular momentum. The coefficient of restitution r of the impact can be computed as shown in equation (3). A confusion sometimes occurs concerning the balance of angular momentum. During an impact, the angular momentum is not conserved for the RB but for the RB-footing system. Similarly, the linear momentum of the RB is not conserved but the linear momentum of the RB-footing system is conserved. Since the footing has an infinite mass, the conservation of momentum at impact of the RB-footing system can not be computed. However, the impact between the RB and the footing is assumed to be a point impact. Therefore, the RB is subjected to a rolling constraint and can not have a reaction moment at the point of impact. Hence the angular momentum is conserved for the RB alone. If a RB is rocking on an isolated base with a finite mass, then

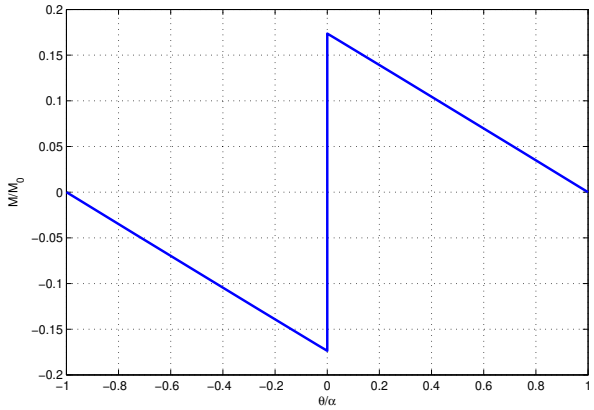

Figure 16: Moment vs. rotation of a RB

the conservation of linear momentum and angular momentum must be conserved for the RB-base system, as explained by Vassiliou and Makris [35].

$$r = \left(\frac{\dot{\theta}_2}{\dot{\theta}_1}\right)^2 = \left(1 - \frac{3}{2}\sin^2\alpha\right)^2 \tag{3}$$

Figure 16 represents the moment versus the rotation of a RB. Once the excitation reaches the required magnitude to initiate rocking, the RB becomes unstable since the resisting moment due to the RB weight decreases as θ increases.

Equation (3) implies that a slender RB looses less energy than squat ones; therefore, the damping ratio depends on the RB slenderness α. Due to dissipation of angular momentum during impact (radiation damping into the RB and the base), the vibration period of subsequent cycles decreases. The horizontal acceleration required to initiate rocking is defined by equation (4).

$$\frac{\ddot{u}_{gmin}}{g} \geq tan(\alpha) \tag{4}$$

Housner [16] also studied the overturning of a RB subjected to constant horizontal acceleration, to sine pulse, and to earthquake type of excitation. He concluded that for two geometrically similar blocks the scale effect makes the larger (i:e. with a smaller p) more stable than the smaller. This scale effect is shown in Figure 17. Since the rocking initiation

only depends on α, it is important to notice that RBs of identical slenderness but with different sizes will start to rock under the same excitation magnitude. However, the larger ones will be more stable.

Finally, Shenton [32] studied the initiation of rocking and sliding for a RB subjected to base excitation. He showed that a slide-rock mode may exist when the friction coefficient of a rocking RB is smaller than its friction coefficient at rest. However, this mode can only occur for $\alpha \leq \pi/4$.

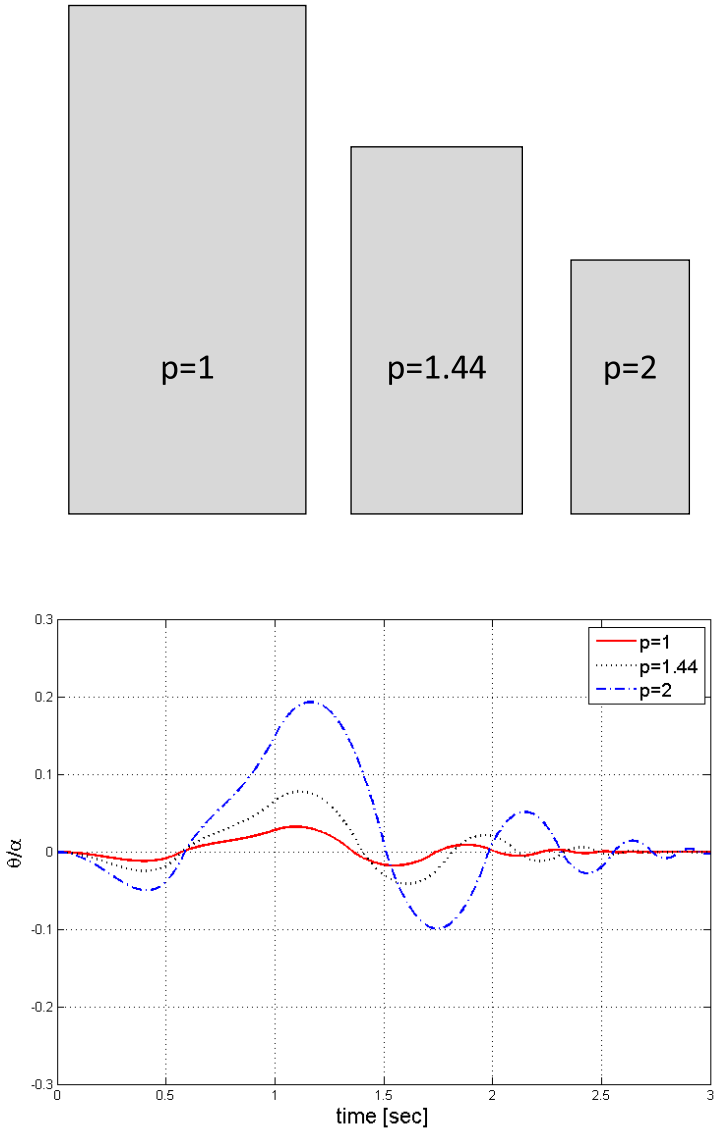

Figure 17: Response of RBs with $\alpha = 25°$ to a Half-Cosine Ground Acceleration Pulse of Amplitude $0.61g$ and Period $T = 2sec$

3.1.2 SDOF Vibration Analogy

Priestley et al. [27] proposed a design methodology to estimate RB rotations when subjected to earthquake horizontal excitation. The method consists of transforming the RB to an equivalent single-degree-of-freedom (SDOF) system with a period and viscous damping. The maximum rotation angle is computed from $\delta = \theta R \cos(\alpha)$, where δ is the displacement of the centroid of the block, which is obtained from a response spectrum of a SDOF system. To define the equivalent viscous damping of a RB system, the relationship between the rotation amplitude in subsequent cycles is used. The equivalent period of the RB depends on the maximum rotation angle θ; therefore, this methodology requires an iteration process. The idea presented by Priestley is used by FEMA 356 [10], but it uses conservatively a lower damping ratio.

From their study, Makris and Konstantinidis [22] concluded that the SDOF oscillator and the RB are two fundamentally different systems. For example, the free vibration of a RB is characterized by an increase of the frequency and a decrease of amplitude. On the contrary, a SDOF oscillator vibrates with constant frequency. Therefore, the response of one of these two systems should not be used to predict the behavior of the other. Additionally, they concluded that the approximate design methodology to estimate block rotations implemented in FEMA 356 is conceptually wrong and should be abandoned.

Makris and Konstantinidis [22] focused their attention in solving the nonlinear dynamic equation of a RB subjected to horizontal ground acceleration. The equation of motion of a rigid block subjected to ground acceleration $\ddot{u}_g(t)$ is written in equation (2). J. Zhang and N. Makris [37] focused on the effect of cyclic loadings on rocking structures.

3.1.3 Rocking termination

It is often assumed that rocking oscillations vanish but do not stop, similar to a harmonic oscillator with viscous damping. But, unlike a damped harmonic oscillator, when the amplitude of a rocking RB decreases, the period of rocking oscillations also decreases. Therefore, the rapid decay of the period may cause rocking interruption at a finite time.

Housner [16] did not elude this question. Instead, he stated that after a few impacts the rocking amplitude becomes so small that other phenomenon such as elastic bouncing will cause rocking to stop. It is proposed in this section to prove that rocking will stop at a finite time, even for a perfectly rigid block.

In order to compute the time of the free rocking response, the equation of motion (2) is linearized. Housner [16] linearized this equation for $\alpha - \theta$ but in this section, the equation of motion is linearized only for θ, while the slenderness angle α is still considered large. The linearized equation is presented in Equations (5a) and (5b).

$$\ddot{\theta} - p^2 \cos(\alpha) \cdot \theta + o(\theta^2) = -p^2 \sin(\alpha) \qquad for \qquad \theta > 0 \tag{5a}$$

$$\ddot{\theta} - p^2 \cos(\alpha) \cdot \theta + o(\theta^2) = p^2 \sin(\alpha) \qquad for \qquad \theta < 0 \tag{5b}$$

Equations (6a) and (6b) represent the solution of Equation (5a) for $\theta(0) = \theta_0$ (with $\theta_0 > 0$) and $\dot{\theta}(0) = 0$. A new frequency parameter is defined as $\tilde{p} = p\sqrt{\cos(\alpha)}$.

$$\theta(t) = tan(\alpha) - (tan(\alpha) - \theta_0) \cdot \cosh(\tilde{p}t) \tag{6a}$$

$$\dot{\theta}(t) = -(tan(\alpha) - \theta_0) \cdot \tilde{p} \cdot \sinh(\tilde{p}t) \tag{6b}$$

After the n-th impact, the maximum rotation is defined as θ_n. The angular velocity at impact n is defined as $\dot{\theta}_n$. At the time of the n-th impact defined as t_n, Equation (6a) can be expressed as Equation (7).

$$0 = \tan(\alpha) - (\tan(\alpha) - \theta_{n-1}) \cdot \cosh(\tilde{p}t_n) \tag{7}$$

Using the hyperbolic function identity $\cosh^2 x + \sinh^2 x = 1$, Equation (7) leads to Equation (8).

$$\cosh(\tilde{p}t_n) = \frac{tan(\alpha)}{tan(\alpha) - \theta_{n-1}} \implies \sinh(\tilde{p}t_n) = \sqrt{\left(\frac{tan(\alpha)}{tan(\alpha) - \theta_{n-1}}\right)^2 - 1} \tag{8}$$

Therefore, the angular velocity at impact n is:

$$\dot{\theta}_n = \tilde{p} \cdot \sqrt{\tan^2(\alpha) - (\tan(\alpha) - \theta_{n-1})^2} \tag{9}$$

The coefficient of restitution r defined in Equation (3) leads to the recursive Equation 10 between the angular velocity at impact n and the angular velocity at impact $n-1$.

$$\tilde{p} \cdot \sqrt{\tan^2(\alpha) - (\tan(\alpha) - \theta_n)^2} = \tilde{p} \cdot \sqrt{r} \cdot \sqrt{\tan^2(\alpha) - (\tan(\alpha) - \theta_{n-1})^2} \tag{10}$$

Hence the maximum rotation after impact n can be expressed as:

$$\theta_n = \tan(\alpha) - \sqrt{\tan^2(\alpha) - r^n \left(\tan^2(\alpha) - (\tan(\alpha) - \theta_0)^2\right)} \tag{11}$$

The quarter period $T_n/4$ is defined as the duration between the time $\tilde{t}_n$ at which the rotation reaches its maximumn after impact n and the time at impact t_{n+1}. Equation (7) is expressed as a function of $\tilde{t}_n + \frac{T_n}{4}$ in Equation (12).

$$0 = \tan(\alpha) - (\tan(\alpha) - \theta_n) \cdot \cosh(\tilde{p}(\tilde{t}_n + \frac{T_n}{4})) \tag{12}$$

Combining Equation (10) and Equation (12), the time at impact $n+1$ is expressed in Equation (13) with respect to the time at impact n. Note that there are two quarter periods $T_n/4$ between two impacts.

$$t_{n+1} = t_n + \frac{2}{\tilde{p}} \sqrt{r^n \left[1 - \left(\frac{\tan(\alpha) - \theta_0}{\tan(\alpha)}\right)^2\right]} \tag{13}$$

Due to the recursivity of Equation (13), the total time of the free rocking motion can be expressed in Equation (14).

$$t_\infty = \frac{2}{\tilde{p}}\sqrt{1-\left(\frac{\tan(\alpha)-\theta_0}{\tan(\alpha)}\right)^2}\cdot\sum_{n=0}^{\infty}\left(\sqrt{r}\right)^n \tag{14}$$

Based on the definition of the reduction factor, for any α, $r < 1$. Hence Equation (14) converges and leads to Equation (15).

$$t_\infty = \frac{2}{\tilde{p}}\sqrt{1-\left(\frac{\tan(\alpha)-\theta_0}{\tan(\alpha)}\right)^2}\cdot\frac{1}{1-\sqrt{r}} \tag{15}$$

The equation of motion was linearized with respect to θ and, since the initial angle θ_0 is finite, the time of rocking interruption t_∞ is approximate. However, this demonstration proves that the free rocking response of a rigid block will lead to an infinite number of impacts but it will stop at a finite time for any slenderness angle α.

3.2 3D Rocking Block

In this section, the RB is allowed to rock on a flat surface in any direction, as described in Figure 18. It is still assumed that the RB does not slide and always remains in contact with the base. The rocking behavior in 3D is largely dependent of the shape of its base. It can be subdivided into two categories: the RB with a polygonal base and the RB with a circular base.

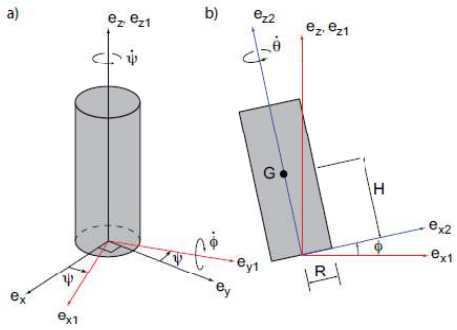

Figure 18: Rolling of a Cylinder on Its Edge (From [33])

After Sanriku-Haruka-Oki earthquake in 1994, Tobita and Sawada [34] noticed that slender granite tombstones were rotated. A sliding block subjected to earthquake excitation may translate but should not rotate so noticeably. Hence it was concluded that the tombstones rotated because of rocking. The multi-directional excitation of an earthquake caused the tombstone to rock in its two transverse directions. Incidentally, the RB was not rocking on its edge but on its corner, allowing it to rotate.

Tobita and Sawada conducted experiments on a shaking table with rigid blocks subjected to skewed earthquake excitations as shown in Figure 20. Once the block uplifts on its corner, it tends to twist around one corner until the center of rotation and the center of gravity are aligned with the excitation, leading to the curious disposition of the tombstone after the earthquake.

The rocking behavior of a cylinder was studied by Srinivasan and Ruina [33]. The cylinder is considered rigid, and its bottom edge is constrained to remain in contact with the supporting surface, as shown in Figure 18. The friction is considered sufficient to prevent

Figure 19: Tombstone Rotated After Sanriku-Haruka-Oki Earthquake (1994)

sliding. It is shown that the cylinder will not rock but will instead roll. Unlike the 2D case, there is no impact between the cylinder and the support. If the cylinder is initially tilted and no angular velocity is applied along its longitudinal axis, it will bifurcate to the left or to the right and roll on its edge. Hence a rocking cylinder is, in fact, only rolling.

In conclusion, 3D rocking motions have two properties unobserved in 2D. One is that they tend to rotate when they have a polygonal base and the other is that they no longer rock but simply roll when they have a circular base. If only rolling occurs, there is no dissipation due to the absence of impacts. A compromise may be found by using a polygonal base with tangent rounded edges; if the block is rocking on one edge then impacts can occur, if it is rocking on a corner, then it rolls until it reaches an edge. This configuration has not yet been studied.

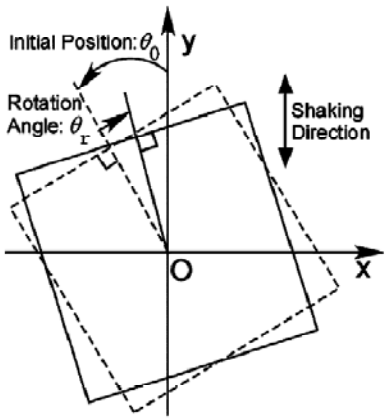

Figure 20: Rotation of a Rigid Block Subjected to a Skewed Earthquake Excitation (from [34])

3.3 Two-block Rocking Assemblies

Psycharis [28] derived the equations of motions for two-block assemblies. It is assumed that the blocks are rigid and that no sliding occurs. As shown in Figure 21, the upper block can rock on top of the lower block. The system is inherently less stable than a single block. For instance, if only the lower block is rocking, the upper block may overturn before it even starts to rock if it is more slender than the lower block.

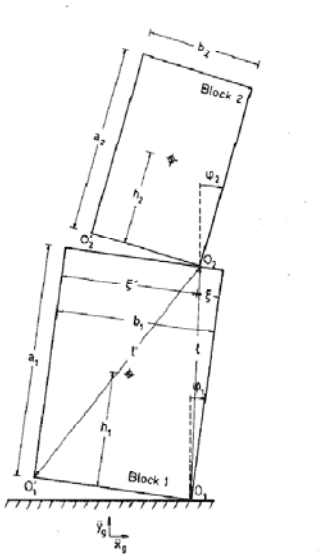

Figure 21: 2 Rigid Blocks Assembly (from [28])

Four different rocking motion modes may occur, as shown in Figure 22. These modes can be described by eight systems of linear dynamic equations, each mode being governed by two different systems of equations, whether the rocking rotations are positive or negative. Furthermore, six equations govern the transition from one mode to the other to conserve the angular momentum, and eight equations govern the initiation of the rocking modes. In order to solve these sets of ODEs, the algorithm must detect each event and then converge to it. Transition equations are solved for the solution of the previous ODE and applied to the new ODE system as initial values, as explained in 3.4.1.

Psycharis computed the solution for a free rocking assembly and for an assembly subjected to an earthquake excitation. It shows that, if the structure does not overturn, the energy is redistributed to the upper block which is therefore subjected to larger rotations.

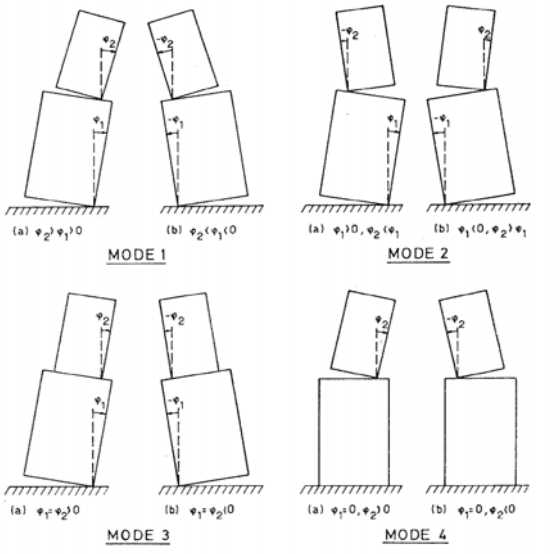

Figure 22: Rocking Modes for 2 Blocks Assemblies (from [28])

As shown in Figure 23, the rotations of the lower block vanish very quickly and the system quickly turns into a single block rocking response of the upper block.

In order to study the behavior of multiple stacked rigid blocks, a numerical method called the distinct element method was used by Konstantinidis and Makris [19].

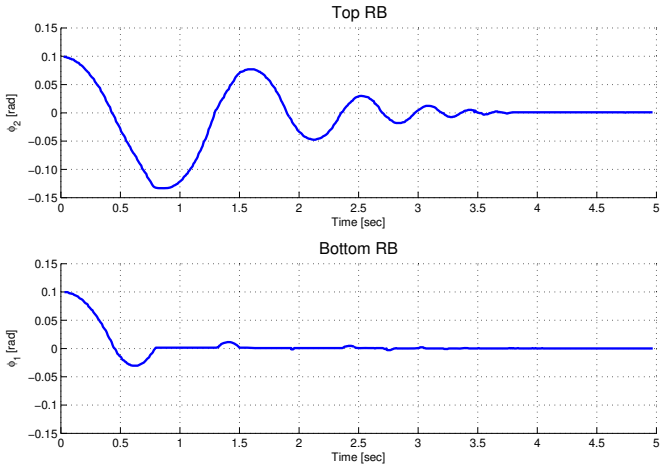

Figure 23: Free Rocking Response of a Two Rigid Blocks Assembly (from [28])

3.4 Single Rocking Block Restrained With a Cable

Rocking behavior may be an efficient way to dissipate energy through the impacts when a structure is subjected to an earthquake excitation. However, the inherent instability shown in 16 limits its use. An unbonded post-tensioning (PT) cable is expected to add stiffness to the system, and therefore improve its stability.

Figure 24 describes the setup studied. Since the cable is unbonded, the post-tension force depends of the strain of the cable, $P(\theta) = P_0 + k\varepsilon(\theta)$, where P_0 is the initial post-tension force (at $\theta = 0$) and k the cable stiffness. The rotation between the axis of the block and the axis of the cable is considered negligible consequently, the post-tension force is modeled as a follower force. The strain of the cable is computed in Equation (16). Using Taylor expansion, the strain can be linearized as shown in Equation (17).

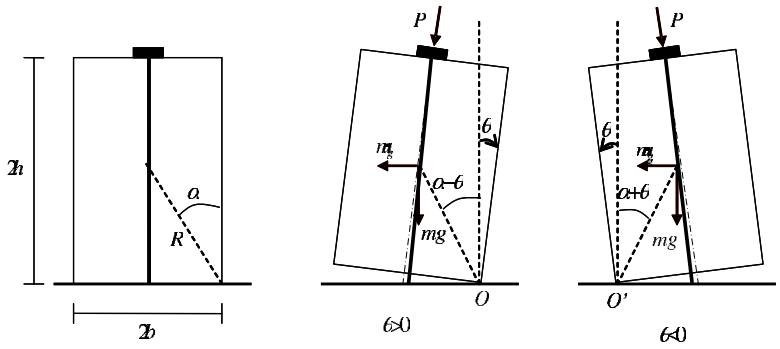

Figure 24: Rocking Block with PT Cables

$$\varepsilon(\theta) = \frac{[4h^2 + 2b^2 - 2b(b\cos(\theta) - 2h\sin(|\theta|))]^{1/2} - 2h}{2h} \tag{16}$$

$$\varepsilon(\theta) \approx \frac{\tan\alpha}{2}\theta + o(\theta^{3/2}) \tag{17}$$

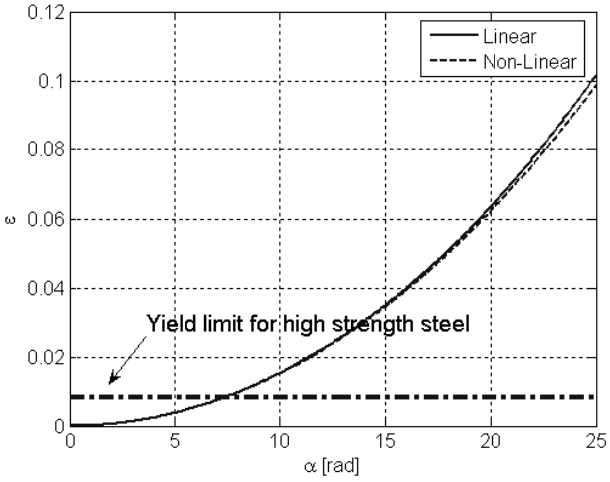

Figure 25: Strain in the Post-Tensioning Cable for $\theta = \alpha$

Figure 25 shows that the strain can be considered linear, especially for slender blocks. Based on this assumption, the post-tension force can be represented by two dimensionless parameters, η_0 and η_α as shown in equation (18). η_0 represents the initial post-tension force at $\theta = 0$ (divided by the weight) and η_α represents the post-tension force when the PT-RB reaches angle $\theta = \alpha$. Hence, if a cable is very soft, the post-tension force remain constant during motion and $\eta_0 = \eta_\alpha$. The balance of angular moment with respect to O and O' leads to Equations (19a) and (19b).

$$P(\theta) = mg(\eta_0 + (\eta_\alpha - \eta_0)\frac{\theta}{\alpha}) \tag{18}$$

$$I_0\ddot{\theta} = -P(\theta)R\sin(\alpha) - m\ddot{u}_g R\cos(\alpha - \theta) - mgR\sin(\alpha - \theta) for \qquad \theta > 0 \tag{19a}$$

$$I_0\ddot{\theta} = P(\theta)R\sin(\alpha) - m\ddot{u}_g R\cos(\alpha - \theta) - mgR\sin(-\alpha - \theta) for \qquad \theta < 0 \tag{19b}$$

Combining equations (18) and (19) leads to equation (20).

$$\ddot{\theta} = -p^2\{\sin(\alpha sign(\theta) - \theta) + \frac{\ddot{u}_g(t)}{g}\cos(\alpha sign(\theta) - \theta) + (\eta_0 sign(\theta) + (\eta_\alpha - \eta_0)\frac{\theta}{\alpha})\sin(\alpha)\} \tag{20}$$

The energy dissipation is incorporated at each impact using the conservation of angular momentum given by equation (3). Therefore, the post-tension cable is assumed to remain elastic and it does not dissipate energy. For a PT-RB, the minimum ground acceleration required to initiate rocking depends only on η_0. The required acceleration to initiate rocking is defined in equation (21). Compared to Equation (4), the effect of the PT cable is evident; it increases the stability of the RB.

$$\frac{\ddot{u}_{gmin}}{g} \geq (1 + \eta_0)\tan\alpha \tag{21}$$

The restoring moment versus the rotation angle of a RB for different post-tension values η_0 is shown in Figure 26. The cable's stiffness is assumed to be negligible, hence $\eta_\alpha = \eta_0$. It is observed that the restoring moment has a negative slope, and its value is still positive for $\theta > \alpha$. Therefore, a RB with post-tension force will overturn for a larger rotation than the case without post-tension force.

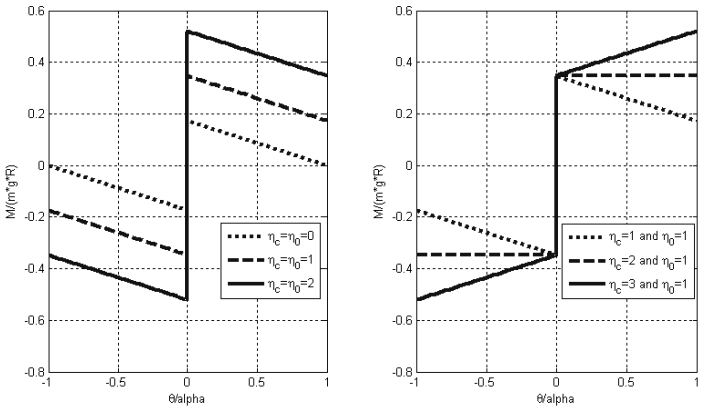

Figure 26: Restoring Moment Versus Rotation for $\alpha = 10°$

Moreover, if the cable's stiffness is large, the RB becomes stable. In fact, the tension increases when the RB rotates and the stiffness of the system becomes positive as shown in Figure 26. Stability is achieved when $\eta_\alpha \geq 1 + \eta_0$. In practice, this criterion may not be achieved because the steel cables cannot undergo such a large strain. Figure 25 shows that the cable may fail for squat blocks in an extreme case where $\theta = \alpha$.

3.4.1 Implementation of the PT-RB Model

The dynamic behavior of a RB with a post-tension cable is examined under different types of excitations in this section. The response is calculated by numerical integration of equation (20), expressed as a 2-DOF first order ODE, using a fourth order explicit Runge-Kutta method (Dormand-Prince pair). The system becomes stiff when θ becomes very large (beyond overturning angle); therefore, an implicit scheme is more efficient to detect overturning.

$$\begin{aligned}
\left\{y(t)\right\} &= \begin{Bmatrix}\theta(t)\\ \dot{\theta}(t)\end{Bmatrix} && \text{with } \left\{f(t)\right\} = \left\{\tfrac{d}{dt}y(t)\right\}\\
\left\{f^{+}(t)\right\} &= \begin{Bmatrix}\dot{\theta}(t)\\ -p^2[\sin(\alpha_\theta(t)) + \frac{\ddot{u}_g}{g}\cos(\alpha-\theta(t))]\end{Bmatrix} && \text{for } \theta > 0\\
\left\{f^{-}(t)\right\} &= \begin{Bmatrix}\dot{\theta}(t)\\ -p^2[\sin(-\alpha_\theta(t)) + \frac{\ddot{u}_g}{g}\cos(-\alpha-\theta(t))]\end{Bmatrix} && \text{for } \theta < 0
\end{aligned}$$

Note that not only the restoring moment but also the velocity are discontinuous for $\theta = 0$ because of Equation (3). The ODE solver has to stop when the rocking event occurs, computes the angular velocity after impact, and restarts with the updated initial conditions. This category of solvers was studied by Shampine and al. [31].

In the papers presented in this chapter, a conventional ODE solver is used to solve the discontinuous equation (20). But the discontinuity occurs at the same time as the rocking event. Therefore, it is much more efficient to solve the continuous function f^+ when $\theta \geq 0$ and f^- when $\theta \leq 0$. Figure 27 represents the continuous functions used by the ODE solver. For instance, if the algorithm tries to converge from $\theta < 0$ to $\theta = 0$ but overshoots, instead of computing the 'true' system response, it is more effective to keep computing the continuous function $f^-(t)$. Once the convergence is achieved, the updated boundary conditions are applied and the algorithm solves for $f^+(t)$. Hence the solver never encounters discontinuities while it is iterating.

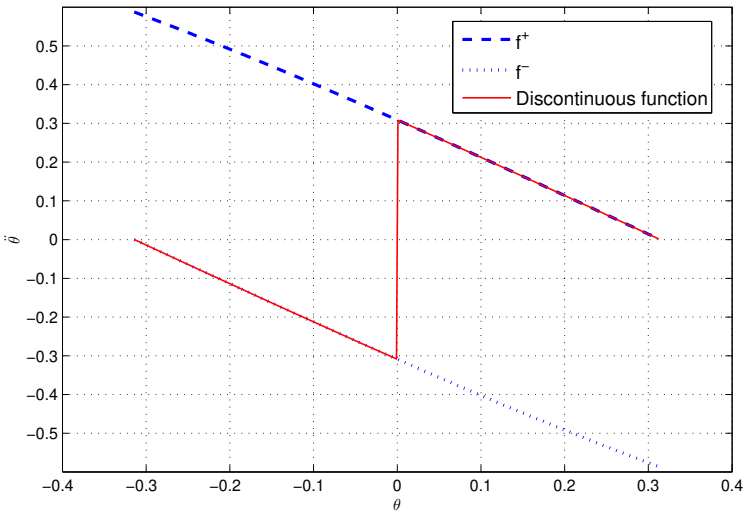

Figure 27: Continuous Functions f^+ and f^- Used By the ODE Solver

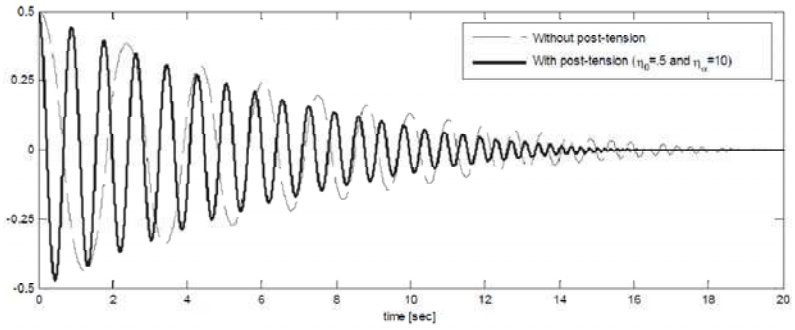

Figure 28: Free Vibration Response With an Initial Rotation $\theta_0 = \alpha/2$. RB Properties Are $p = 2.0(1/sec)$,$\alpha = 10°$

3.4.2 Free Vibration Response

Figure 28 shows the free vibration response of a free-standing and PT-RBs. The initial rotation of the RB is $\theta_0 = \alpha/2$. It is observed that the period decreases as the rotation angle decreases. The post-tension cable does not add any damping but, since the post-tensioned RB oscillates faster than the free-standing RB, the amplitude of rotation decreases faster. Otherwise, the behavior of the two RBs is very similar. Since no overturning will occur for the given initial conditions, both RBs remain stable.

3.4.3 Response to a Ground Acceleration Pulse

When an unprestressed RB is subjected to a constant ground acceleration sufficient to initiate rocking, it overturns. Therefore, the push-over analysis is not suitable to study the earthquake stability of rocking structures. It was shown in this section that a prestressing cable can stabilize a RB, but their dynamic response remain highly non-linear. It is proposed in this section to study the behavior of a PT-RB to a half cosine ground acceleration pulse. This type of loading was already studied by Konstantinidis and Makris [19] for unprestressed RBs.

Figure 29 shows the response of an unprestressed RB to a ground acceleration pulse. For $\ddot{u}_g \leq 0.25g$, the RB does not rock, but for $\ddot{u}_g \geq 0.45g$ the RB overturns. It was shown that the initial prestressing force of a PT cable allows rocking initiation to be controlled. The rocking motion should occur during a large earthquake to dissipate energy. Therefore, the cable has to be tuned to allow rocking but to limit it such that the amount of rotation is

acceptable. Figure 30 shows that it is possible to limit the maximum rotation of the RB and prevent overturning by increasing η_α, even if there is no initial prestressing force (i.e. $\eta_0 = 0$).

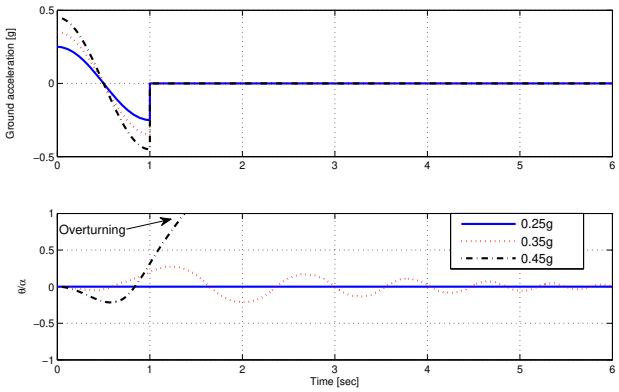

Figure 29: Response of an Unprestressed RB to a Half-Cosine Pulse for Several Amplitudes ($p = 2[1/\text{sec}]$, $\alpha = 15°$)

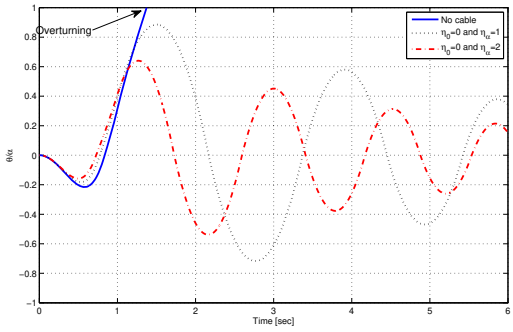

Figure 30: Response of PT-RBs to a Half-Cosine Pulse of Amplitude $\ddot{u}_g \leq 0.45g$ and Period $T = 2[\text{sec}](p = 2[1/\text{sec}]$, $\alpha = 15°)$

3.5 Rocking Spectra

As proposed by Makris and Konstantinidis [22], it is possible to compute rocking spectra, comparable to oscillation spectra widely used nowadays. An oscillation spectrum shows the maximum acceleration of a single DOF system for a given natural frequency, a damping ratio, and an earthquake excitation. Similarly, the rocking spectra represent the maximum rotation of a rigid block for a given frequency parameter p, a slenderness angle α, and an earthquake excitation.

Rocking spectra for PT-RBs are presented in this section. Similarly to spectra computed by Makris and Konstantinidis [22], it gives the maximum rotation of a PT-RB for different parameters. In some cases, the post-tensioning cable has an amplifying effect. For instance, in Figure 31, for $\alpha = 10°$, $2\pi/p = 6sec$ and $\eta_\alpha = \eta_0 = 0.5$, the PT-RB undergoes a rotation approximately 30% higher than the unprestressed RB. This observation still holds for $\eta_\alpha = 5\eta_0$ and $\eta_\alpha = 10\eta_0$. Since the frequency of rocking will increase with the use of the PT cable, resonance may occur for some specific earthquakes. The time history acceleration of an earthquake is very random, and since the RB response is highly non-linear, some frequencies may be excited when a PT cable is added. The resonance of PT-RB is usually balanced by the added stability, and for large prestressing forces ($\eta_0 \geq 1$), observations show that the cable is always beneficial.

The complex resonance phenomenon may lead to surprising results. Thus, the results of the rocking spectra cannot be extrapolated as easily as the results given by oscillation spectra. Two major differences must be noted. For oscillation spectra, it is possible to scale the response to simulate an earthquake excitation of a larger amplitude. Furthermore, multi-DOF elastic oscillators can be decomposed into orthogonal modes, hence the spectra can be used to design multi-DOF structures. This is not the case with multiple blocks rocking structures.

Unlike free rocking blocks, the PT-RB can rotate beyond α and return, rather than overturn. Since the resisting moment has a positive slope as described in Figure 16, it can in theory rotates beyond the angle α. However, the spectra presented here do not show the maximum angle when it exceeds the overturning angle of an unprestressed RB. It is considered that at such large rotations, it will experience very large strains (see Figure 25).

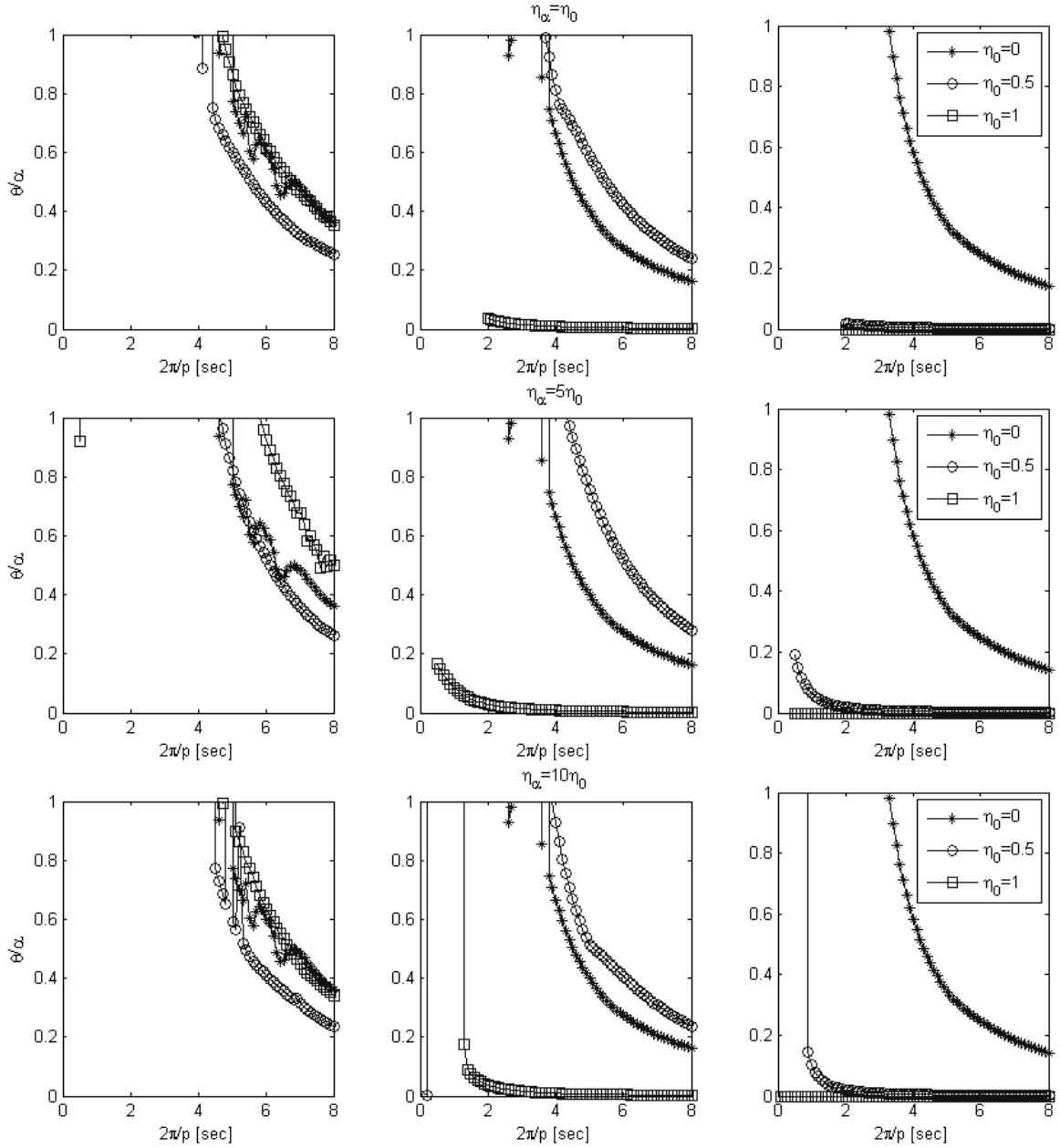

Figure 31: Rocking Spectra of PT-RBs, Subjected to Kobe Earthquake (Japan,1995, Takatori Station, Longitudinal), α is Equal to Respectively 5°, 10°, and 15°

3.6 Design Strategy Using a Rocking Base

The rocking mechanism can be used as a dissipative system for large structures subjected to earthquake excitation. Chen et al. [4] studied the rocking dissipation of slender viaduct columns. In their study, the rocking mechanism is rarely used because it is hard to predict overturning and also because it is hard to adjust the initiation of rocking. Namely, if the rocking behavior is used as a seismic isolation, the structure must start to uplift before it undergoes major damages. It was shown that the rocking impacts dissipate energy. But, if the column is slender, this dissipation will be minimal. However, when the base of the column is uplifted, it limits the resisting moment within the column. Furthermore, the non-linear oscillations of the rocking structure, the earthquake excitation is unlikely to resonate.

The use of post-tensioned rocking system for seismic response modification for a standard ordinary California bridge is presented here. The bridge section presented in Figure 32 was first studied by Ketchum et al. [18].

The column is considered rigid and the girder is modeled as a lumped mass, equal to the mass of the two adjacent mid-spans. The stiffness of the girder is neglected, so the bridge column can be modeled as a single degree of freedom. Rocking is allowed only between the pile cap and the column and at the foot of the column. For a typical $100'$ span, the rocking parameters become $p = 1.1225[1/sec]$ and $\alpha = 4°$. Note that the lumped mass on top of the column increases the block slenderness ($\alpha_{column} = 7.1°$). In order to get a stable rocking column, the post-tension force parameters η_0 and η_α can be adjusted. Also, the foot of the column may be widened in order to increase α.

In order to tune the rocking parameters properly, several design objectives have to be considered. The rocking mechanism is used in order to reduce the demand on the column. It helps to reduce the moment and shear in the column. In addition, the forces transferred to the footing and the deck are also lowered. Another design objective is to ensure that the bridge deformations remain acceptable. If the rocking rotations are too large, the structure may overturn. Therefore, the rocking parameters must be chosen adequately in order to limit the column's demand as well as to limit the bridge deformation. Since the response of the structure is highly non-linear, a trial and error strategy is used.

The unprestressed column will start rocking for $\ddot{u}_g = 0.07g$. Given that rocking has to occur for $\ddot{u}_g \geq 0.2g$ in order to limit the moment the foot of the column, $\eta_0 = 1.86$ based on Equation (21).

The cable is first assumed to be very soft (i.e. small diameter), hence $\eta_0 = \eta_\alpha$. The bridge

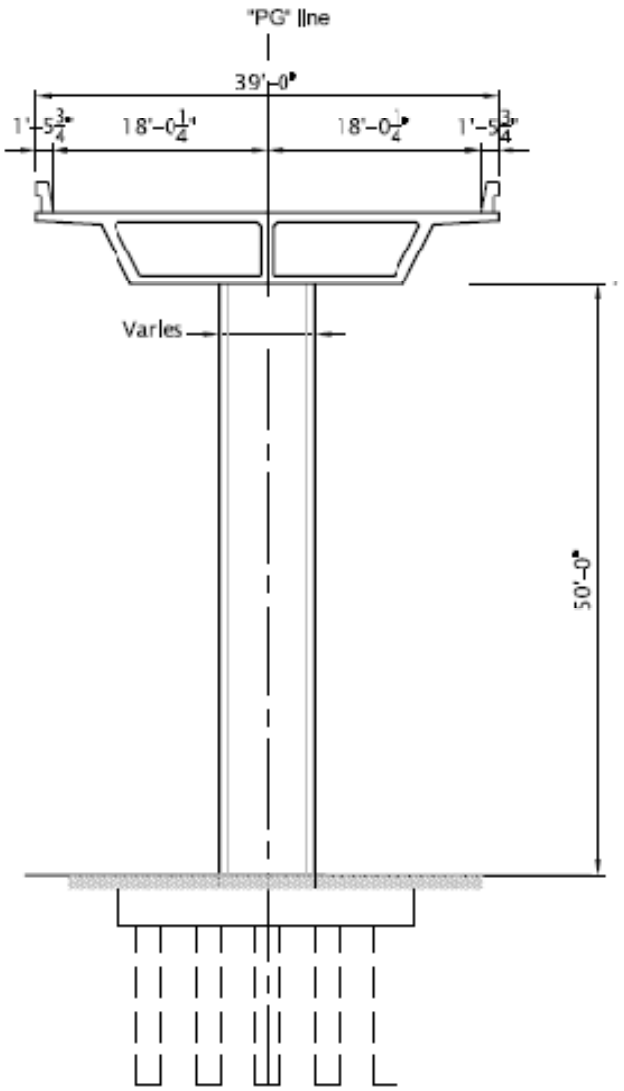

Figure 32: Typical Section of a Multi-Span Bridge

is subjected to Tabas earthquake record motion (1978). Figure 34 shows the rotation of the column during the excitation. $\eta_0 = 0$ represents the case with no post-tensioning cable the structure overturns almost immediately. For $\eta_0 = \eta_\alpha = 1.86$, the structure can withstand the earthquake. But the rotation of the column exceeds 80% of α. Furthermore, there is almost no dissipation. The structure is still largely oscillating 20 seconds after the end of the excitation.

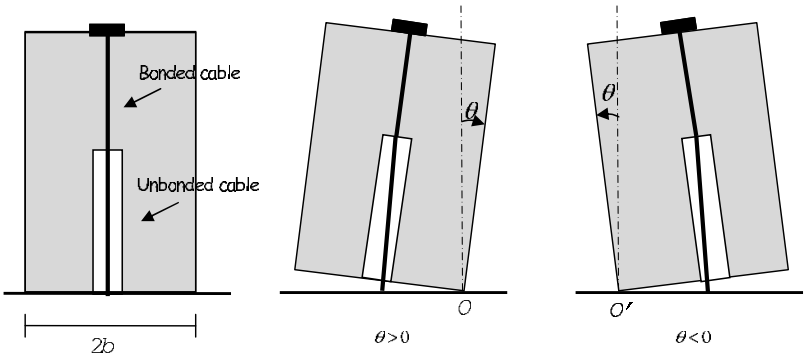

Figure 33: Bridge Column subjected to Tabas EQ With $\eta_0 = 0$ and $\eta_0 = 1.86$

In order to reduce the amplitude of the rotation, the cable stiffness $\frac{EA}{L}$ can be increased. Hence, a cable with a larger diameter can be used. However, it is also possible to partially bond the cable to reduce the length allowed to elongate. As a consequence, η_α will increase. But the small dissipation comes from the slenderness of the column. Even though the foot of the column could be widened to increase α, the dissipation would remain small. Other dissipation devices can be added to slender structure such as this one.

A new run is performed with $\eta_{alpha} = 10\eta_0$. Figure 35 shows that the rotation is significantly reduced. Its maximum is 24% of α.

The maximum force in the post-tension cable is $F_{pMax} = 5.9Weight$. For the bridge column studied here, this capacity can be obtained using a $5in^2$ steel cable with a yielding strength of $270ksi$. But such cable would be too soft. In order to obtain the parameter η_α, the cable can be partially bonded as shown in Figure 33. The cable has to be unbonded over a length of about $30ft$ to satisfy the mechanical properties used above.

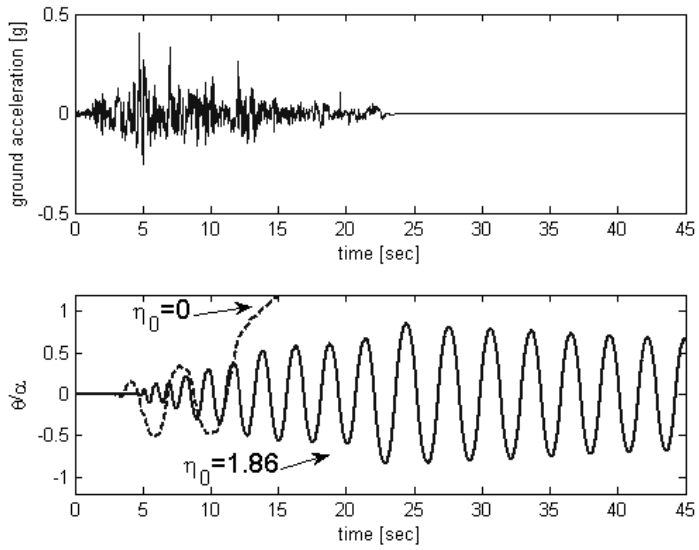

Figure 34: PT-RB with a partially bonded cable

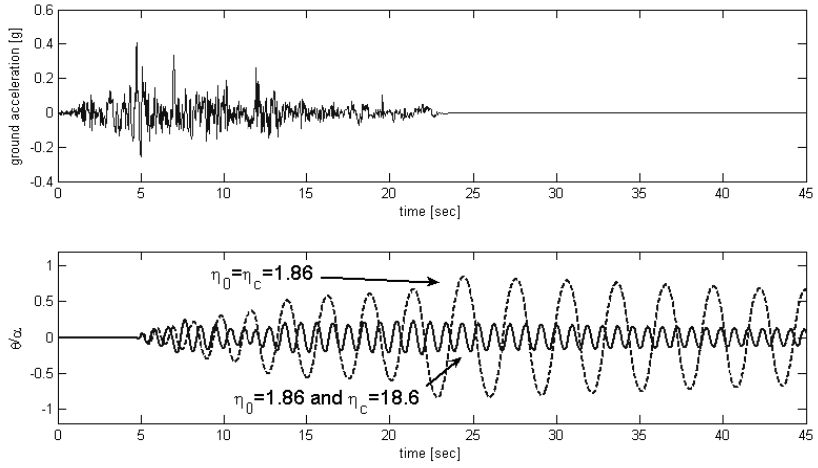

Figure 35: Bridge column subjected to Tabas EQ With $\eta_0 = 1.86$ and $\eta_\alpha = 18.6$

This simplified model shows the potential benefits of rocking behaviour in large structures. The moment at the base of the column will be considerably reduced, allowing the designers to reduce the moment capacity of the column and the footing. It also shows that the damping due to rocking is very small for slender structures such as bridges. Figures 34 and 35 show that the oscillations are still very large, $20sec$ after the end of the excitation; thus, an extra damping device may be required at the base.

In conclusion, a PT-RB is an effective seismic response modification mechanism. Its principal benefits are:

- Effective control of rocking initiation
- Limitation of the rocking amplitude
- Vibration period shift, making it difficult for the structure to enter resonance

This makes the structure less sensitive to earthquake excitation. But the dissipative property observed on squat blocks is negligible for very slender structures. Hence rocking connections should be coupled with external damping devices to control the attenuation of motion.

3.7 Conclusion

A PT-RB is an effective seismic response modification mechanism. Its principal benefits are:

- Effective control of rocking initiation
- Limitation of the rocking amplitude
- Vibration period shift, making it difficult for the structure to enter resonance

This makes the structure less sensitive to earthquake excitation. But the dissipative property observed on squat blocks is negligible for very slender structures. Hence rocking connections should be coupled with external damping devices to control the attenuation of motion.

The equations governing a rigid block subjected to rocking are fairly simple but they cannot be represented by an oscillating system. Hence the spectral analysis widely used in

earthquake engineering cannot be applied here. Makris and Konstantinidis [22] have developed rocking spectra, allowing the designers to know the maximum rotation that a rigid structure may experience for a given earthquake. However, the oscillation spectra are convenient because they can be used for multi DOF systems using modal analysis with a statistical approach. Furthermore, oscillation spectra can be blended together in order to represent the likelihood of an earthquake event for a given region. They can be scaled since the oscillation systems behave linearly. None of these properties applies to the rocking spectra, hence their use is much more limited.

The double RB assemblies were presented in section 3.3. The complexity of the implementation is due to the very large number of events. In fact, a single RB has a rocking initiation defined by one equation, versus 8 equations for a double RB. A single RB in motion may be subjected to only one impact event, versus 6 for a double RB. If a three rigid blocks assembly was to be implemented, the amount of events would be so large that it would be almost impossible to define them all. Furthermore, such a vast amount of events would be extremely hard to solve for conventional ODE solvers because of the likelihood that several events happen during the same time step. Hence we can conclude that analytical rigid body models are not suitable for multi-DOF rocking assemblies.

At last, the purpose of the research presented in this thesis is to study the behavior of bridges subjected to rocking. But the rigid block assumption cannot hold for slender structures because the structural elements of a bridge are not rigid but deformable. The material deformations may interact with the rocking rotation. Furthermore, it is likely that a bridge structure will require several rocking surfaces (between the deck and the column, for instance). These problems were an incentive to address the mechanics of rocking in a different manner. It has been already shown that the finite element method allows to represent complex material deformations, it is proposed to design a connection element capable of modeling the rocking rotation. Such element could be used in combination with existing finite elements to represent the behavior of a deformable rocking structure.

4 Rocking Element

4.1 Introduction

The rocking rigid body model is very convenient to analyze the response of single degree of freedom systems. It only has a few non-dimensional parameters. However, for systems with multiple rocking surfaces, the complexity rises tremendously. Different rocking modes may appear; thus, the algorithm has to detect when each rocking event is triggered as explained in [31] and it also has to detect the transition between two different rocking modes. Two superimposed rigid blocks lead to ten different rocking modes transitions [28], so three superimposed rigid blocks analysis is merely intractable. Therefore, the analytical equations of staggered rigid blocks is not conceivable to study large structures. A finite element model may be more suitable.

Furthermore, a flexible block may have a significantly different rocking behavior. In order to use rocking devices on slender structures such as bridges, the deformations of the structural elements must be taken into account as they may alter the rocking behavior when deformed elastically, inducing or precluding overturning, compared to a rigid body. This leads to the conclusion that the rocking surface cannot be modeled independently from the rest of the structure.

The goal in this chapter is to develop a finite element model representing rocking at the interface between two prismatic (frame) finite elements. Rocking is assumed to occur in the plane of the frame (2-dimensional rocking) and the frame elements are assumed to have no thickness; i.e., the shape of the cross-sections at the rocking interface is irrelevant; only the thickness dimension of the frame element matters. The width of the rocking surface is defined as a parameter of the rocking element and it is independent of the width of the adjacent frame elements. In addition, it will allow the consideration of the large displacements and deformations of the frame elements in the structure.

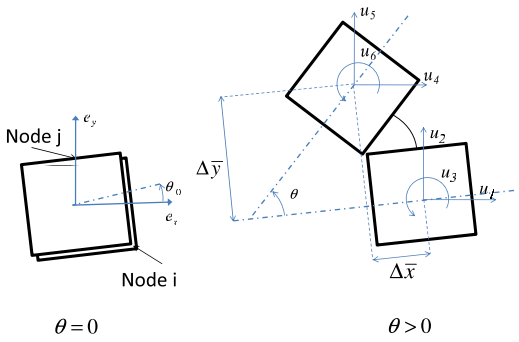

Figure 36: Description of the Rocking Element

4.2 Description of the Element

The rocking element is a point element. It has two independent nodes overlapping at rest. Each node can be connected to another element such as a beam. The kinematics of the element are limited to the plane of the frame (2D modeling), so each node has three degrees of freedom, two translations and, one rotation. It is considered that no sliding will occur at the rocking interface. The two parameters p and α used in Chapter 3 cannot be applied in this case since they both depend on the geometry of the block. The new element will have a rocking radius R and a rotational stiffness k_r. The rocking radius defines the distance between the nodes and their center of rotation. The rotational spring k_r shall be set to zero when modeling a free rocking behavior. Even a post-tensioning cable restraining rocking shall not be modeled using this rotational spring, a bar element connecting the anchoring points will be far more realistic and the added computational cost will be negligible. However, this spring can be useful when representing a deformable footing.

Note that the element does not have a constitutive law, except for the rotational stiffness k_r, which is usually equal to zero (free rocking configuration). Therefore, if the element is not subjected to any external force and a rotation is imposed at one end, the resisting moment will be zero. However, when the element is subjected to an axial force, the rocking rotation θ will generate a resisting moment. In fact, the element may be free to rotate (i.e., no rotational stiffness), but the center of rotation does not correspond to the center of the element because of the kinematic constraints. Hence the resisting forces of the element depend on the forces applied to the element of the rest of the structure.

The displacements and the rotations of the nodes expressed in the global coordinate system are stored in the vector u. The forces and the moments at the nodes are stored in the vector p. The two nodes can translate and rotate separately but, in order to model rocking without sliding, these translations and rotations are dependent. Hence only one internal degree of freedom, the angle, remains.

The element has an orientation, so there is an initial angle θ_0 that defines the angle between the rocking surface and the e_x-axis as shown in Figure 36. When rocking occurs, the kinematic equations are the following:

$$\Delta\overline{x} = -sign\,(\theta)\,R\,(1-\cos\theta) \tag{22a}$$

$$\Delta\overline{y} = R|\sin\theta| \tag{22b}$$

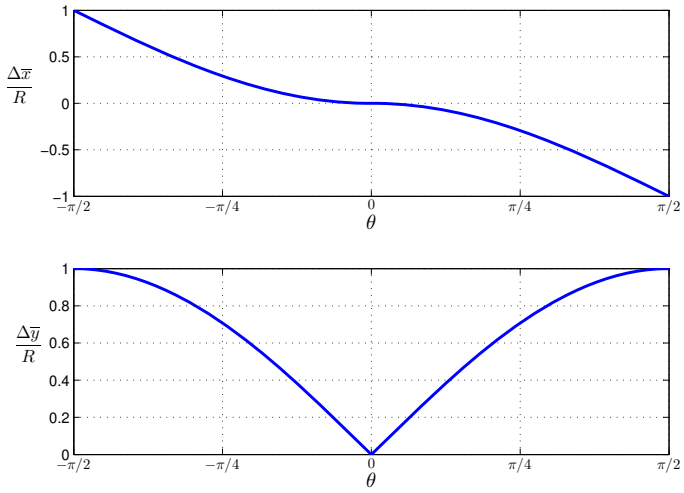

Figure 37: Kinematics of the Rocking Element

The kinematic constraints are imposed using the Lagrange multiplier method. Before rocking occurs, the two nodes must overlap. Therefore, the algorithm applies the following three constraints.

$$g_1(\mathbf{u}) = u_4 - u_1 = 0 \tag{23a}$$
$$g_2(\mathbf{u}) = u_5 - u_2 = 0 \tag{23b}$$
$$g_3(\mathbf{u}) = u_6 - u_3 = 0 \tag{23c}$$

Once rocking is initiated, then the three constraint functions defined in Equations (23a), (23b), and (23c) are replaced by the two constraint functions (24a) and (24b). These two constraints impose the vertical and horizontal displacements consistent with the radius R for a rotation θ. The center of rotation is located at a distance R from the nodes. The initial angle θ_0 defines the initial orientation of the rocking surface. These constraints also prevent sliding. The relative displacements between the nodes are represented in Figure 37. Note that the horizontal displacement is smooth; however, the vertical displacement has no first derivative for $\theta = 0$.

$$g_1(\mathbf{u}) = (u_4 - u_1)\cos(u_3 + \theta_0) + (u_5 - u_2)\sin(u_3 + \theta_0) + sign(u_6 - u_3)R(1 - \cos(u_6 - u_3)) \tag{24a}$$
$$g_2(\mathbf{u}) = -(u_4 - u_1)\sin(u_3 + \theta_0) + (u_5 - u_2)\cos(u_3 + \theta_0) - R|\sin(u_6 - u_3)| \tag{24b}$$

4.3 Initiation of Rocking

A block uplifts when one end of its rocking base is no longer subjected to compression so the element will initiate rocking when the axial compression multiplied by the radius of the base is less than the moment applied at the node . It is important to note that the element can be subjected to a rigid body motion; so, in general, the direction of the axial force is not aligned with the vertical axis.

In equation (25) the forces and moments p_i are associated with the displacements and rotations u_i and the internal rotation θ is equal to zero since rocking has not occured. When rocking is initiated, the constraints are changed. The three constraint functions (23) are replaced by the two constraint functions (24). A Lagrange multiplier will disappear, so the structure of the global stiffness matrix will change. This event has to be handled with great care by the algorithm. It corresponds to a sudden change in the boundary conditions of the structure, hence the transition should occur when the system respect the constraints

associated with the non-rocking state (23) and the constraints associated with the rocking state (24). This transition should occur when the rocking initiation event is satisfied and when the internal rotation in the rocking element is $\theta = 0$.

$$p_3 > -R \begin{pmatrix} -\sin(u_3 + \theta_0) & \cos(u_3 + \theta_0) \end{pmatrix} \begin{pmatrix} p_4 - p_1 \\ p_5 - p_2 \end{pmatrix} \tag{25}$$

If the algorithm overshoots when the rocking is initiated, the moment in the element will far exceed the moment defined by equation (25). The release of a constraint will then lead to a sudden drop of the moment and generate noise while, in fact, the resisting moment should be continuous when rocking is initiated. Therefore, when the event occurs, the algorithm has to step back and reduce the time step in order to converge to the rocking initiation event. This issue was discussed in chapter 3.4.1, for the rocking event detection (at each impact) and not for the rocking initiation event.

As a structure undergoes free rocking, the amplitude is reduced and the oscillations become shorter after each impact. Eventually, the rocking rotations are too small and the algorithm should interrupt rocking to minimize computational cost.

4.4 Implementation of the Constraints

In order to represent the rocking motion properly, the rest of the structure has to be modeled with elements accounting for large displacements. The location of the center of masses with respect to the center of rotation of rocking will play a central role in the rocking behavior and in the loss of stability of the structure. The beam elements used in this thesis are elastic corotational beam elements [6], embedded in FEDEASLab [11]. This program allows the user to call any existing routine in Matlab as well as a robust linear algebra solver.

The rocking elements are associated with constraints. Therefore, an energy potential for the entire structure (rocking and elastic elements) has to be minimized and to satisfy the constraint functions $g_i(\mathbf{u})$, using the Lagrange multiplier method.

$$\Pi_{tot}(\mathbf{u}, \lambda) = \mathbf{\Pi}(\mathbf{u}) + \lambda \mathbf{g}(\mathbf{u}) \tag{26}$$

$$\Longrightarrow \quad \begin{cases} \frac{\partial \Pi_{tot}}{\partial \mathbf{u}} = R(\mathbf{u}) + (\frac{\partial \mathbf{g}}{\partial \mathbf{u}})^{\mathbf{T}} \lambda - \mathbf{F} \\ \frac{\partial \Pi_{tot}}{\partial \lambda} = g(\mathbf{u}) \end{cases} \tag{27}$$

Equations (26) and (27) describe the governing equations of the structure with the constraints. u represents the displacements at the free degrees of freedom (DOF) , $R(u)$ represents the resisting force associated with the free DOFs, F represents the applied force, including the inertia forces, and $g(u)$ represents the constraint functions associated with the free DOFs connected to a rocking element.

Since these equations are non-linear, this potential will be minimized using an incremental and iterative algorithm. Equation (28) shows that the total stiffness matrix is symmetric but not positive definite. Hence the Cholesky solving algorithm cannot work because the pivots are equal to the diagonal terms and cannot be zero. The matrix can still be inverted with a permutation algorithm, but the computational cost increases. In such cases, it is usually preferred to enforce the constraints with approximate methods [17].

$$K = \frac{\partial R}{\partial u}, L = \frac{\partial g}{\partial u} \implies \begin{bmatrix} K & L^T \\ L & 0 \end{bmatrix} \begin{pmatrix} \Delta \mathbf{u} \\ \Delta \lambda \end{pmatrix} = \begin{pmatrix} \Delta \mathbf{F} \\ \Delta \bar{\mathbf{g}} \end{pmatrix} \tag{28}$$

The penalty method consists of multiplying the constraint functions by a very large penalty number such that, when the potential is minimized ,the constraint function has to remain small.

$$\Pi_\kappa(\mathbf{u}) = \mathbf{\Pi}(\mathbf{u}) + \frac{\mathbf{1}}{\mathbf{2}} \kappa \mathbf{g}(\mathbf{u})^{\mathbf{2}} \quad with \quad \kappa \gg 1 \tag{29}$$

In order to set the constraints to zero, κ must be very large. This may compromise the condition number of the stiffness matrix but the penalty factor can be reduced without compromising the constraint if it is combined with an iterative algorithm, using the Augmented Lagrangian method. This iterative method is presented in Figure 38.

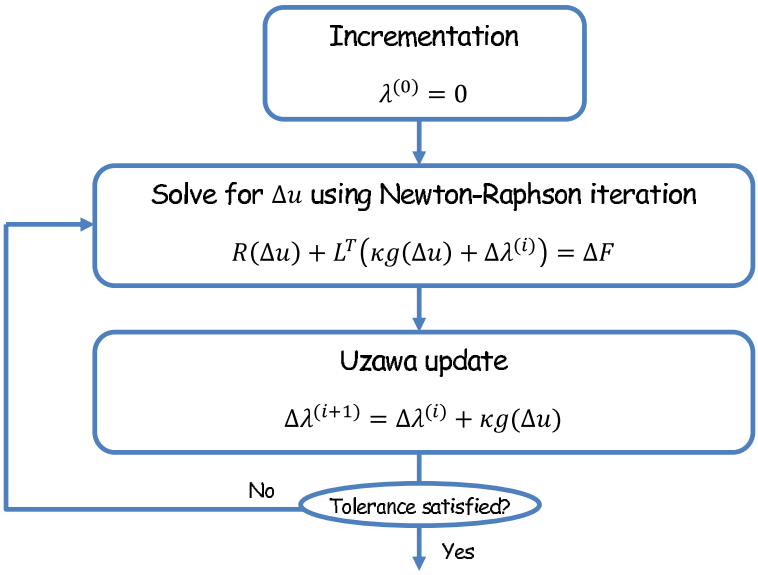

Figure 38: Augmented Lagrangian Method

For each *Augmented Lagrangian* iteration, the algorithm has to perform a *Newton-Raphson* iteration until convergence occurs. In order to optimize the computational cost, the algorithm was implemented such that the *Augmented Lagrangian* iterations will occur very rarely. If the penalty parameter κ is very large, then the Augmented Lagrangian iteration may be satisfied within one step.

As shown in Figure 39, the constrained vertical displacement in the rocking element has a discontinuous gradient, hence *Newton-Raphson* iteration may fail to converge and since this gradient is infinitely steep for $\theta = 0$ it is not Lipschitz continuous, so more enhanced iterative method such as BFGS may also fail to converge [6].

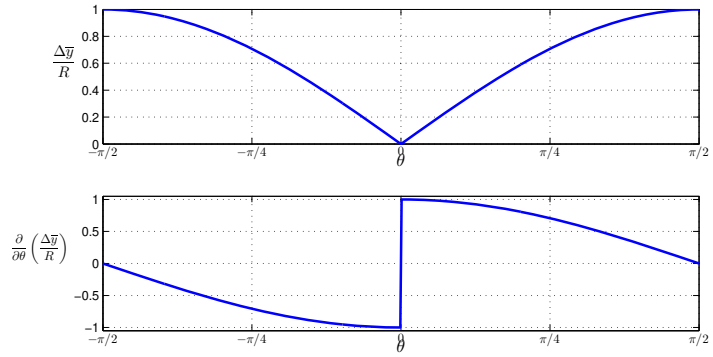

Figure 39: Vertical Constraint of the Rocking Element Versus Rotation

Therefore, a different approach was used. Instead of trying to find an algorithm that converges, despite the discontinuity, the vertical constraint function was 'smoothed.' When θ is within an interval ε near zero, Equation (22b) is interpolated with an order 4 polynomial. Hence its derivative is continuous at zero. This method makes the element more robust because it allows the user to use any iterative algorithm, suitable for the rest of the structure. In order to enforce the continuity at the edge of the interval ε , the function is made so that it is no longer equal to zero for $\theta = 0$. In Figure 40, a very large interval ε was chosen for clarity. Equation (31) represents the smoothed constraint functions used when $|\theta| < \varepsilon$, with the polynomial coefficients expressed in Equation (30)

$$\begin{pmatrix} a_1 \\ a_2 \\ a_3 \end{pmatrix} = \begin{pmatrix} -\frac{1}{8\varepsilon^2}\sin(\varepsilon) - \frac{1}{8\varepsilon^3}\cos(\varepsilon) \\ -\frac{1}{2}\sin(\varepsilon) - 6\alpha\varepsilon^2 \\ \sin(\varepsilon) - \alpha\varepsilon^4 - \beta\varepsilon^2 \end{pmatrix} \tag{30}$$

$$g_{1\varepsilon} = (u_4 - u_1)\cos(u_3 + \theta_0) + (u_5 - u_2)\sin(u_3 + \theta_0) + sign(u_6 - u_3)R(1 - \cos(u_6 - u_3)) \tag{31a}$$

$$g_{2\varepsilon} = -(u_4 - u_1)\sin(u_3 + \theta_0) + (u_5 - u_2)\cos(u_3 + \theta_0) - R(a_1(u_6 - u_3)^4 + a_2(u_6 - u_3)^2 + a_3) \tag{31b}$$

Inevitably, the 'softening' parameter ε will reduce the intensity of the impact, so it will affect restitution. Figure 42 represents the rotation of a rocking element for a column subjected to free rocking behavior. The initial angle of the column is equal to its slenderness angle (i.e. $\theta_{ini} = \alpha$). It shows that for $\varepsilon \geq \theta_{ini}$, the rocking element does not dissipate any

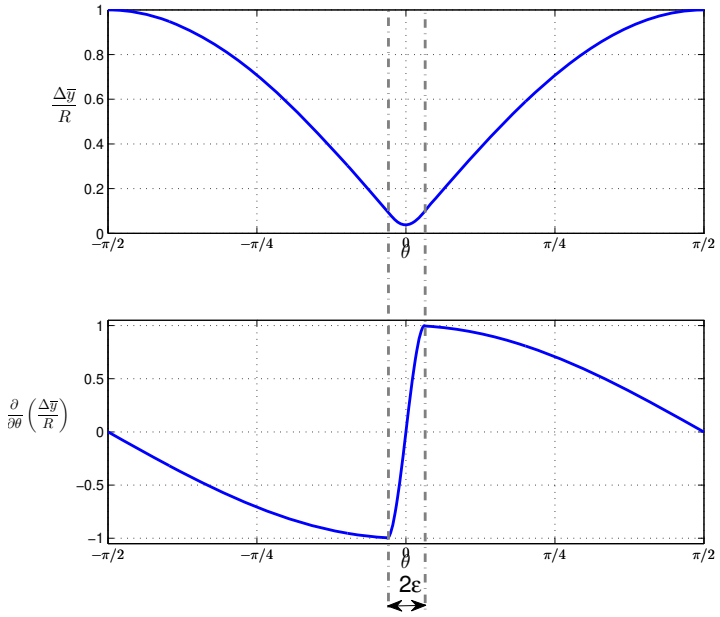

Figure 40: Vertical Constraint of the Rocking Element With a Polynomial Interpolation

energy (dashed blue plot). However, for $\varepsilon \leq \theta_{ini}/100$, the dissipation during each impact is represented with sufficient accuracy (solid red plot). A fraction of the slenderness angle of the column can give a good calibration parameter for ε. Unfortunately, this angle is not inherent to the rocking element; it depends on rest of the structure. Unlike the rigid block model studied above, a rocking element contains very few intrinsic properties. Leaving aside the rotational stiffness (often set to zero), the rocking element property is only a radius R and an initial angle θ_0. However, in order to be implemented in a finite element code, the approximation parameter ε should have a default value.

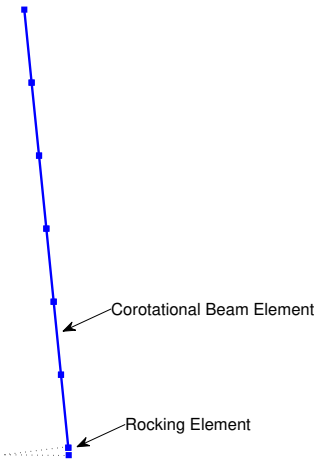

Figure 41: Column With a Rocking Base

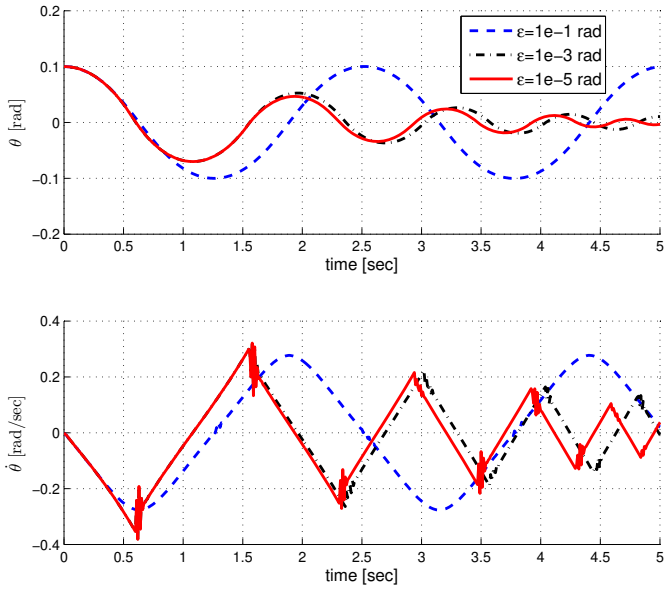

Figure 42: Rocking Column Rotation and Angular Velocity for Different Values of ε

4.5 Integration Scheme

In order to solve the dynamic equation in a time step analysis, the time integration scheme is usually explicit for 'fast dynamic problems' and implicit for 'slow dynamic problems'. Dynamic problems are considered fast when the time scale allows to track shock wave propagation. It usually refers to structures subjected to impact. Conversely, dynamic problems are considered slow when the frequencies of the excitation are of the same order as the natural frequencies of the structure.

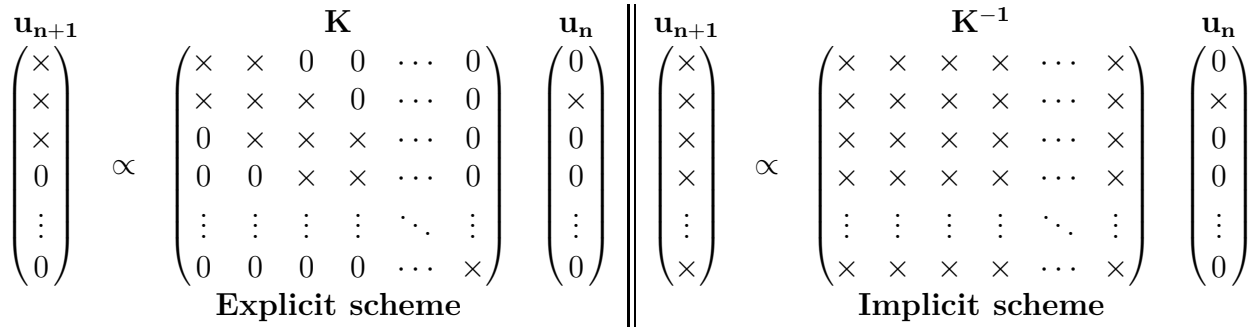

Figure 43: Structures of the Integration Schemes

As shown in Figure 4.5, the displacement of a degree of freedom at time t_n can only affect the neighboring degrees of freedom at time t_{n+1} when the time integration is explicit. On the contrary, an implicit scheme has the capacity to modify all the degrees of freedom within one time step.

In order to remain stable, an explicit scheme such as the central difference method uses time steps shorter than T_n/π, where T_n is the shortest natural period of the system. The column in the model presented in Figure 41 is very stiff so as to compare the results with the solution given by the rigid block model in Chapter 3. So for the rocking systems studied here, the required time step has to be less than $10^{-8} sec$. However, analytical solutions of rocking equation of motion (Chapter 3) indicate that oscillations occur at periods of approximately $1 sec$ for rocking blocks representing typical bridge structures. Therefore, despite the impact caused by the rocking element, an implicit scheme is preferred for solving rocking problems in typical structures.

Figure 41 represents the structure used to calibrate the time integration scheme. It is a 20 feet tall reinforced concrete column with a rocking radius of $1m$. In order to represent a column rocking on its base, the rocking radius should be equal to half the width of the rock-

ing column (i.e. $R = b/2$). The geometric and material parameters are chosen to represent a realistic bridge column with a hollow section. An initial rotation of $0.1rad$ is applied to the column and the free oscillation response is computed using a Newmark implicit scheme ($\beta = 1/4$ and $\gamma = 1/2$). The initial time step is $1e-2sec$, but the integration algorithm is able to perform time-step division when the *Newton-Raphson* iterations fail to converge.

Figure 44 represents the rotation and the angular velocity response of the rocking element for the initial conditions shown in Figure 41. Based on the results presented in Chapter 3, the column is expected to rock freely and to radiate the energy released during impact through the column. Hence, the rotation at the base should only decrease; however,the solid blue plot in Figure 44 shows that the rotation being amplified, which leads to the instability of the structure. It is due to the numerical noise of the angular velocity $\dot{\theta}$. After each impact, the noise worsens. The velocity at the first impact should be the upper bound but, after a few impacts, the noise generated exceeds this limit in amplitude. This numerical noise is often observed in structures subjected to impact [14]. High frequency noise in the displacement response can easily be solved by adding viscous damping but, in this case, the high frequency noise is in the velocity response . The Newmark scheme used here is energy conservative; therefore, only a different integration scheme with a numerical dissipation can solve this issue.

The HHT method [14], also known as the α-method, is a modified Newmark scheme. Equation (32) represents the implementation with the Augmented Lagrangian contribution. The added parameter α controls high-frequency damping. It can then be used to filter out the high frequency noise observed in the angular velocity.

$$M\ddot{u}_{n+1} + C\dot{u}_{n+1} + (1+\alpha)(R(u_{n+1}) + \lambda_{n+1}\frac{\partial g}{\partial u}(u_{n+1})) - \alpha(R(u_n) + \lambda_n\frac{\partial g}{\partial u}(u_n)) = F_{n+1} \tag{32a}$$

$$u_{n+1} = u_n + \Delta t\dot{u}_n + \Delta t^2((1/2-\beta)\ddot{u}_n + \beta\ddot{u}_{n+1}) \tag{32b}$$

$$\dot{u}_{n+1} = \dot{u}_n + \Delta t((1-\gamma)\ddot{u}_n + \gamma\ddot{u}_{n+1}) \tag{32c}$$

The spectral radius defines the change of the displacement norm between steps n and $n+1$, so $\rho = \frac{||u_{n+1}||}{||u_n||}$. It is computed using the response of a linear system $M\ddot{u}_{n+1}+C\dot{u}_{n+1}+Ku_{n+1} = F_{n+1}$. If the spectral radius $\rho = 1$, then the integration scheme does not dissipate energy. If $\rho > 1$, the scheme is unstable. Figure 45 represents the spectral radius of the HHT integration scheme versus the time-steps/natural-period ratio. It shows that the Newmark method

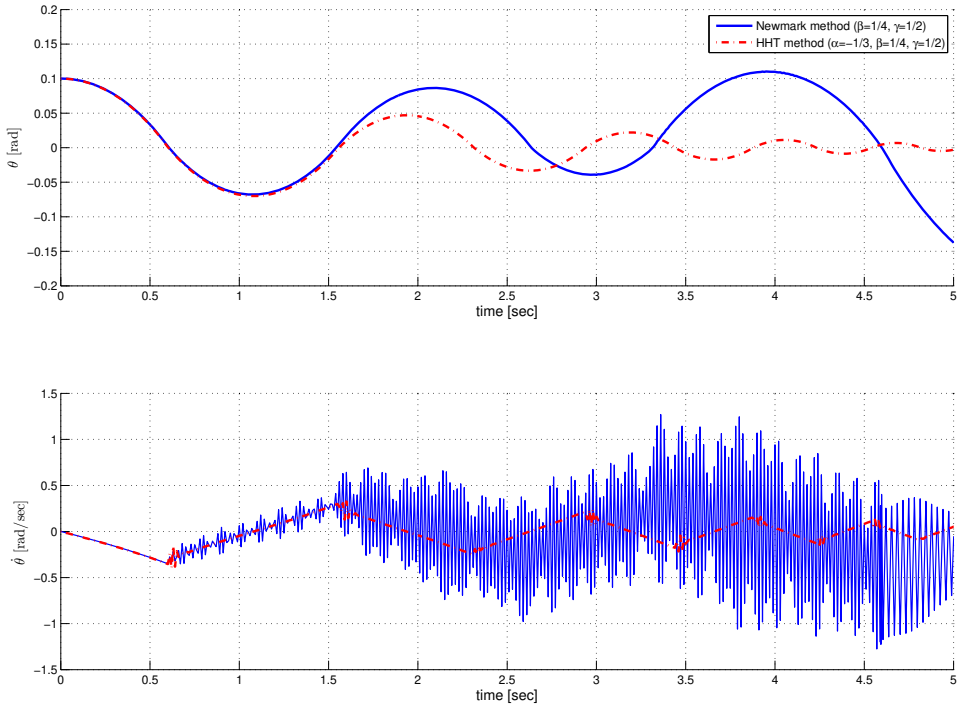

Figure 44: Rocking Element Response to a Free Oscillation (Newmark Scheme $\beta = 1/4$ and $\gamma = 1/2$)

is not dissipative for $\beta = 1/4$ and $\gamma = 1/2$. Since the solution is not exact, the conservation of energy leads to numerical noise generation. It is observed that this noise occur in the high frequency range and should be filtered. The spectral radius for the HHT method is equal to 1 for low frequencies (i.e. $\frac{\Delta t}{T} << 1$), but it filters the high frequencies. Hence it is very suitable to solve the issue presented in Figure 44. The dashed plot shows that the HHT integration scheme represents a reasonable solution without the noise observed in the angular velocity.

The implementation of the HHT integration algorithm is summarized in Figure 46.

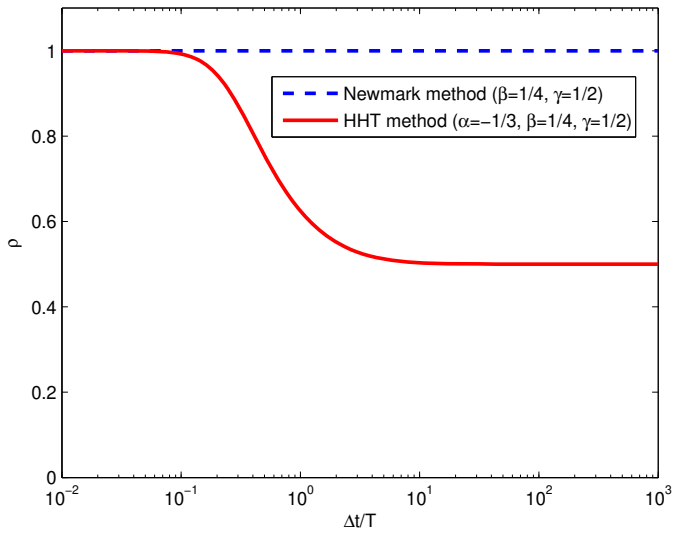

Figure 45: Spectral Radius of the HHT Integration Method

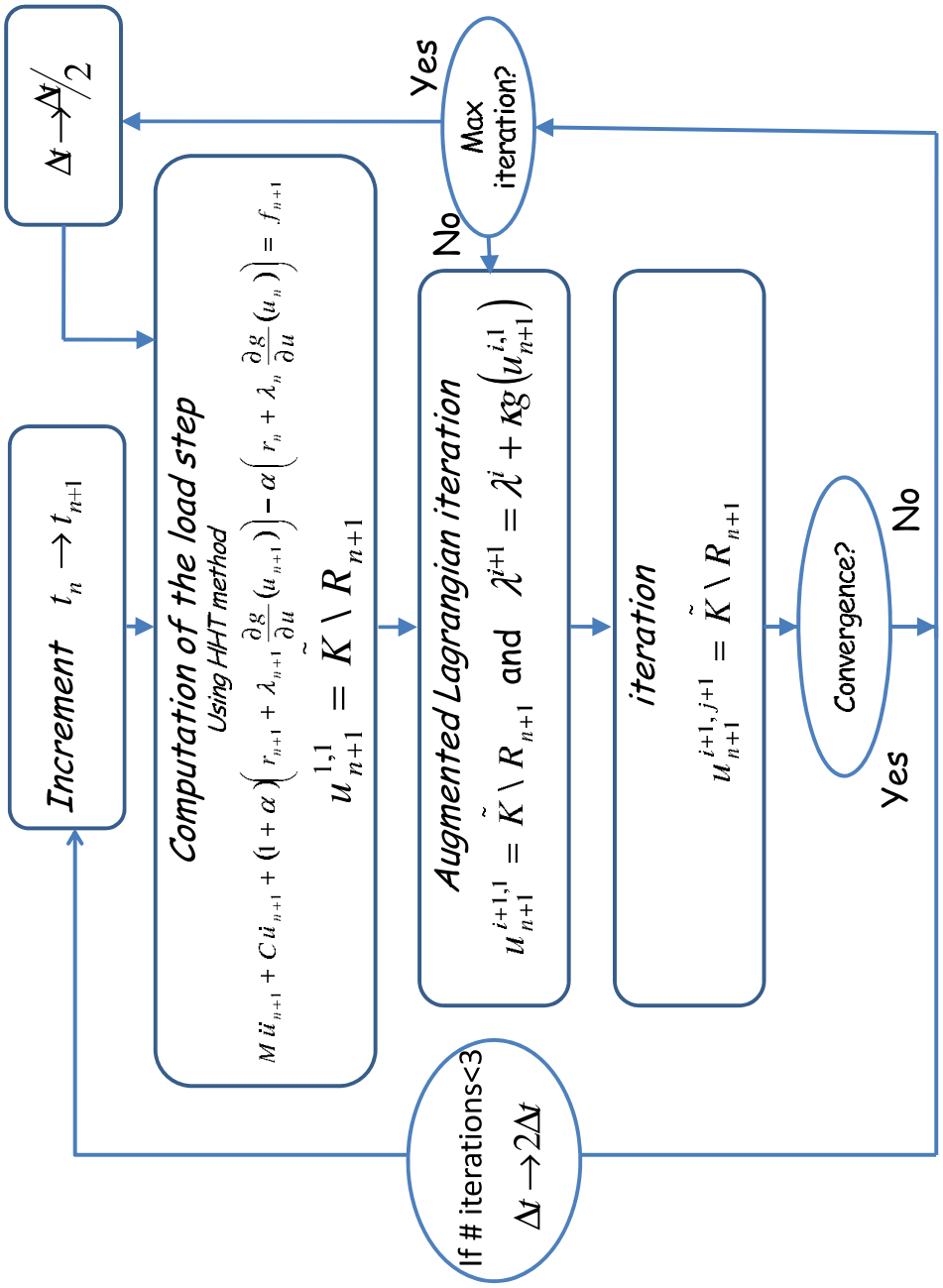

Figure 46: Summary of the HHT Algorithm Implementation

4.6 Comparison with Rigid Block Solutions

In order to compare the rocking behavior of a beam with a rocking element to that of a rocking rigid block, a free rocking test was performed. A squat block with the properties presented in Table 1 was modeled. The formulation of the geometry is corotational when elastic beam and rocking elements are used in FedeasLab.

Geometric parameters	Height	=	$6m$
	Width	=	$2m$
Material parameters	EI	=	$4.64e10\ N \cdot m^2$
	EA	=	$1.02e11\ N$
	ρ	=	$6400\ kg/m$
Equivalent rigid rocking block parameters	p	=	$1.525 rad/sec$
	α	=	$18.4°$

Table 1: Column Properties

In the rigid block model introduced by Housner [16] , energy dissipation is observed. In fact, the balance of angular momentum leads to a loss of angular velocity after each impact, defined in Equation 3. If the column studied in this example is considered rigid, then the angular velocity loss should be equal to 25% per impact. The equations governing the rigid block rocking motion do not satisfy the conservation of energy, but the equation of dynamics governing the model presented in this section does conserve energy. Therefore, after each impact, this energy is expected to appear as a shock wave propagating in the beam. Viscous damping can be added to dissipate energy, but the HHT integration scheme will also dissipate energy for very high frequencies. It is expected that the rocking element solution will tend to the rigid block solution if the beam is very stiff.

Furthermore, the beam will be subjected to large rigid body motions so, if the damping matrix is proportional to the mass matrix, the dissipation will be unrealistic. The rotation of the base is a rigid motion so it should not lead to any dissipation. Instead, the energy released during impact should generate a vanishing shock wave in the beam. Hence viscous damping should be proportional to the beam stiffness matrix only. This issue is discussed in details in Section 5.3. In the present example, the shock wave propagation vanishes only due to the HHT integration scheme.

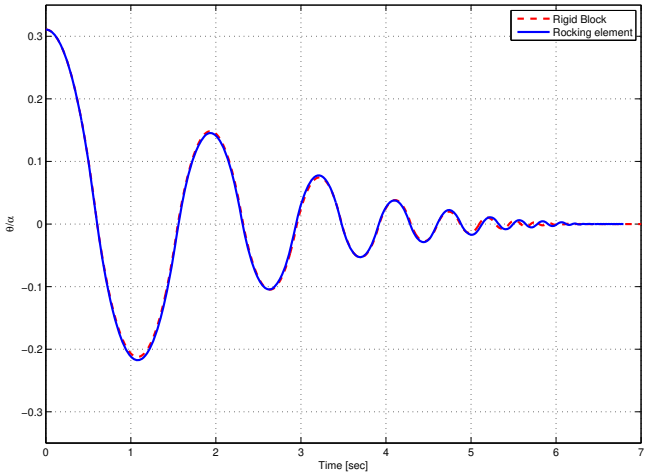

Figure 47: Free Rocking Response of a Rigid Block and a Stiff Beam With a Rocking Element

Figure 47 compares the rotation of a stiff beam and a rocking element with a rigid block in free rocking. The beam model developed herein is very suitable to represent the rocking behavior of a rigid block. To exaggerate the comparison, the geometric parameters chosen here are very penalizing for the rocking element model. The slenderness ratio is 3. It leads to very large impacts that dissipates a significant amount of energy, leading to very large shock wave radiations. When the rigid block modeled was more slender, the computation would be at least as accurate as the one represented herein. This example shows that the rocking element approach fulfills the expectations in describing the motion of single degree of freedom rocking objects.

4.7 Rocking Termination

It was shown in Section 3.1.3 that even though the number of rocking impacts is infinite, the free rocking response will stop at a finite time but, due to the 'softening' parameter ε described in Section 4.4, the rocking element will act as a very stiff rotational spring when $\theta \simeq 0$ and the rotation will continue indefinitely with a very small amplitude.

There are two options to handle termination of rocking motion:

- The rocking rotation can be locked under a certain value
- The element can be allowed to rock even for very small rotations

A criterion, intrinsic to the element, must be chosen to stop the rocking but a rocking rotation is considered to be small when compared to the rest of the structure. Here, the option to do nothing about stopping the small magnitude rocking motions is examined. A rigid block is excited in free rocking, followed by a ground acceleration pulse equal to 75% of the required ground acceleration to initiate rocking. Figure 48 shows that, once the rocking motion vanishes, the system behaves like a column at rest. Despite this large excitation, the block does not rock; its rotation does not increase. This is consistent since the structure can be considered at rest. Therefore, small magnitude rocking can be allowed to remain in the model without affecting the solution. However, as the rocking rotations become smaller, the frequency of impacts increase. Hence the time steps shorten and the computational time of monitoring just minor motions becomes extremely large.

The properties of the rocking elements are not sufficient to be determined when the tip displacement of the column or some controlling point of the structure becomes negligible. An 'autonomous' strategy should be preferred to simplify the use of this element. In order to avoid an ill-conditioned stiffness matrix, the user should use units such that the stiffness matrix and the mass matrix of each element remain close to one. If the HHT integration scheme is used, then the condition number of the matrix $K_{eff} = K_t + \frac{1}{\Delta t^2} \cdot \frac{1}{\beta(1+\alpha)} M$ should be considered. It can be assumed that if rocking rotations are less than $1e-10rad$ and rocking velocities are less than $1e-7rad/[time-unit]$, the rocking motion is negligible and rocking will be terminated. These two parameters are very severe, but they guarantee the stability of the algorithm even when the matrix K_{eff} is poorly conditioned.

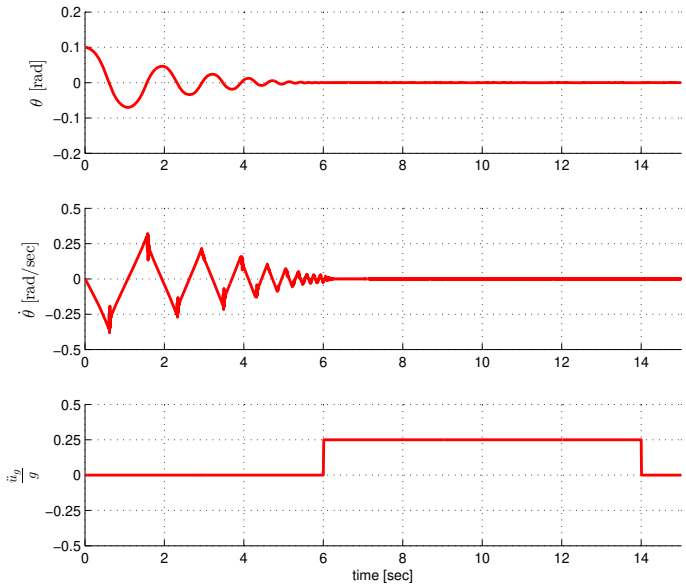

Figure 48: Free Rocking Response, Then Subjected to a Large Ground Acceleration

4.8 Behavior of a Two-block Assembly

As explained in section 3.3 the governing equations of two rigid blocks stacked were derived in [28]. This model is much more complex than the single rigid block model. The equations for three or more rigid blocks would be even more difficult to derive. Such configuration is very sensitive to small geometric variations. This can quickly lead to an overturning of the structure, due to the inherent instability of the assembly. A two-block structure is modeled here in order to compare the results of simulation, using the rocking element to the analytic solution for rigid blocks presented by Psycharis, even though such configuration could hardly be used in earthquake engineering.

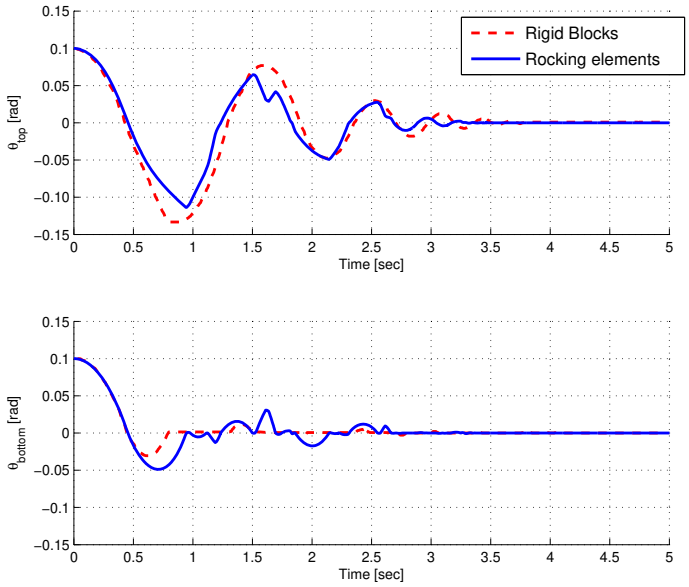

Figure 49: Free Rocking Response of a Two Rigid Blocks Assembly and a Two Beams Assembly With Rocking Elements at Interfaces

Figure 49 compares the response of a two rigid bodies assembly with the beam and rocking elements assembly subjected to an initial rotation. The geometric parameters are presented in Table 2; they are similar to the ones used in [28]. The rocking elements successfully represent the two-block assembly behavior. The error is more noticeable than that observed in Figure 47. However, it can be explained by the high sensitivity of the model. The solution varies noticeably when a slight change is made to the mass distribution (lumped

Top block	Height	=	$2.5m$
	Width	=	$1m$
	Density	=	$2.5e3kg/m^3$
Top block	Height	=	$1.25m$
	Width	=	$1.25m$
	Density	=	$2.5e3kg/m^3$

Table 2: Blocks Properties

or distributed) to the stiffness, or to the natural damping. In order to preserve stability, it is necessary to add viscous damping. The damping ratio is set to 2% and the damping matrix is proportional to the tangent stiffness matrix. It is continuously updated during computation, as explained in 5.3. This is to be expected since the rigid block model assumes that radiating shock waves will be damped. The rocking between the two blocks initiates only after the first impact between the bottom block and the footing. This is successfully represented by the rocking element. In fact, during the free fall before the first impact, the compressive force at the interface between the two blocks is very small. The initiation of rocking defined in Equation 25 shows that premature rocking initiation can occur. However, the HHT integration scheme and a sufficiently small time step prevent this problem.

4.9 Conclusion

In this chapter, the implementation of a rocking element was presented. It consists of a zero-length two nodes element capable of representing the behavior of a rocking surface between prismatic elements. The kinematics of this element are limited to the plane of the frame. The rocking parameters presented in Chapter 3 are no longer suitable for this modeling approach. Therefore, new parameters intrinsic to the element, namely, the rocking radius R and its orientation θ_0, were introduced.

This element behavior is not governed by a material constitutive law but by kinematic constraints. The element has one degree of freedom, namely, the relative rotation between the two nodes but, the center of rotation is not located at the nodes. The kinematic constraints force the rotation to occur around a center located at a distance R from the nodes. So, when this element is used in a model, the solution cannot be obtained with a conventional energy minimization method. Instead, the energy minimization must also respect the kinematic constraints. An approximated solution called the *Augmented Lagrangian* method was implemented.

Several computational issues had to be addressed during the implementation of the solving algorithm. First, the element can cause rocking to initiate and to terminate. By doing so, the number of constraints change during the computation. Furthermore, one of the kinematic constraints is not *Lipschitz* continuous and may prevent the *Newton-Raphson* iteration method to converge. At last, the rocking impacts may cause noise in the velocity response that must be filtered by the integration scheme.

A stiff column was modeled with a rocking element at its base and the rocking response was compared with the response of a rigid body. The solution obtained was very consistent. The rocking response of two stacked rigid blocks was also approximated with success by using stiff frame elements and rocking elements at their interface.

Thus, this element can be used to model the effect of rocking on deformable structures. It is extensively used in the rest of this thesis address several issues concerning bridge columns subjected to earthquake and has helped overcoming the severe limitations of the rigid block model presented in Chapter 3. For instance, the fiber elements capable of representing beams with inelastic material behavior can be used to compute the earthquake response of a slender reinforced concrete structure allowed to rock.

5 Rocking Analysis of Elastic Columns

5.1 Introduction

In Chapter 3, the behavior of a free standing rigid block subjected to earthquake ground motion was studied. It was shown that the rocking impacts can radiate energy. Furthermore, the frequency of rocking varies with the amplitude. Since the rocking motion changes the dynamic response, a rocking structure is unlikely to resonate. Over the last decade, many researchers focused on rocking mechanism for large structures subjected to earthquake. Kwan and Billington designed bridge columns with a rocking footing in [20] and [21]. M. Garlock et al. [13] designed a self-centering steel frame capable of rocking. Finally, Eatherton et al. [8] studied the behavior of a shear wall allowed to rock with a post-tensioning cable and a custom dissipation device.

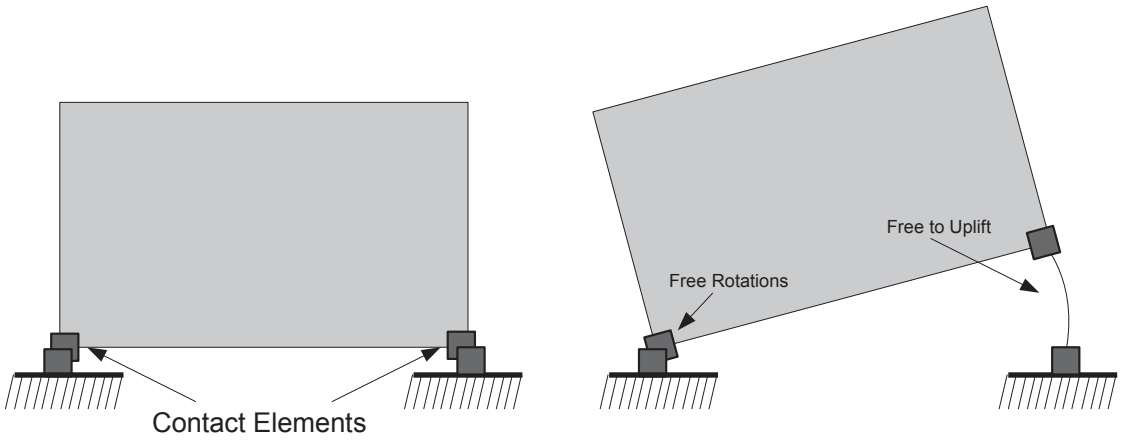

Figure 50: Common Model Configuration for a Rocking Frame

It is important to note that rocking walls are modeled with a different element from the one presented in Chapter 4. A contact element is added at each end of the wall, as shown in Figure 50. When the element is in tension, the two nodes can freely move apart but, when the element is in compression, the distance between the two nodes is set to zero. Such element also prevents slipping. It allows free rotation such that the structure can be uplifted when there is contact on only one node. The wall itself can be modeled with shell elements or with an assembly of frame and truss elements. The structure can be subjected to rocking

only if at least two nodes of the frame are connected to the footing with this contact element. But for slender structures such as bridges, the columns are modeled with frame elements. Therefore, the column and the footing are bonded with only one node, preventing the use of contact elements described above. This is when the rocking element presented in Chapter 4 can be used.

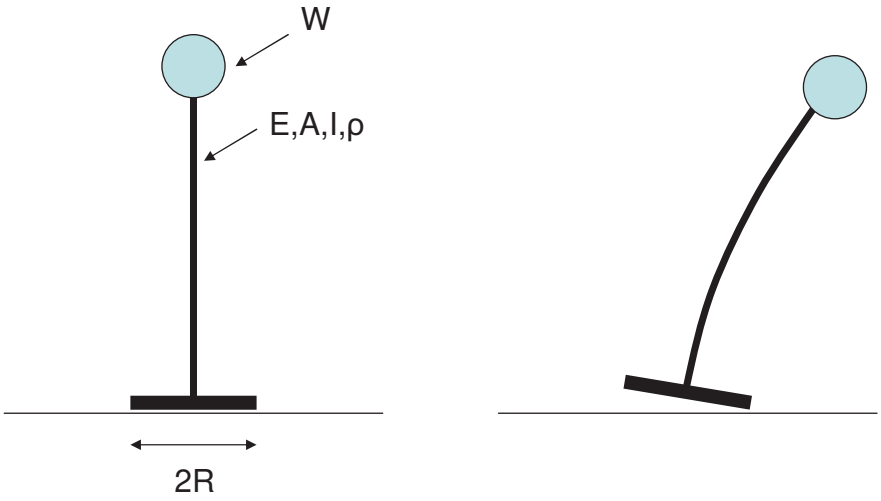

Figure 51: Elastic Column With a Lumped Mass and a Rocking Base

5.2 Rocking-Bending Interaction

Figure 51 represents a deformable column with a distributed mass and a lumped mass at the top. The base of the column is allowed to rock. The column consists of a $400mm$x$400mm$ square steel tube with $12mm$ wall. The structure properties are presented in Table 3. In this Chapter, the Young's Modulus E_s is scaled extensively in order to emphasize the influence of column stiffness on the structure response.

The structure was chosen such that, even without rocking, very large inertia forces are expected. The first mode of the structure has a natural period of $T_n = 0.315sec$. Figure 52 represents the Pseudo-Acceleration Response Spectrum of the considered earthquake. It shows that the acceleration of the mass (that is lumped at the top of the column) would be large for a SDOF system, responding with column oscillatory bending.

Column	Height h	=	$6m$
	Young's Modulus E_s	=	$200GPa$
	Cross Section Area A	=	$18,624mm^2$
	Cross Section Inertia I	=	$4.677e8mm^4$
	Linear Density ρ	=	$96.7kg/m$
Lumped mass	Mass	=	$3000kg$
Footing	Rocking Radius	=	$1m$

Table 3: Model properties

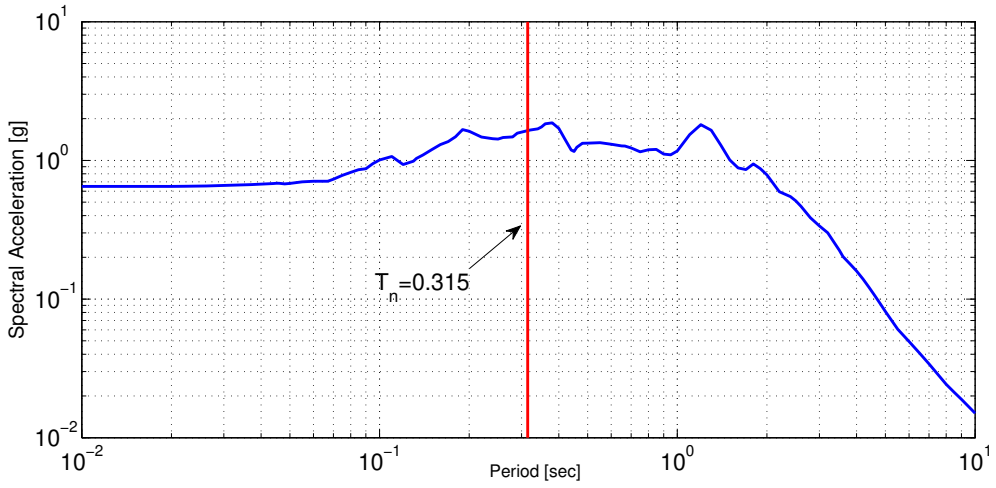

Figure 52: Unscaled Pseudo-Acceleration Response Specrum With 2% Damping - Kobe EQ(1995) - Takatori Record - Longitudinal

Figure 53 represents the horizontal acceleration of the lumped mass. It was obtained by a time history analysis of the structure when rocking is prevented. The damping matrix was built such that the first mode has a 2% damping. The result is in accordance with the Pseudo-Acceleration Response Spectrum (Figure 52).

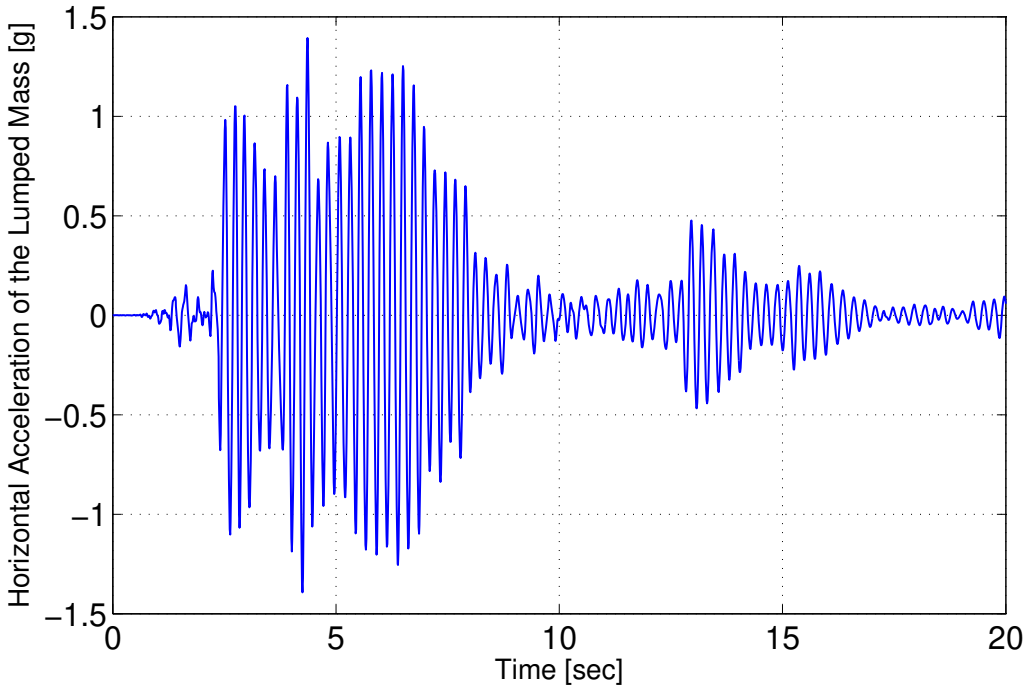

Figure 53: Acceleration Response of the structure subjected to Kobe (1995)

This column-mass structure represents an elastic column predominantly excited in its first mode when subjected to the Kobe earthquake. A first computation is performed with a clamped base (no rocking) and a second computation is performed with a rocking base and a rigid column. Figure 54 shows the results obtained. The oscillation period of the rocking column is much longer than the oscillation period of the elastic column.

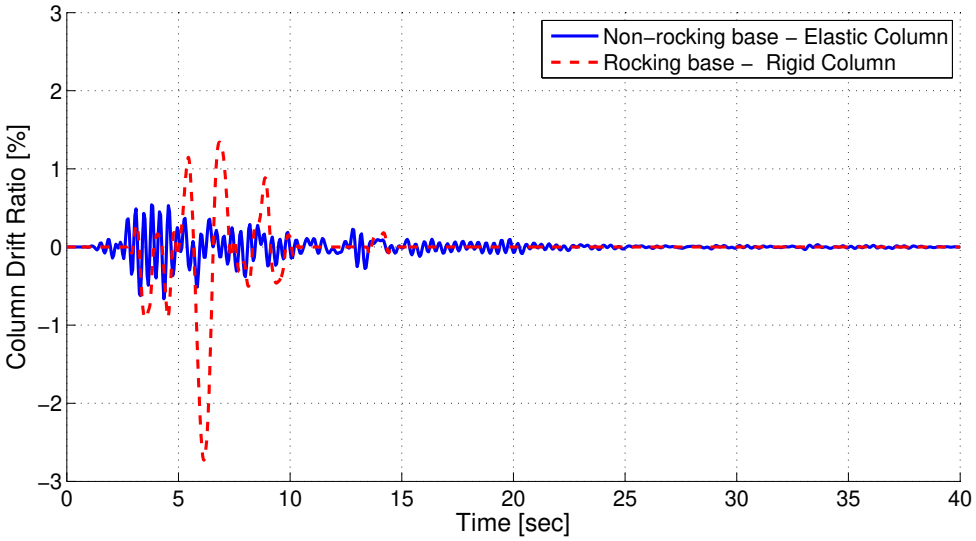

Figure 54: Displacement Response of a Clamped Elastic Column and a Rocking Rigid Column - Kobe (1995)

Currently, the rocking behavior is represented by a rigid block model, as presented in Chapter 3. Hence the interaction between the rocking rotation and the elastic deformations can not be computed. The rocking element presented in Chapter 4 can represent such interaction. It is proposed here to focus on the importance of such interaction in order to be able to judge if it can further be neglected. Figure 55 represents the rocking base rotations of a rigid column and of an elastic column. Both columns, detailed in Table 3, were allowed to rock and they both had the same rocking base. The base rotation of the elastic column is slightly less than the base rotation of the rigid column. Furthermore, the number of rocking impacts is greatly reduced for the elastic column. For the elastic column, the kinetic energy accumulated while the column was returning to its initial position is partially transformed in bending energy. Hence the rocking rotations are reduced when the column is elastic and rocking is more likely to be interrupted.

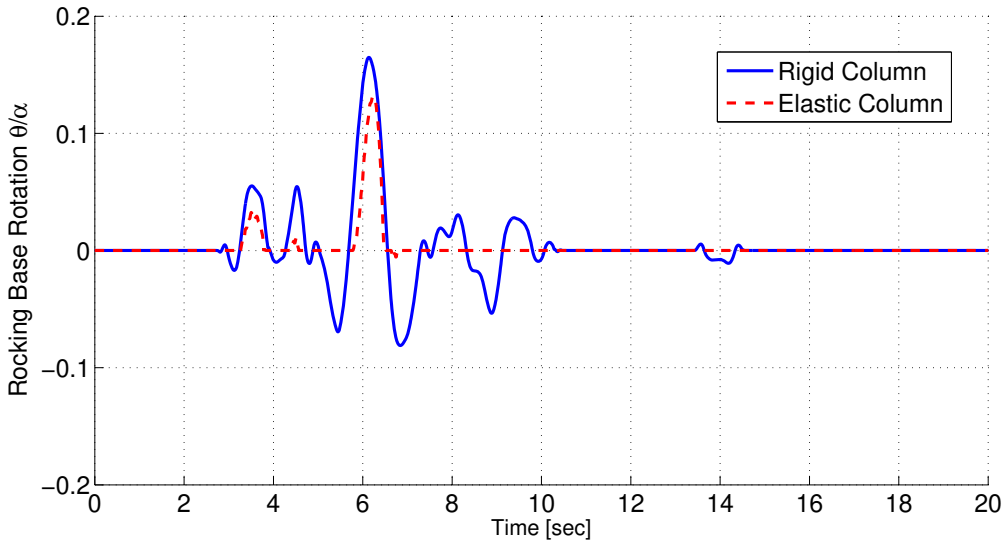

Figure 55: Base Rotations of a Rigid Column and an Elastic Column When Subjected to Kobe EQ(1995)

5.3 Damping

In Chapter 4, the rigid block is replaced with a very stiff elastic column in order to compare the results with the rigid block model. The impact generates a fast shock wave as well as high-frequency numerical noise in the angular velocity. The HHT integration scheme was chosen in order to filter out these high frequencies. The integration scheme reduces the noise in the high-frequency range. Such technique is considered to be a numerical trick, whereas viscous damping is oftentimes considered more realistic; such statement, however, is arguable since the viscous damping is usually built with respect to the global response of a structure and has nothing to do with material properties. Therefore, both can be considered as a convenient numerical tool and they do not model a physical property of the model. It is proposed here to study the viscous damping calibration for a free rocking column.

Equation 33 represents the Rayleigh damping matrix. The parameters a_0 and a_1 are calibrated to match given damping ratios of the first two modes of the structure [5].

$$C = a_0 \cdot M + a_1 \cdot K \tag{33}$$

At first, a damping matrix proportional to the mass matrix will be computed. A column subjected to free rocking rotation is modeled. Its properties are summarized in Table 3, but the Young Modulus is equal to $10E_s$. The modal analysis must be performed at rest because, if the rocking element is active, the first mode is complex. So the displacement vector is set to zero and the rocking surface is inactive. It is equivalent to a modal analysis of a clamped column. The parameter a_0 is chosen such that the first mode of the column has a damping ratio of 2%. Figure 56 shows the result obtained. The period of rocking is significantly longer than the period of the undamped system. Since the masses are lumped at the nodes, the mass matrix and the damping matrix are diagonal. Hence, if the structure undergoes rigid body motion, the mass-proportional damping matrix will damp it. Such issue is often encountered in contact mechanics. When a deformable object is subjected to very large rigid body displacements, this motion must be undamped in order to remain realistic. Therefore, a mass-proportional damping matrix is not suitable for the problem studied here.

A stiffness proportional matrix is now considered. The parameter a_1 is chosen to damp the first mode of the non-rocking structure with a damping ratio of 2%. Note that the constraints within the rocking element are approximated with a penalty factor and added to the stiffness matrix. This penalty factor must not contribute to the damping matrix otherwise, the kinematic constraints would be severely damped. Even though the rocking element contributes to the stiffness matrix, it must be noted that this contribution is due to the numerical strategy chosen to handle the constraints (penalty method or *Augmented*

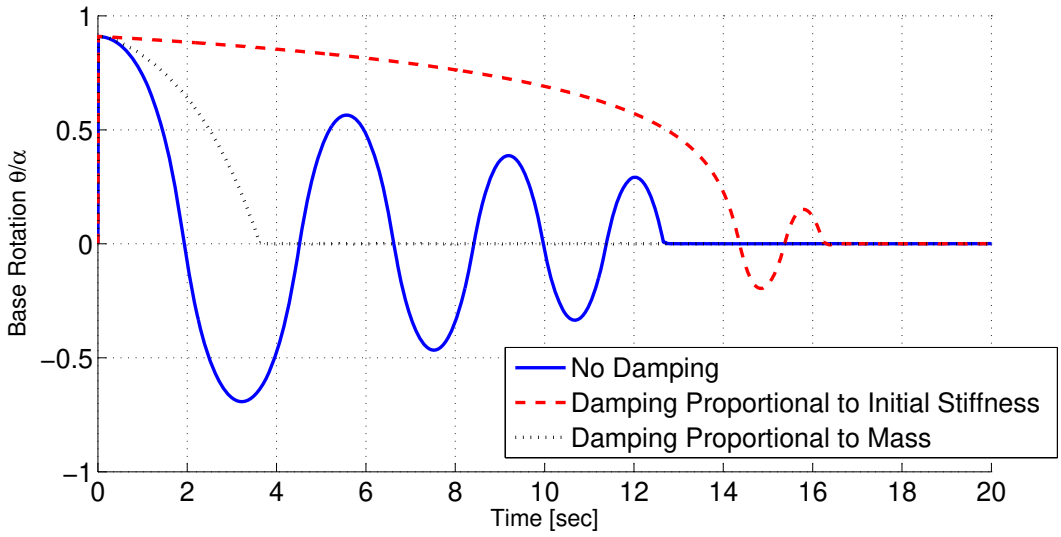

Figure 56: Free Rocking With Constant Damping Matrices

Lagrangian). Unlike other stiffness contribution, they are not associated with material deformations but with rigid body motion, so they should not be damped. In the algorithm, the stiffness matrix is built by adding each element stiffness matrix. But to build the damping matrix, the algorithm substracts the contribution of the rocking element from the stiffness matrix before computing Equation 33. Figure 56 shows the result obtained. The rocking period is extremely longer than the rocking period of the undamped system. Thus, this damping matrix is also not adequate. It was chosen to be proportional to the stiffness matrix, but this stiffness matrix is constantly updated to respect the corotational transformations, whereas the damping matrix remains constant. Here, the rigid body motion is again disturbed by the damping matrix. In order to avoid such issue, the damping matrix must also be updated. The parameter a_1 remains constant but, for each increment and for each iteration, the damping matrix is now updated proportionally to the stiffness matrix. Again, the contribution of the rocking element to the stiffness matrix is substracted because it is associated with rigid body motion. Figure 57 represents the solution obtained.

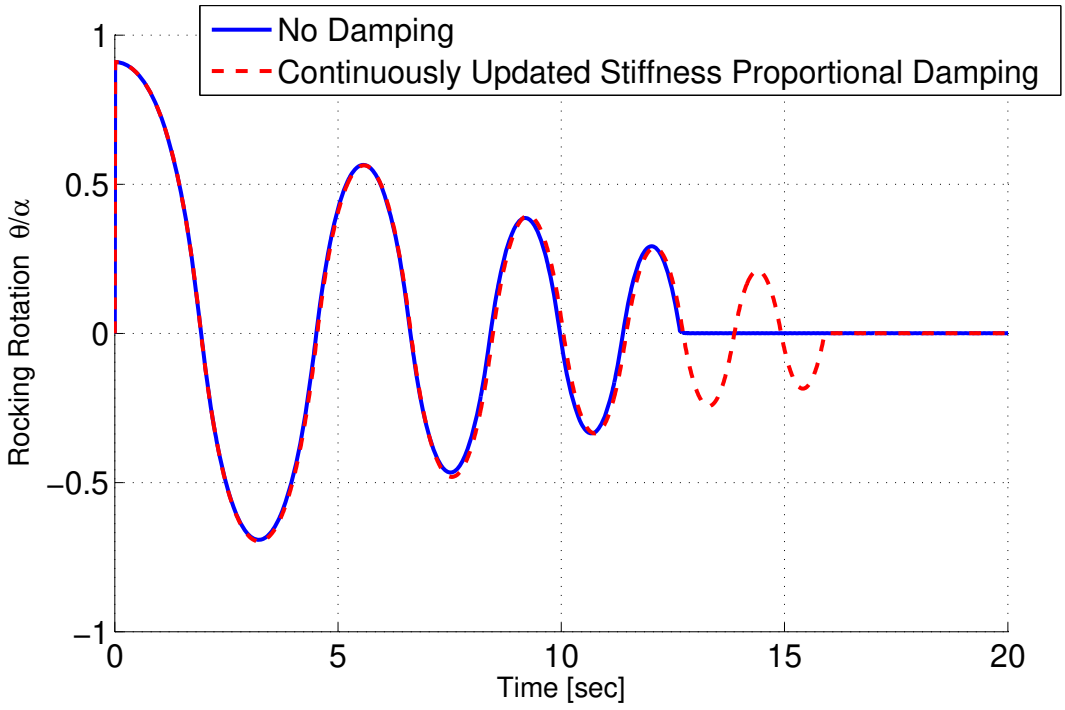

Figure 57: Free Rocking With an Updated Damping Matrix

The updated stiffness-proportional damping matrix does not disturb the free rocking motion. The solution is now realistic and the column can damp the shock waves generated at each impact an updated damping matrix can cause other issues, especially when it is used with non-elastic materials. In fact, if the material softens, the damping matrix may not be positive definite instead of being damped, some frequencies can be amplified and lead to numerical instability.

In this thesis, the rocking element is intended to be used with large structures subjected to earthqake excitation. Furthermore, these structures are restrained with unbonded post-tensioned cables to reduce the rocking amplitude. Therefore, the rigid body motions should be less important than the rigid body motions observed during free rocking tests. Hence a more simple mass proportional damping matrix could be sufficient. In order to confirm this assumption, the response of a cable-restrained column was performed. The column properties are summarized in Table 3 but, again, the Young modulus is set to $10E_s$. The column is restrained with a steel cable ($EA_{cable} = 200e6N$, no initial prestress). Such properties are close to those later used in Chapter 7, in which design of bridges is being considered. The

damping matrix is calibrated such that the first mode of the structure at rest has a damping ratio of 2%. Figure 58 represents the rocking rotation of the column when subjected to Kobe earthquake.

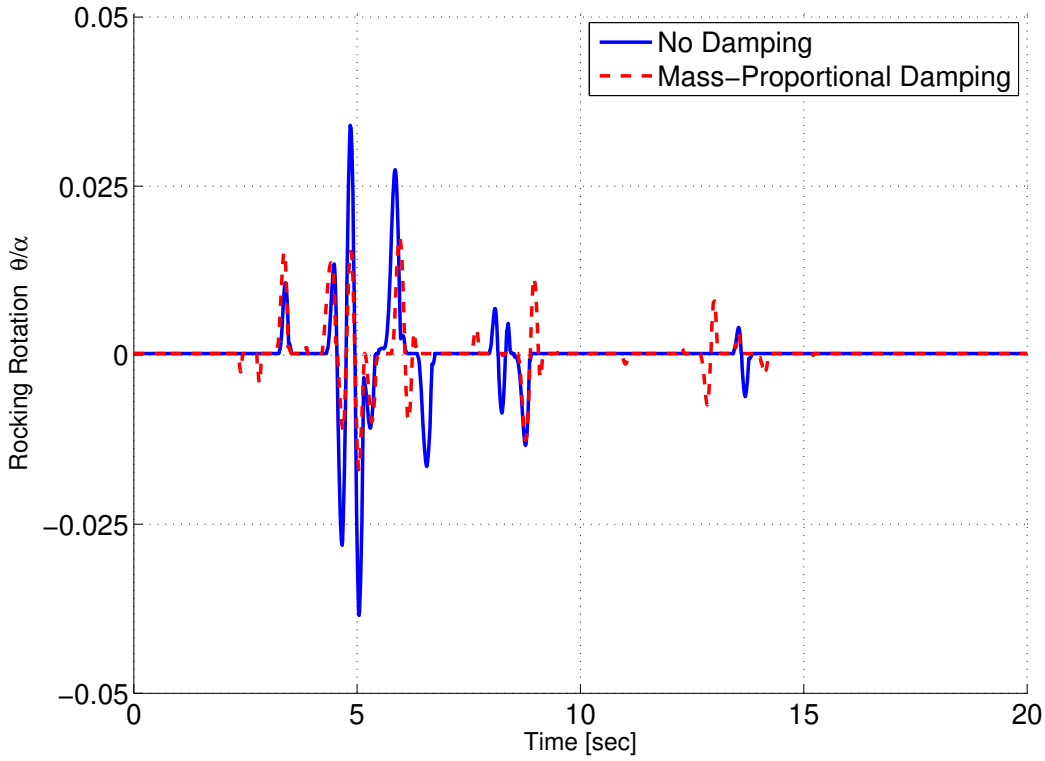

Figure 58: Rocking Rotation of a Cable Restrained Cantilever Column - Kobe EQ (1995)

A shown in Figure 58, even for an earthquake excitation, the mass-proportional matrix significantly changes the results. The rotation period is longer than the first harmonic period of the structure used to calibrate the damping matrix. Hence even though the rocking rotations remain small, they are severely damped.

The use of a continuously updated stiffness-proportional damping matrix was also investigated but, as explained earlier, this type of damping matrix can be non positive-definite and generate numerical instability. Indeed, with such damping matrix, the algorithm failed to converge for this example.

Although viscous damping is used in structural engineering to represent the energy dissipation of a structure, if this energy dissipation was only viscous, then a factor associated with the strain rate $\dot{\epsilon}$ could be specified for a given material. Instead, the Rayleigh damping matrix is calibrated based on the first few modes of the entire structure; hence a_1 is defined for a given structure and not for a given material. Therefore, viscous damping is calibrated using an empirical approach. It is proven to be very convenient for most structural engineering applications but, since it is not founded on physical ground, its reliability must be verified for each application. In order to limit the elastic oscillations of large deformable structures, viscous damping is essential. In Chapter 6 and Chapter 7 a 2% mass-proportional viscous damping was used. This damping matrix is necessary to damp the elastic oscillations, but it must be noted that, when the rocking rotations become very large, the damping will generate inaccurate results.

5.4 The effect of elastic deformations on rocking behavior

In Chapter 3, it was shown that, when a rigid block rocks, some energy is lost during impact. This energy must be dissipated in order to respect the conservation of angular momentum, hence the rigid block is assumed to be capable of absorbing it during the impact. This model, presented by Housner in 1963 [16], is now used in most papers to describe rocking behavior. It is very useful to represent stiff objects such as equipment or large construction blocks [37]. Indeed, the harmonic oscillations generated by the impact are much faster than the rocking oscillations, hence the shock wave is quickly damped and elastic deformations are negligible. But the behavior of a free rocking elastic column with a lumped mass may be different. Such column may undergo very large elastic deformations, hence their combined rocking and flexural motion may be complex.

In order to observe the effect of elasticity, three columns are modeled. The columns have the properties described in Table 3, but each one has a different Young modulus: E_s, $10E_s$ and $15E_s$. All three columns are undergoing free rocking motion with the same initial angle. There is no viscous damping and the HHT parameter is set to $\alpha = -1/12$ in order to preserve the high frequencies oscillations. In fact, when α tends to zero, the HHT integration scheme does no longer filter out the high frequencies, when $\alpha = -1/12$, it may compromise the stability but, in this example, it is essential to capture accurately the column's bending oscillations. In the other examples studied in this thesis, $\alpha = -1/6$ in order to favour robustness.

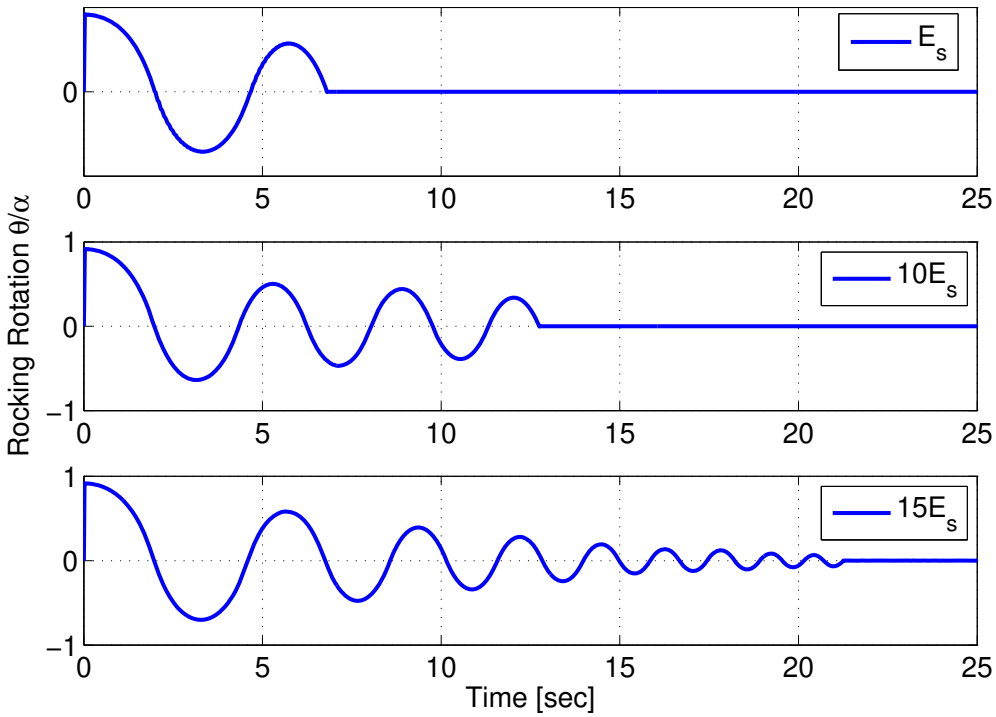

Figure 59: Free Rocking of a Column for Different Young's Moduli

Figure 59 shows the results obtained for the same initial angle with different Young moduli. It is observed that the stiffer the column, the longer it rocks. Eventually, the column is stiff enough to converge towards the rigid block solution. This is an important difference, when compared with the results obtained in Chapter 3. An elastic column rocking on a rigid surface may suddenly stop rocking. In fact, the kinetic energy due to the rocking motion is transformed into bending energy, which prevents uplift. Hence, instead of creating a rotation around the opposite corner, the column simply stops rocking. Figure 59 also shows that the period of rocking and its amplitude are the same for each column, regardless of their stiffness. It is interesting to note that a rigid column and an elastic column whose geometric properties are the same will rock the same way but that the elastic column will stop rocking whereas the rigid column will not.

Figures 60 and 61 represent the horizontal tip displacement of the column when the Young modulus is equal to respectively E_s and $10E_s$. It can be observed that, when the rocking

stops, the column oscillates. The amplitude after the rocking interruption is much smaller because there is no more rigid body motion at the base of the column. But the rocking kinetic energy leads to bending oscillations. In Figure 61, it can be noted that the bending oscillations are dissipated but not in Figure 60. This is because the bending oscillations in Figure 61 are faster and the HHT integration scheme only filters the high frequnecies.

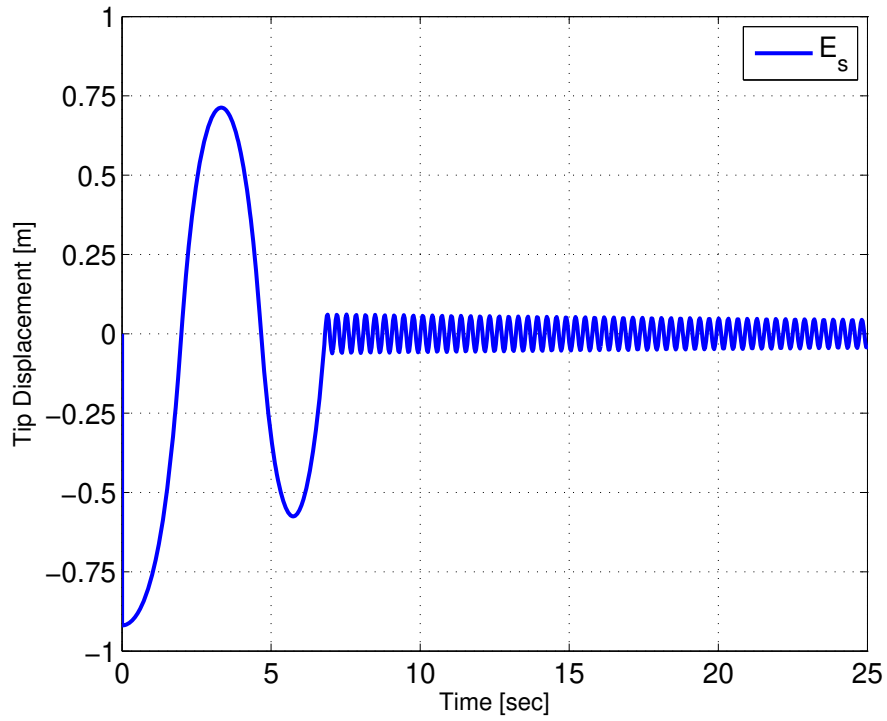

Figure 60: Tip Displacement of an Elastic Rocking Beam with Young Modulus equal to E_s

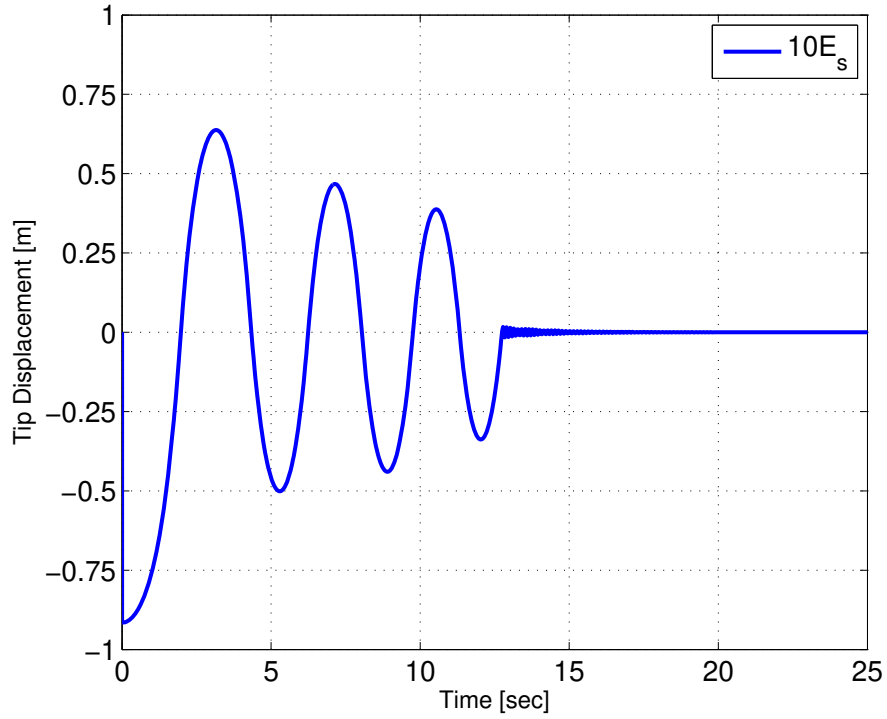

Figure 61: Tip Displacement of an Elastic Rocking Beam with Young Modulus equal to $10E_s$

It is proposed to evaluate the amplitude of the bending oscillations due to the rocking interruption. Several approximations will be made to build the simplified model. The column is modeled as an *Euler-Bernoulli* beam with linear geometry. The axial deformations are neglected and only the lumped mass is represented. Figure 62 represents the simplified model used here. The last rocking rotation observed is called θ^r_{last}. It represents the maximum rotation before the last impact; there is no angular velocity in this instance.

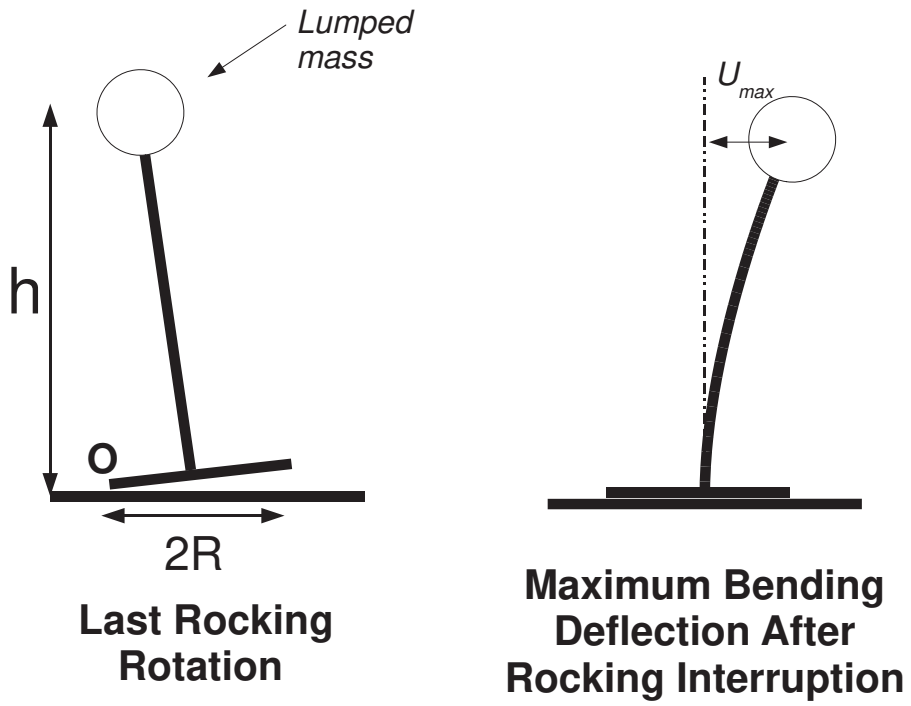

Figure 62: Simplified Model of an Elastic Rocking Beam

The column rotates around point O before impact and lands on its base. It is considered that the landing does not radiate energy, so the energy is conserved. The kinetic energy due to rocking is written in Equation 34

$$E_{rocking} = \frac{1}{2} I_0 \dot{\theta}^2_{impact} \tag{34}$$

In order to compute the angular velocity at impact $\dot{\theta}_{impact}$, the equation of motion (2) described in Chapter 3 has to be solved. It is proposed to linearize it for $(\alpha - \theta)$, as explained by Housner [16]. It gives Equation (35) with $p^2 = \frac{mg\sqrt{R^2+h^2}}{I_0}$ and α, the angle representing the aspect ratio ($\alpha = \arctan(\frac{R}{h})$).

$$\ddot{\theta} - p^2\theta = -p^2\alpha \tag{35}$$

Equation (36) is obtained by solving Equation (35) for $\theta(0) = \theta^r_{last}$ (the last rocking rotation observed) and $\dot{\theta(0)} = 0$.

$$\dot{\theta}_{impact} = -p\sqrt{\alpha^2 - (\alpha - \theta^r_{last})^2} \tag{36}$$

Combining Equation (35) and Equation (36), the rocking kinetic energy is expressed with respect to θ^r_{last} in Equation (37).

$$E_{rocking} = \frac{1}{2} I_0 p^2 (\alpha^2 - (\alpha - \theta^r_{last})^2) \tag{37}$$

It is now proposed to compute the bending energy. Equation (38) describes the deflected shape of the column. $v(x)$ represents the deflection, and the origin of x is the base of the column. This deflected shape is derived from the general *Euler-Bernouilli* beam equations, assuming that the base of the column is clamped and no moment is applied at the top. U_{max} represents the maximum bending deflection at the top of the column once rocking stops.

$$v(x) = -\frac{U_{max}}{2h^3}x^3 + \frac{3U_{max}}{2h^2}x^2 \tag{38}$$

Equation (39) represents the bending energy of the column.

$$E_{bending} = \frac{1}{2}\int_0^h EI \left(\frac{\partial^2 v}{\partial x^2}\right)^2 \mathrm{d}x \tag{39}$$

Equation 40 is obtained by solving (39) for the deflected shape given in Equation (38).

$$E_{bending} = \frac{3EI}{2h^3} U^2_{max} \tag{40}$$

Since $E_{bending} = E_{rocking}$, the maximum tip displacement U_{max} is expressed with respect to θ^r_{last} in Equation (41).

$$U_{max} = \sqrt{\frac{h^3}{3EI} mg\sqrt{R^2 + h^2}(\alpha^2 - (\alpha - \theta^r_{last})^2)} \tag{41}$$

In order to confirm that the rocking interruption observed in this chapter can be explained with this simplified model, the maximum tip displacement observed after the rocking interruption is compared with the estimated tip displacement obtained with this model.

	θ^r_{ini} [rad]	Estimated U_{max} [m]	Observed U_{max} [m]	Error
E_sI	0.094	$5.53e-2$	$6.02e-2$	8.1%
$10E_sI$	0.056	$1.45e-2$	$1.59e-2$	8.8%
$15E_sI$	0.011	$5.7e-3$	$5.0e-3$	14%

Table 4: Comparison of the rocking-elastic transition results with the simplified model

5.5 Conclusion

In this chapter, the behavior of an elastic beam subjected to rocking was studied. The rocking element presented in Chapter 4 allows to represent an elastic beam rocking on its base. It was shown that, when an elastic column subjected to an earthquake rocks, it behaves differently from a rigid block (Figure 55).

Viscous damping was discussed in Section 5.3. It was shown that, if the damping matrix is proportional to the mass matrix or to the initial tangent stiffness matrix, the rocking motion is severely damped and become unrealistic. This is particularly true for very large rocking rotation. Only a continuously updated stiffness-proportional damping matrix can properly represent the rocking behavior of a column. But such matrix can lead to numerical instability and should be avoided for complicate problems. Hence it was decided to use a mass-proportional damping matrix but only if the rocking rotations remain small. This is usually the case for structures subjected to an earthquake and equipped with a restraining cable. A mass-proportional damping matrix, however, is not suitable to compute the problems with a large initial rotation such as a free rocking block.

At last, the rocking interruption due to column bending was discussed. It was observed that, when columns are tilted and allowed to rock freely, the stiffer columns will rock longer. A softer column will land and the rocking kinetic energy will lead to column bending. A simplified model of the rocking column was presented in order to explain how the rocking interruption affects the column bending.

6 Behavior of Bridge Columns Allowed to Rock

6.1 Introduction

Previous Chapter showed that deformable columns may have a different rocking behavior than rigid blocks presented in Chapter 3. The behavior under earthquake excitation was greatly influenced by the material deformations, and the column's elasticity caused rocking termination. In this chapter it is proposed to study the influence of inelastic material deformations on the rocking behavior of a cantilever column. Figure 63 represents the system configuration. The geometric and material properties are summarized in Table 5. The column supports a large lumped mass and is free to rock at its base. The column material is elastic, except in Section 6.3 where the column is elastic-perfectly plastic. A 2% mass-proportional viscous damping is modeled. It is restrained with an unbonded post-tensioning cable that is anchored to the column at $2m$ high and not at the top. It was shown in Section 3.6 that using a shorter cable can reduce the rocking rotations without increasing the cable diameter. However in this configuration the cable may undergo very large strains.

Column	Height h	=	$12m$
	Axial Stiffness EA	=	$2.5e8kN$
	Flexural Stiffness EI	=	$2.0e8kN \cdot m^2$
	Linear Density ρ	=	$20,900kg/m$
	Damping Ratio ζ	=	2%
Restraining Cable	Young's Modulus E_s	=	$200GPa$
	Cross Section Area A_f	=	$2,000mm^2$
	Cable Length L_{cable}	=	$2m$
	Prestressing Force q_0	=	$2000kN$
Lumped mass	Mass	=	$100,000kg$
Footing	Rocking Surface Width	=	$3m$

Table 5: Model properties of the Rocking Column With a Short PT Cable

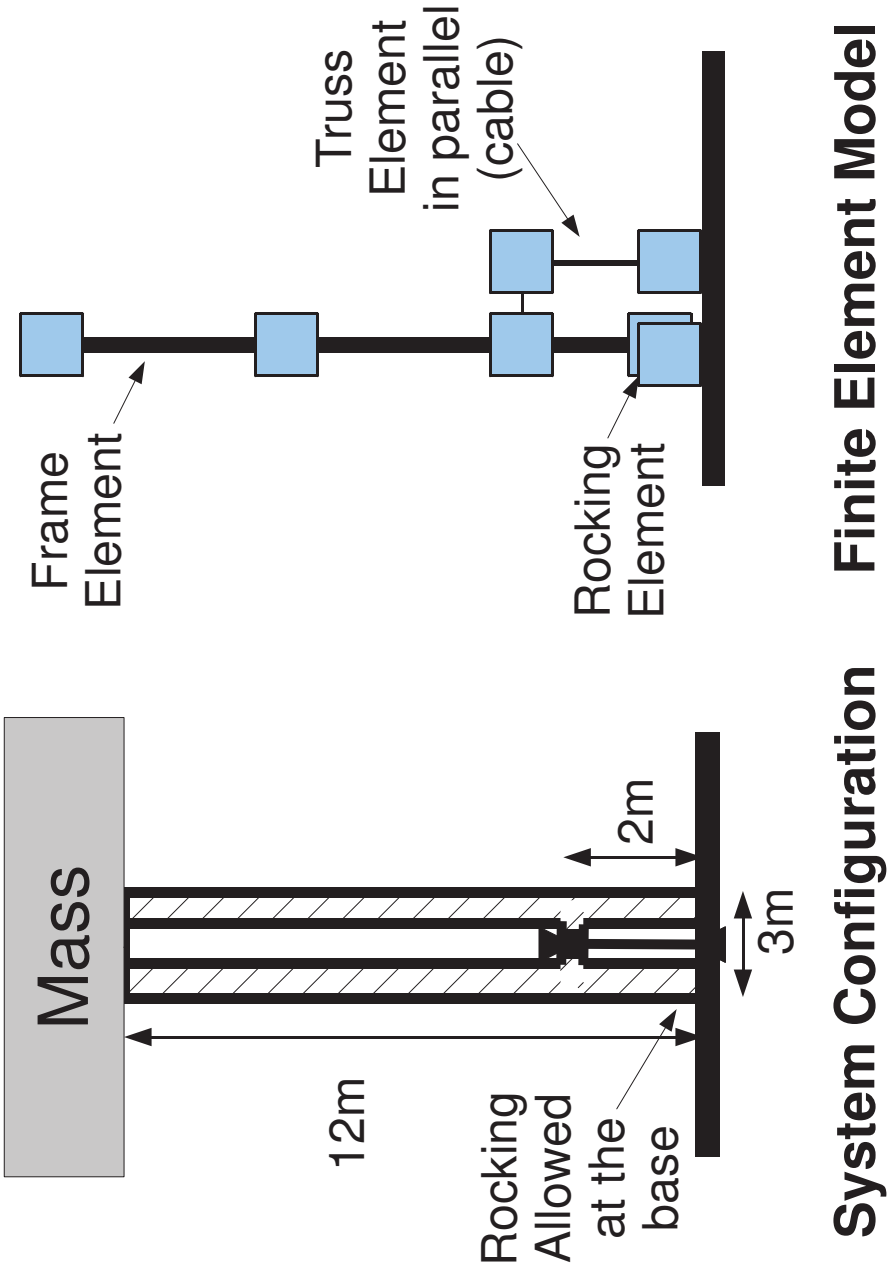

Figure 63: Cantilever Column with a Short Restraining Cable

It is first proposed to study the consequences of a failure of the post-tensioning cable. The purpose of this cable is to limit the rocking rotations, hence if it fails the structure may overturn. This cable is then replaced with a post-tensioning tie-rod. A cable may undergo brittle failure, but a tie-rod can withstand moderate plastic deformations. However, as the tie-rod yields the initial prestressing force will be reduced hence the column may also overturn.

Secondly, the yielding of the column is studied. As a cantilever column rocks, it may exceed its plastic capacity and a plastic hinge will form at the base. This plastic hinge will dissipate energy so it may reduce the rocking rotation. But it will also lead to a larger drift of the lumped mass and may cause the structure to collapse.

Finally, the use of a dissipative fuse connecting the base of the column to the footing is discussed. It consists of a mild-steel rod located along the neutral axis of the column. It can withstand very large plastic deformations in tension and compression. Hence it may help to restrain the rocking rotations and prevent damage of the rest of the structure.

6.2 Yielding and Failure of the Restraining Cable

In this section it is proposed to study the consequences of a cable failure while the structure is rocking. It is impossible to represent the moment-rotation relationship of the rocking element because it is not governed by a material constitutive law but by kinematic constraints as explained in 4.2. So instead, Figure 64 represents the restoring moment of the entire structure versus the rocking rotation, assuming that the structure is rigid. It represents the relationship described in Equation (42), which is derived from the post-tensioned rigid blocks analysis performed in Section 3.4.1. But in this case the slenderness angle of the structure $\alpha = \arctan(\frac{R}{h})$ is dissociated from the angle $\alpha_{cable}\arctan(\frac{R}{h_{cable}})$, where h is the height of the column, h_{cable} is the length of the cable and R is half the width of the rocking surface. m and g represent respectively, the lumped mass and the gravity constant. The other parameters η_0 and η_α correspond to restraining cable parameters as defined in Chapter 3. They are calibrated to match the cable properties of the example studied here.

$$\begin{aligned} M_r(\theta) = {} & m \cdot g \cdot \sqrt{h^2 + R^2} \cdot (\sin(sign(\theta)\alpha - \theta)) \\ & + m \cdot g \cdot \sqrt{h_{cable}^2 + R^2} \cdot (sign(\theta)\eta_0 + (\eta_{alpha} - \eta_0)\frac{\theta}{\alpha_{cable}} \sin(\alpha_{cable})) \end{aligned} \tag{42}$$

In Figure 64, the dashed red plot represents the static restoring moment of the column with a post-tensioning cable and the solid blue plot represents the static restoring moment of the structure once the cable failed. When the column is close to its initial position (i.e. θ is close to zero), the restoring moment is equal to $\pm 4,000kN \cdot m$ with the cable and $\pm 2,000kN \cdot m$ without the cable. Furthermore, without the cable the structure has a softening behavior. So based on the static analysis of this rigid model, it is expected that the cable failure will lead to very large rocking rotations and eventually overturning.

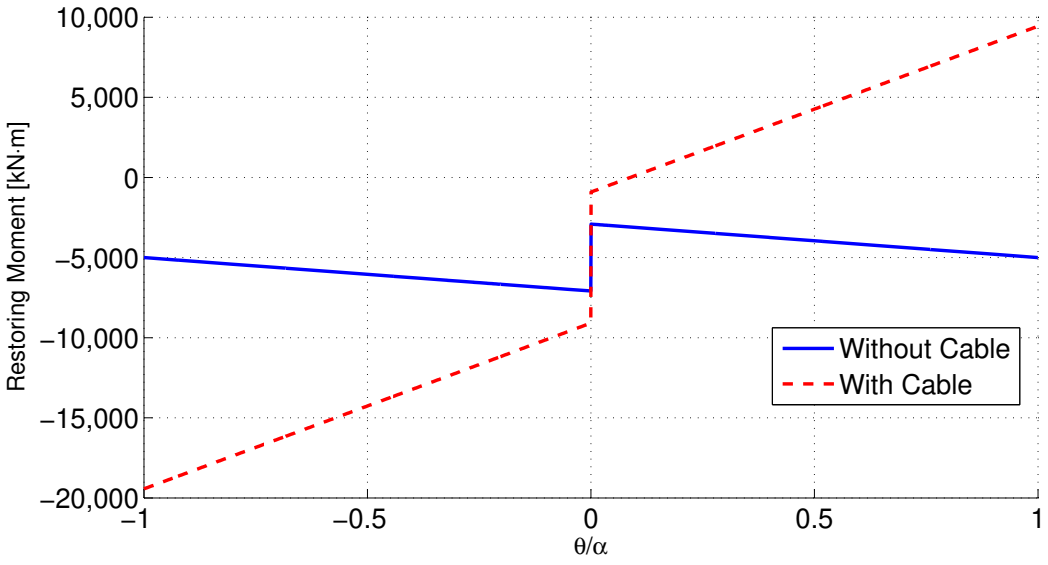

Figure 64: Static Restoring Moment versus θ for a Column assumed to be rigid

The elastic column presented in Figure 63 is now studied. The post-tensioning cable is modeled with a truss element. This element cannot be loaded in compression and it may undergo a brittle failure in tension if the stress exceeds $f_u = 1,800MPa$. The column is subjected to the Takatori station longitudinal record of the Kobe earthquake (1995).

Figure 65 represents the column's drift ratio and the cable stress. Only the first $10sec$ of the earthquake response are represented. The maximum drift ratio observed is 7.6%. But due to the viscous damping used in this model, this value is conservative. Actually, in Section 5.3 it was shown that the mass-proportional damping matrix may underestimate the rocking rotations when they are too large. So when the cable fails the column's drift ratio becomes very large and the column stability may not be preserved.

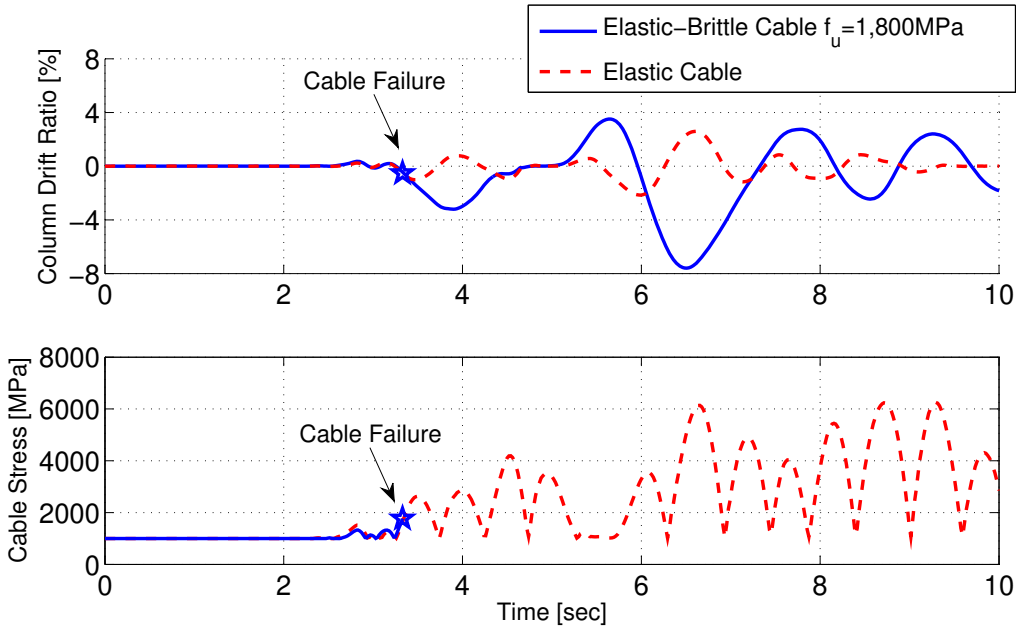

Figure 65: Drift Ratio of the Column and PT stress with Brittle Cable Failure $f_u = 1,800MPa$ - Kobe EQ (1995)

Figure 66 represents the resisting moment at the base of the column with an elastic cable and an elastic-brittle cable. The resisting moment is larger when the cable remains elastic, as expected based on the rigid block behavior presented in Figure 64. It can also be noted that once the cable failed, (solid blue plot), the resisting moment oscillates between $\pm 1,920 kN \cdot m$, which is also consistent with the rigid block behavior presented in Figure 64. However, when the column impacts on the footing, it causes the resisting moment to exceed $10,000 kN \cdot m$. Once the cable has failed, the rocking rotations are larger, so the impacts are also much more severe.

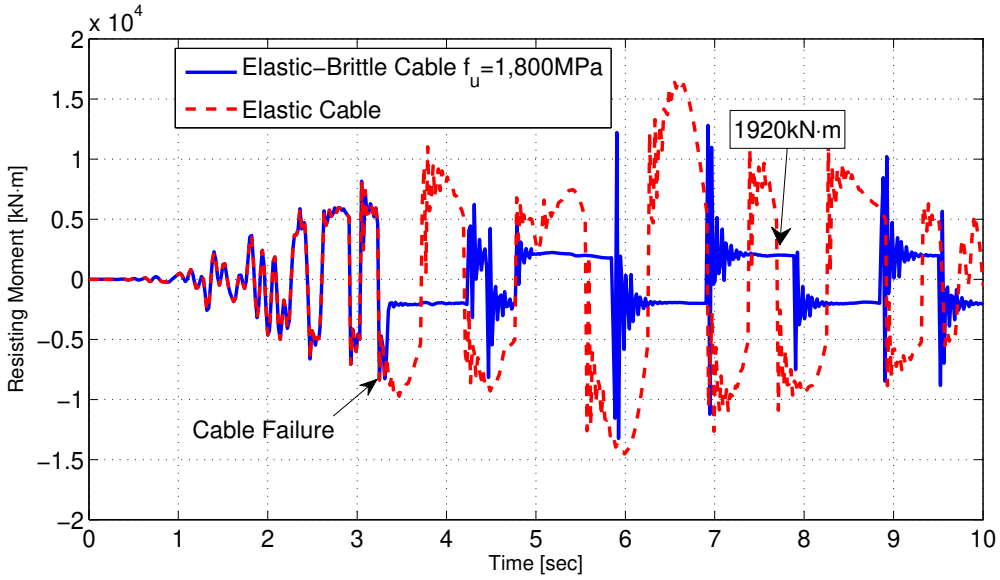

Figure 66: Resisting Moment at the base of the Column with Brittle Cable Failure $f_u = 1,800 MPa$ - Kobe EQ (1995)

It is proposed to replace the post-tensioning cable with a tie-rod of the same diameter. This tie-rod (often called *Dywidag bar* in the industry) has an elastic limit $f_y = 1,200MPa$ [7]. It consists of a solid steel section rod with the same Young modulus than a PT cable ($E_s = 200GPa$). It cannot be loaded in compression but it can withstand moderate plastic deformations in tension. So the elastic-brittle truss element representing the cable is replaced with an elastic-perfectly plastic truss element. This element has no resisting force when loaded in compression.

Figure 67 shows the structure's response with an elastic-perfectly plastic tie-rod when it is subjected to Kobe earthquake. Only the first $10sec$ of the earthquake response are represented. It shows that the prestressing force of the tie-rod is entirely lost at time $t = 5sec$. Therefore, the column's drift ratio is larger than the column equipped with an elastic cable. The plastic elongation of the tie-rod increases only if the column's drift ratio exceeds the maximum amplitude observed at previous time steps. Eventually, the plastic strain of the tie-rod reaches 4%, and it does no longer restrain the rocking rotations. The column's maximum drift ratio is 215% higher than the maximum drift ratio of the column equipped with an elastic cable.

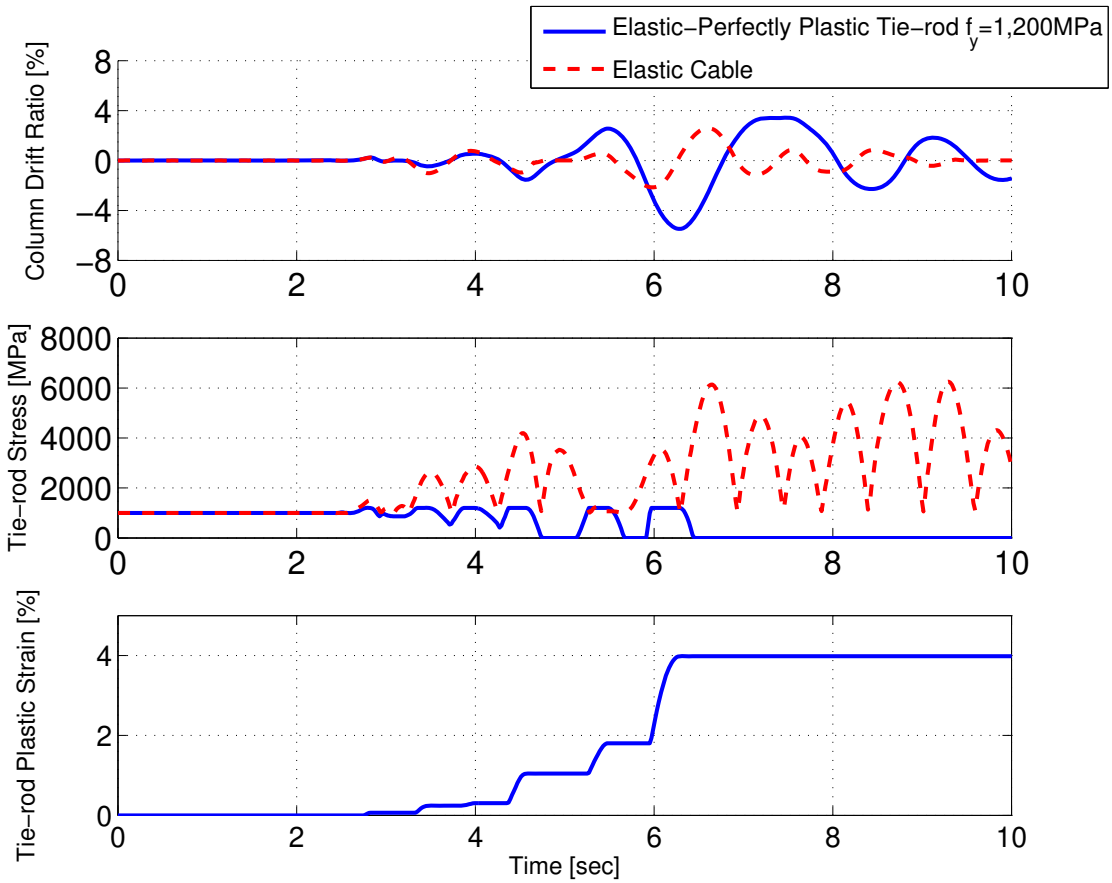

Figure 67: Drift Ratio of the Column and PT stress with Elastic-Perfectly Plastic Tie-rod $f_y = 1,200MPa$ - Kobe EQ (1995)

Figure 68 represents the resisting moment at the base of the column with an elastic cable and with an elastic-perfectly plastic tie-rod. Due to the very large rocking rotations, the column equipped with a tie-rod undergoes very large impacts resulting in moment shock waves. After $t = 7sec$, the resisting moment between impacts is close to the restoring moment of the rigid model ($\pm 2,000kN \cdot m$) observed in Figure 64. So it confirms that once the tie-rod has severely yielded, it does no longer restrain the rocking rotation and becomes ineffective.

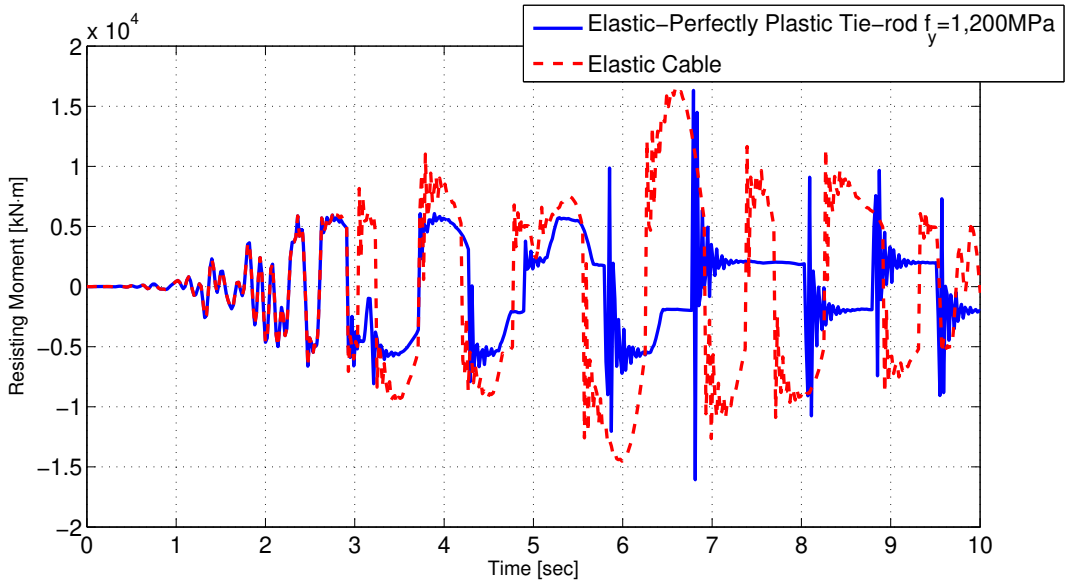

Figure 68: Resisting Moment at the base of the Column with Elastic-Perfectly Plastic Tie-rod $f_y = 1,200MPa$ - Kobe EQ (1995)

So in order to preserve the integrity of the structure, the post-tensioning cable should remain elastic. It was shown that when the column is equipped with an elastic cable, the cable stress exceeded $6,000MPa$. But the best PT cables available in the industry are rated for only $1,800MPa$. So a longer cable should be used in order to limit the maximum strain (and therefore the maximum stress), and the cable diameter should be increased adequately to preserve its stiffness.

6.3 Elastic-Perfectly Plastic Column

In this section, it is proposed to study the rocking behavior of a column when a plastic hinge forms at its base. The column configuration presented in Figure 63 is modeled. The properties of the structure are presented in Table 5. The PT cable is assumed to remain elastic. The column's axial and shear deformations are elastic, but flexure deformations are elastic-perfectly plastic. The plastic capacity of the column is $M_p = 6,000kN \cdot m$. Since the moment is maximum at the base of the column, it is expected that a plastic hinge will form as described in Figure 69.

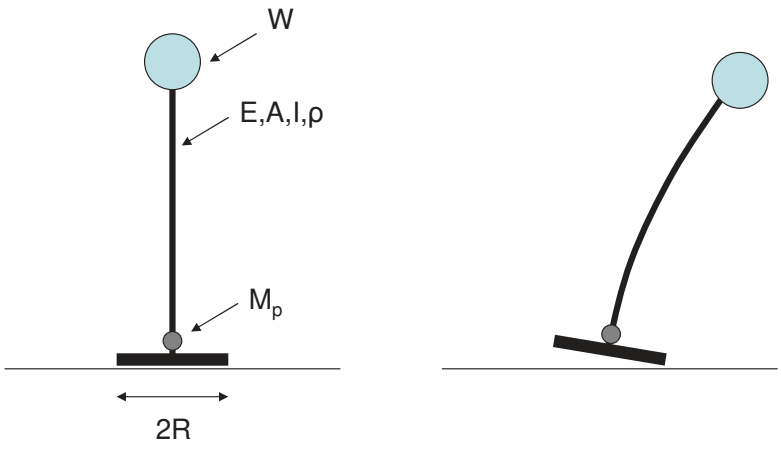

Figure 69: Elastic Column With a Lumped Mass, a Plastic Hinge and a Rocking Base

Figure 70 represents the column drift ratio and the rocking rotation at the base of the column for an elastic column and for an elastic-plastic column. First it can be noted that the rocking rotations are greatly reduced when a plastic hinge forms at the base (dashed red plot). Figure 71 represents the resisting moment at the base of the column. As expected, the resisting moment of the elastic-plastic column (dashed red plot) never exceeds $M_p = 6,000kN \cdot m$. Otherwise both plots are very similar, and the plastic hinge does not seem to affect the pattern of the rocking impacts during the earthquake.

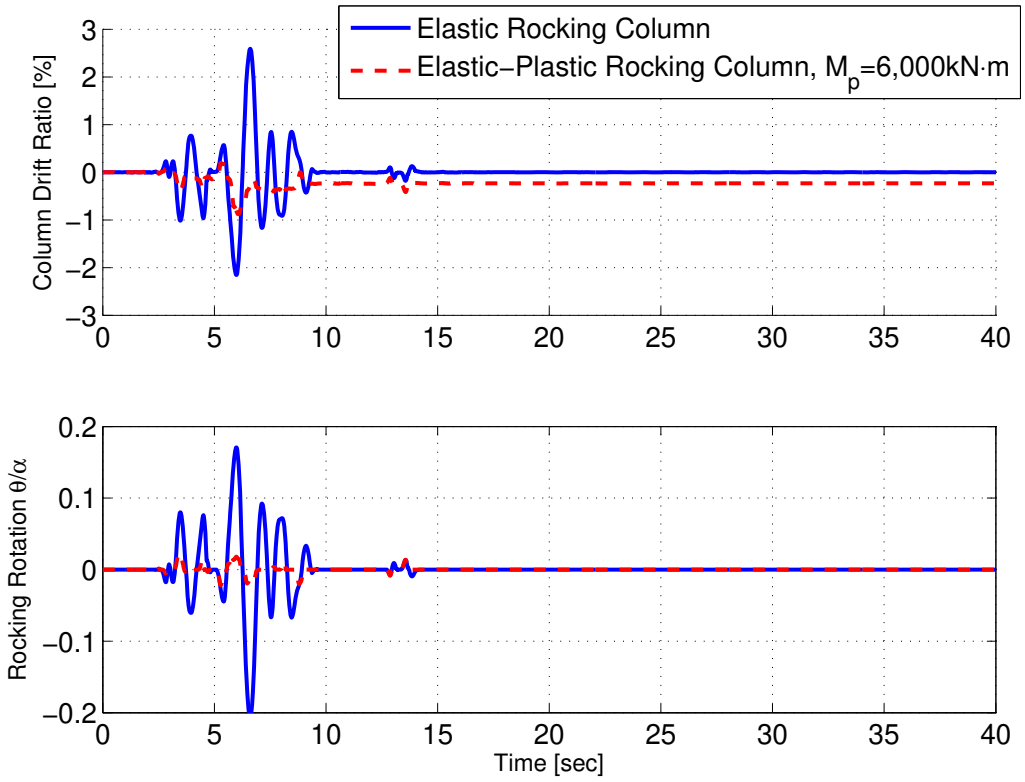

Figure 70: Column Drift Ratio and Rocking Rotation for an Elastic Column and an Elastic-Perfectly Plastic Column - Kobe EQ (1995)

As the rocking rotation increases, the resisting moment at the base of the column also increases because of the PT cable elongation. Eventually, the resisting moment at the base of the column reaches the plastic capacity M_p, the rocking rotation is bounded and only

plastic rotation can occur. As a consequence, in the bottom plot of Figure 70, it can be observed that the rocking rotation of the elastic-plastic column cannot exceed $\theta = 0.022\alpha$.

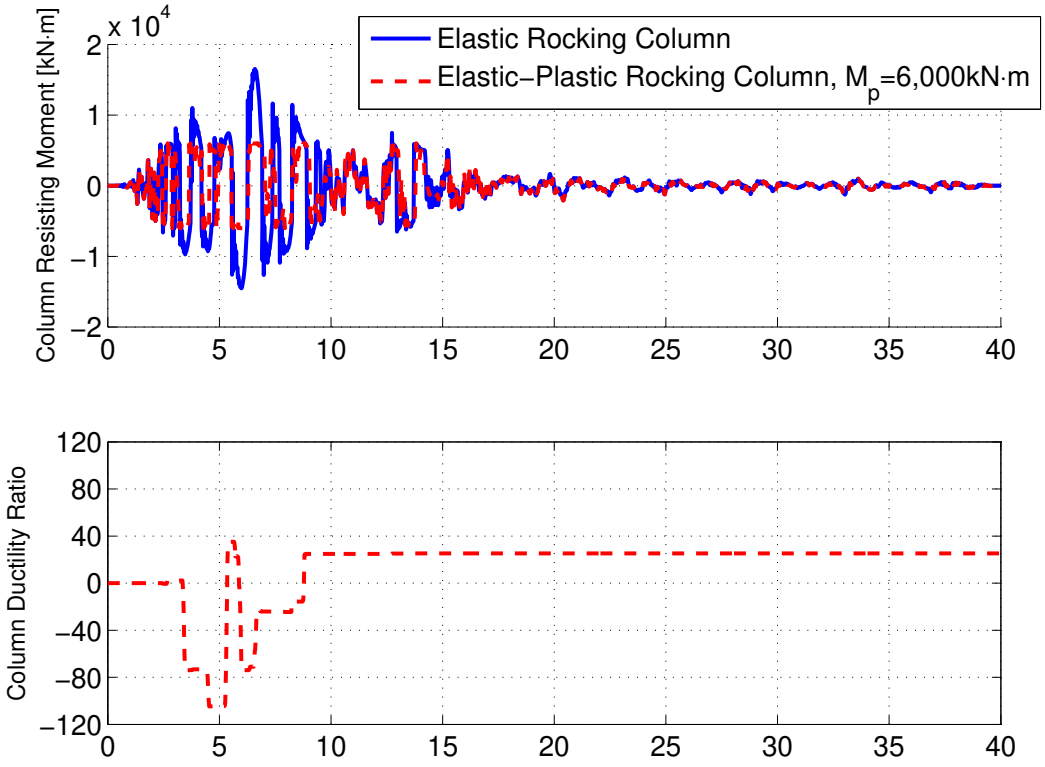

Figure 71: Resisting Moment at the Base of the Column and Plastic Hinge Rotation for an Elastic Column and an Elastic-Perfectly Plastic Column - Kobe EQ (1995)

The bottom plot in Figure 71 represents the plastic hinge ductility ratio of the column, i.e. the plastic rotation over its maximum elastic rotation. The maximum ductility ratio is equal to 105. Despite the very large amount of rocking oscillations, the sign of the plastic rotations changes only 3 times during the earthquake. So the column yields only for very large rocking rotations, when the PT cable has elongated significantly.

The plastic hinge also dissipates the shock waves observed during the impacts. It was shown in Chapter 3 that squat blocks radiate more energy during rocking impact than slender

blocks. Since this column is slender (aspect ratio of 8), the energy radiated by the rocking impacts is small. Therefore, when a rocking impact occur, the column yields but the plastic rotation does not change significantly.

Overall, the plastic hinge greatly reduces the column's drift ratio. However, a strong limitation of the model must be noted. When the plastic hinge forms at the base of the column, the properties of the rocking element remain unchanged. But in practice, when a column yields at its base, the local damage may change the rocking properties. This damage may simply lead to a reduction of the rocking radius, or it may change the shape of the rocking surface and cause rolling. Damage on the rocking surface is not investigated in this thesis and is left for further research.

6.4 Rocking Column with a PT Cable and a Dissipative Fuse

It was shown that a PT cable can limit the rocking rotation when the column is subjected to a moderate earthquake but it may not be sufficient. In fact, a short PT cable may fail and a post tensioning tie-rod will become useless after one large rocking rotation as shown in Section 6.2. Therefore, it is proposed in this section to combine the use of a PT cable with a dissipative fuse. Figure 72 shows the system configuration. The fuse is modeled with a truss element, connecting the base of the column with the footing. Unlike a PT cable, it can be loaded in tension and compression. Its material properties correspond to a mild-steel, with a low elastic limit and capability of withstanding large plastic cycles. The PT cable is connected to the top of the column in order to limit its strain when the column rocks. The system properties are summarized in Table 6.

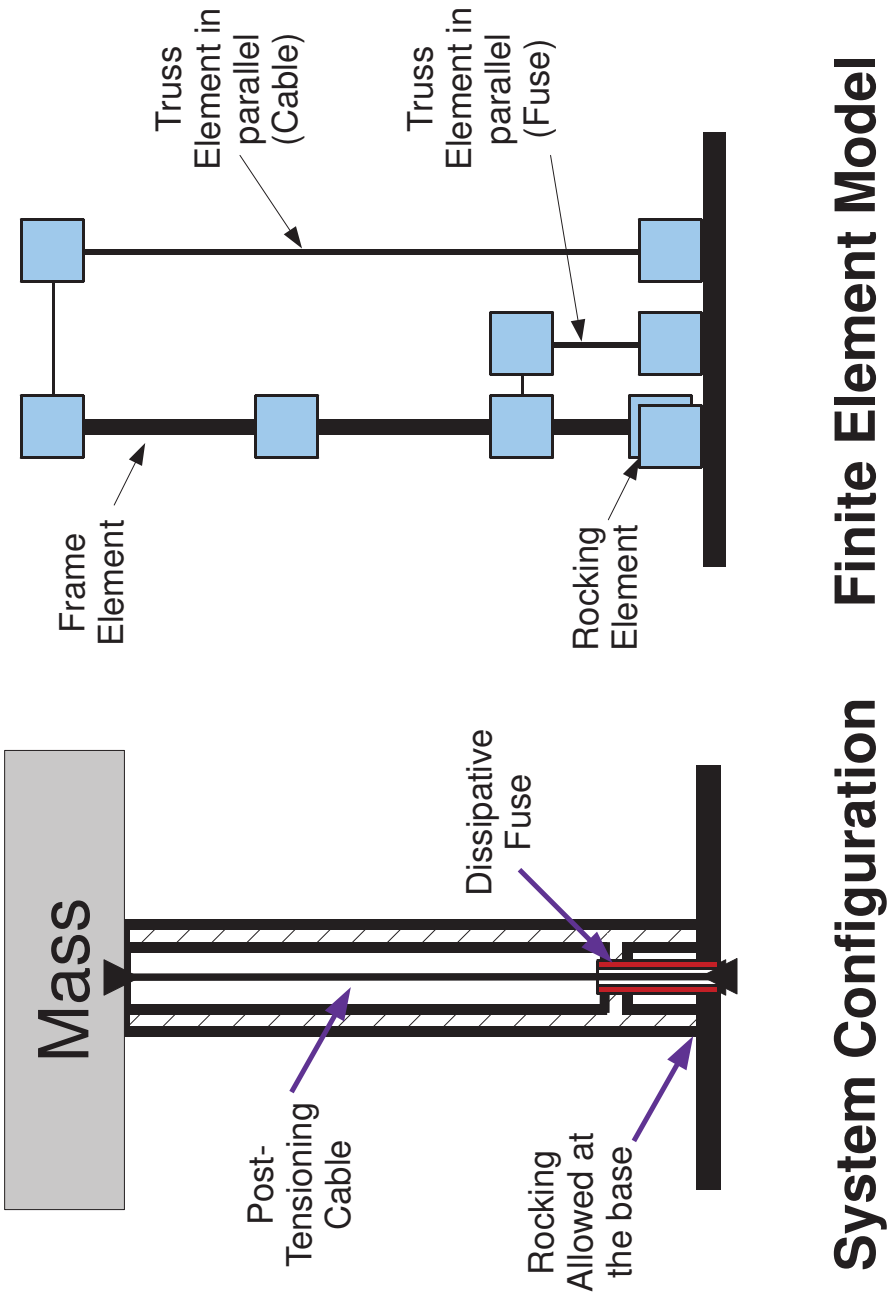

Figure 72: Column with an Unbonded Restraining Cable and a Dissipative Fuse

Column	Height h	=	$12m$
	Axial Stiffness EA	=	$2.5e8kN$
	Flexural Stiffness EI	=	$2.0e8kN \cdot m^2$
	Linear Density ρ	=	$20,900kg/m$
	Damping Ratio ζ	=	2%
Restraining Cable	Young's Modulus E_s	=	$200GPa$
	Cross Section Area A_c	=	$2,000mm^2$
	Cable Length L_{cable}	=	$12m$
	Prestressing Force q_0	=	$2000kN$
Dissipative Fuse	Young's Modulus E_s	=	$200GPa$
	Cross Section Area A_f	=	$16,000mm^2$
	Fuse Length h_{fuse}	=	$2000mm$
	Isotropic Hardening H_i	=	$\frac{E_s}{20}$
	Elastic Limit f_y	=	$200MPa$
	Ultimate Strength f_u	=	$1000MPa$
Lumped mass	Mass	=	$100,000kg$
Footing	Rocking Surface Width	=	$3m$

Table 6: Model Properties of the Rocking Column With Fuse and PT Cable

The structure presented in Figure 72 is subjected to the Takatori station longitudinal record of the Kobe earthquake (1995). Figure 73 shows the rocking rotations of the column. Only the first $20sec$ of the earthquake response are represented. When no fuse is used (solid blue line), the rocking rotations are very large. Because the PT cable is anchored at the top of the column, it is less effective than the elastic short cable used previously in this chapter, however, it also prevents the cable to undergo very large strains. When the fuse is added (dashed red plot), the rocking rotations are greatly reduced. Figure 74 shows the resisting moment at the base of the column. It should be noted that, when the rocking rotations are large, the resisting force of the dissipative fuse causes the resisting moment at the column's base to increase. However, the maximum moment observed is larger for the column with no fuse because the rocking impacts cause very large shock waves at the base. Hence, in this example when a fuse is used, the resisting moment at the base of the column and the rocking rotations are reduced.

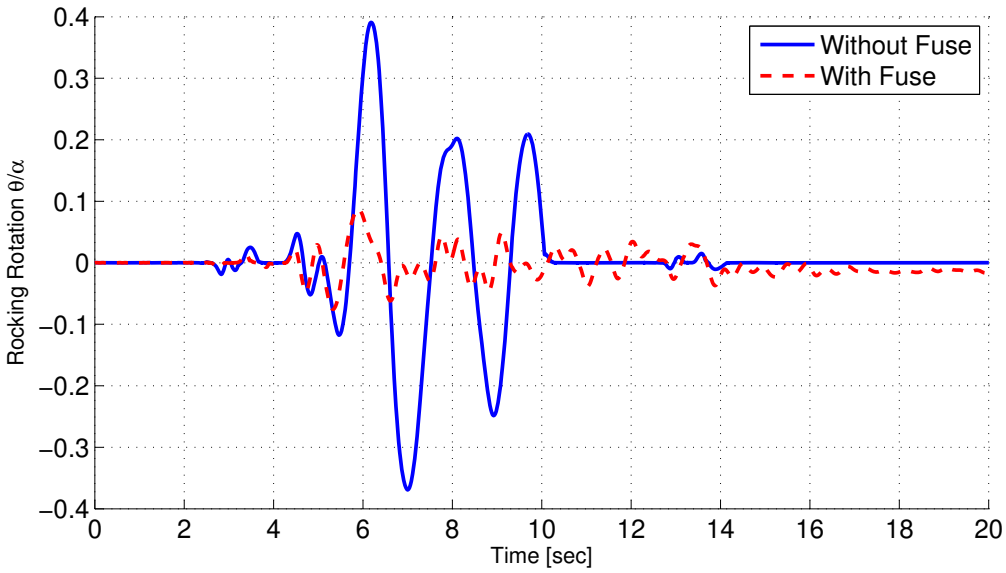

Figure 73: Rocking Rotation of a Column with an Unbonded Restraining Cable and a Dissipative Fuse - Kobe (1995)

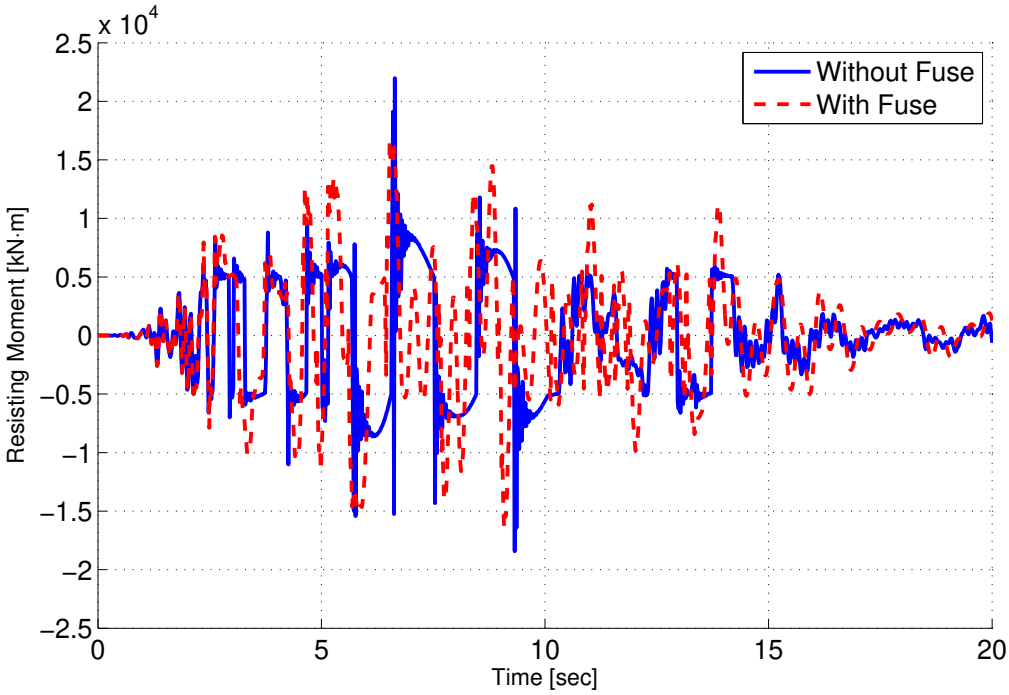

Figure 74: Resisting Moment at the Base of a Column With an Unbonded Restraining Cable and a Dissipative Fuse - Kobe (1995)

An unexpected behavior can be observed after time $t = 10sec$ in Figure 73. The column with a fuse continues to rock, whereas the column that is not equipped with a fuse stops rocking. The role of the fuse is to restrain rocking rotation, so why a fuse can cause rocking to occur when a column without a fuse does not rock at all?

This contradiction can be explained by analyzing the consequences of the plastic elongation of the fuse. When the column is uplifted, the fuse yields in tension and restrains the rocking rotation as shown in Figure 75, but, when the column returns to its initial position, the fuse is now loaded in compression due to the plastic elongation that occured previously. Hence the fuse acts against the weight of the structure and prevents the rocking surface to close. This is confirmed with the fuse response presented in Figure 76. The resisting force of the fuse is normalized with respect to the total weight of the structure added with the prestressing force of the PT cable ($P + W = 1392kN$). It shows that the fuse is alternately loaded in tension and compression and, after time $t = 16sec$, the normalized resisting force is always less than -1. In other words, after time $t = 16sec$, the weight of the structure and the prestressing force are entirely supported by the fuse and the rocking element is in tension. Consequently, the structure cannot return to its initial position and remains tilted toward one side. This is confirmed in Figure 73 where, after $t = 16sec$, the rocking rotation remains negative.

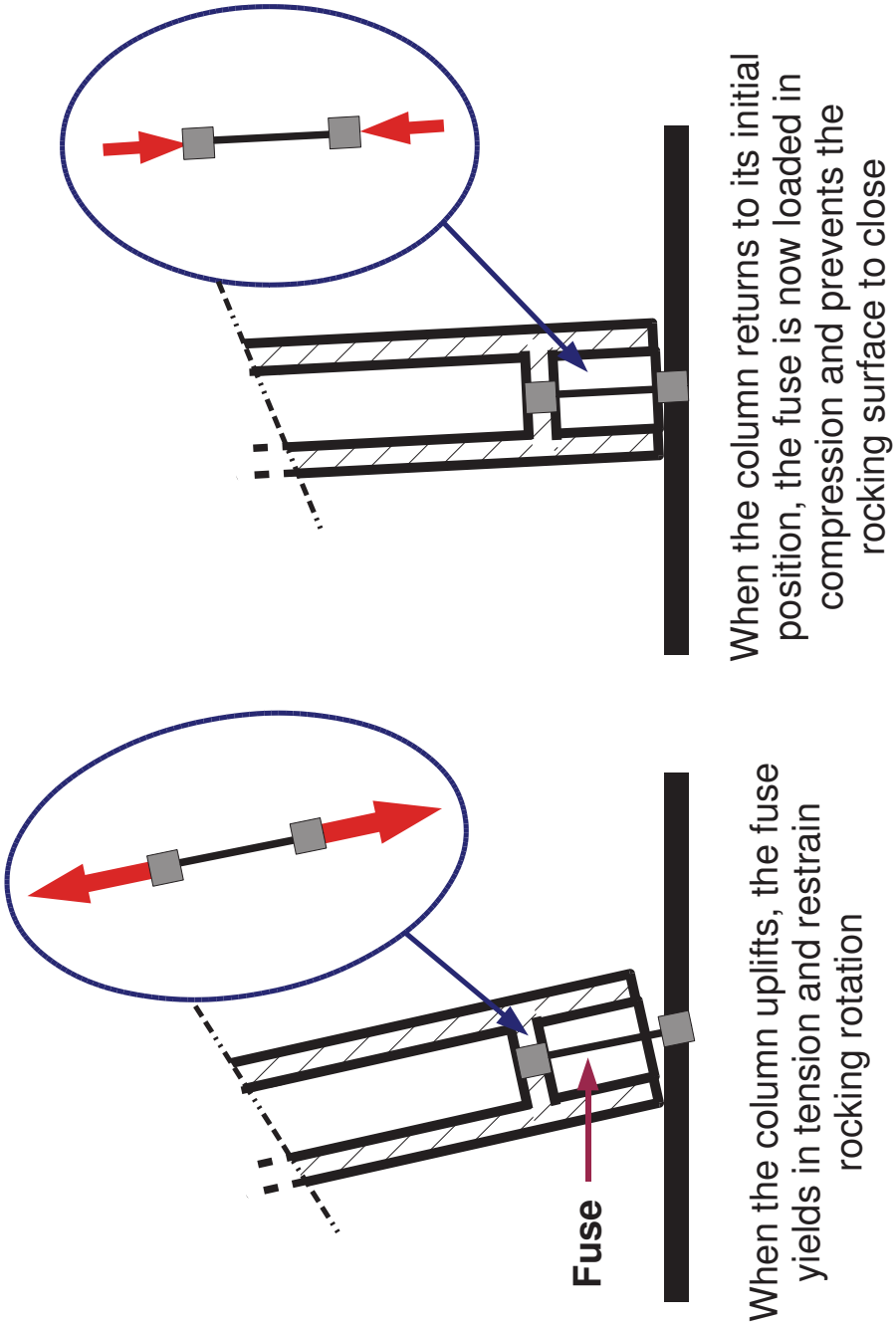

Figure 75: The Fuse Prevents the Column to Return to its Initial Position

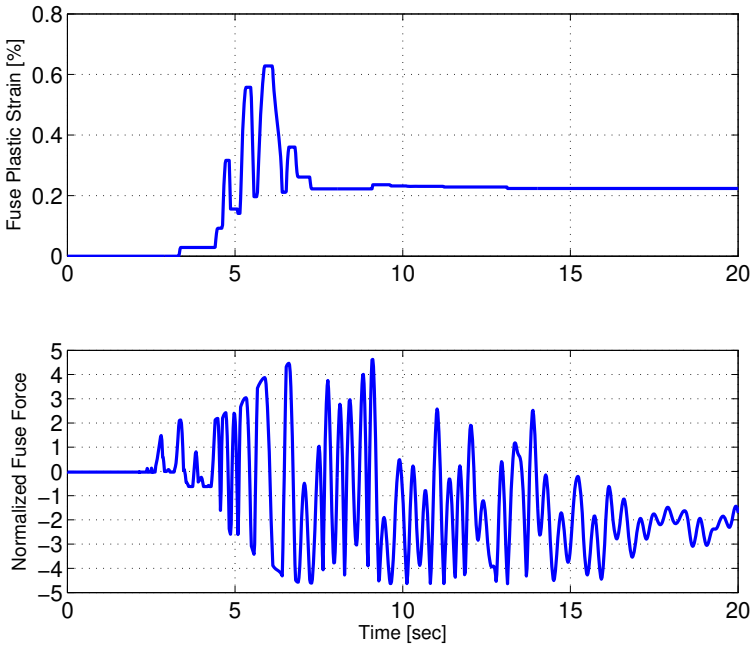

Figure 76: Fuse Resisting Force Normalized with Respect to the Weight of the Structure added with the Prestressing Force of the PT Cable and Fuse Plastic Strain for a Column With an Unbonded Restraining Cable and a Dissipative Fuse - Kobe (1995)

Based on this observation, the fuse can be redesigned such that its resisting force cannot exceed the total weight of the structure. The new fuse properties are shown in Table 7. This fuse does not harden ($H_i = 0$) and it yields when the resisting force reaches $R_{max} = A_f f_y = 1000kN$. Since the weight of the structure added with the prestressing force of the PT cable is $P+W = 1392kN$, the structure should always return to its initial position.

New Dissipative Fuse	Young's Modulus E_s	=	$200GPa$
	Cross Section Area A_f	=	$5,000mm^2$
	Fuse Length h_{fuse}	=	$2000mm$
	Isotropic Hardening H_i	=	0
	Elastic Limit f_y	=	$200MPa$

Table 7: Model Properties of the Second Dissipative Fuse

Figure 77 shows the rocking rotations at the base of the column with this new fuse. Only the first $20sec$ of the response is represented. It should be noted that the maximum rocking rotation increases significantly with the new fuse design but, as predicted, with the new fuse design, the column now returns to its initial position when the earthquake excitation becomes negligible. Thus, for a large excitation, this new fuse doe not restrain the rocking rotation as well as the first one. However, when the excitation vanishes, rocking is terminated and there is no residual drift.

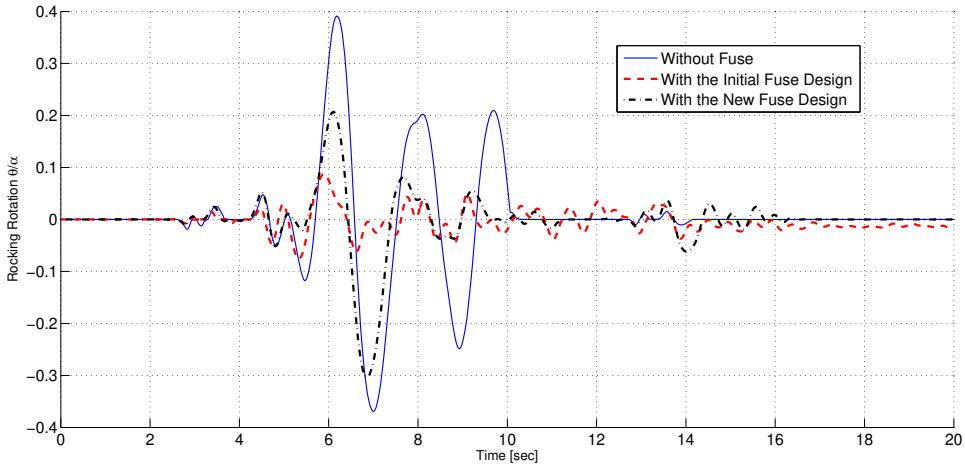

Figure 77: Rocking Rotation of a Column with an Unbonded Restraining Cable and the New Dissipative Fuse - Kobe (1995)

Figure 78 shows the PT cable stress during the earthquake excitation. It shows that the cable stress is greatly reduced when a fuse is used. This is an expected result since the cable strain depends on the amplitude of the rocking rotation, and the fuse does restrain the rocking rotations. Hence the PT cable stress is also reduced since the cable is linear elastic.

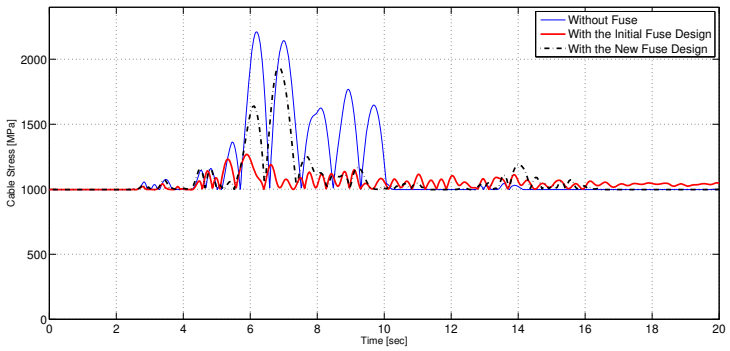

Figure 78: PT Cable Stress for a Column With an Unbonded Restraining Cable and a Dissipative Fuse - Kobe (1995)

The results presented in this section show that the dissipative fuse is an effective device to reduce the amplitude of the rocking rotations. It also damps the rocking impacts thus, as a result, the resisting moment at the base of the column is not disturbed by shock waves. However, when the fuse undergoes plastic elongation and returns to its initial position, it may be loaded in compression. At the end of the earthquake excitation, if the residual force in the fuse is greater than the weight of the structure, then the column may have a residual drift.

6.5 Conclusion

In this chapter, the rocking behavior of a column equipped with a PT cable and subjected to non-elastic deformations was studied. At first, the failure of the PT cable was investigated. It was shown that it can lead to extremely large column's drift ratio. Hence, if a cable is used, its capacity must be such that no failure can occur when the structure is subjected to a severe earthquake. It was then proposed to replace the post-tensioning cable with a prestressing tie-rod. These tie-rods have a lower strength but they can undergo moderate plastic deformations. The yielding of the tie-rods, however, was also very penalizing. Even a reasonable plastic deformation leads to a total loss of the prestressing load. Furthermore, once the tie-rod yields due to a large rocking rotation, it becomes slack and ineffective, as shown in Figure 67. It was shown in Chapter 3 that the initial post-tensioning force can control the rocking initiation, whereas the cable stiffness may have the advantage to keep rocking rotation low. Since bridge columns are usually slender, the use of a PT cable is essential. In this chapter, however, it was shown that to preserve the integrity of the structure, the PT cable should remain elastic. Hence instead of using a short cable anchored near the base of the column, it may be necessary to use a longer cable with a larger diameter that is anchored at the top of the column.

Secondly, a plastic hinge forming at the base of a rocking column was studied. One concern was that the rocking rotation cumulated with the plastic hinge rotation would lead to the overturning of the structure but it turned out that, once a plastic hinge was formed at the base of the column, the overall drift ratio was reduced. The kinetic energy due to rocking was dissipated by the permanent rotations of the plastic hinge. Therefore, the rocking rotations were greatly reduced and the structure remained stable despite the plastic hinge rotation. It must be noted, however, that despite the plastic hinge rotation forming at the base of the column, the properties of the rocking element were assumed to remain unchanged. In practice, it is likely that, when damage occurs at the base of the column, the geometry of the rocking surface will change. This issue is not discussed in this thesis and is left for further research.

Finally, the use of a dissipative fuse at the base of the column was studied. As expected, it helped to reduce the amplitude of the rocking rotation during a large earthquake excitation. A curious behavior, however, was discovered. When the column returns to its initial position, the elongated fuse may prevent the rocking surface to close and rocking rotations may continue even for a minor earthquake excitation. This issue was explained in details in Section 6.4. Overall, the use of a fuse combined with a PT cable was very effective to restrain the rocking rotation, but it may cause the structure to have a residual drift after the earthquake excitation if the fuse is too strong.

7 Behavior of Bridges with Rocking Columns

7.1 Introduction

The behavior of a deformable rocking column was studied in Chapter 5. Interaction between the rocking behavior and the deformations of the column was observed. Chapter 6 focused on the behavior of the structure when permanent deformations occur with rocking and it was shown that a cable failure must be avoided. Hence it was preferred to leave the restraining cable unbonded along the entire height of the column in order to reduce the cable elongation during rocking. Furthermore, it was proposed to use a mild-steel fuse at the base of the column in order to dissipate energy during rocking and enhance stability.

The use of rocking footing for bridge columns was studied by Kwan and Billington in [20] and [21] and rocking foundations were studied by S. Gajan and B. L. Kutter [12]. A rocking footing may be unavoidable in precast construction. Since the reinforcing steel cannot be easily connected at the prefabricated elements interface, only a post-tensioning cable is used to hold the elements together. In this thesis the columns are intentionally allowed to rock, in order to mitigate the harmonic excitation of the structure. To facilitate rocking on the footing, the connection between the top of the column and the superstructure is also allowed to rock.

In this chapter, the behavior of two bridge configurations is investigated. The first configuration is a single-column bridge with two symmetric spans. At the abutments, the girder is free to rotate and translate longitudinally. The second configuration is a three-span bridge with two columns having different height with the same cross-section; thus, the two columns have a different aspect ratio. The bridge columns are allowed to rock at both ends. They are restrained with an unbonded PT cable anchored at the footing and the girder. For each bridge configuration, the behavior of three types of column connections are studied:

- Columns monolithically connected to the girder and the footing
- Columns allowed to rock at both ends and restrained with a PT cable
- Columns allowed to rock at both ends and restrained with a PT cable and a dissipative fuse at the base.

The first bridge configuration is represented in Figure 79. The girder is free to rotate and translate horizontally at the abutments but rocking is not allowed. A rocking element is placed at the top and the bottom joint of the column. The column is post-tensioned between the footing and the bridge deck, using an unbonded cable with a length equal to the column height. One of the column connections studied in this chapter will be equipped with a fuse. This fuse is modeled, using a truss element with a corotational geometry description. It is connected with the footing and the bottom of the column, at a height of $1m$. No fuse is used at the top in order to make sure that the column's resisting moment remains below the girder's moment capacity. A fuse at the base of the column may also prevent it from slipping on its footing.

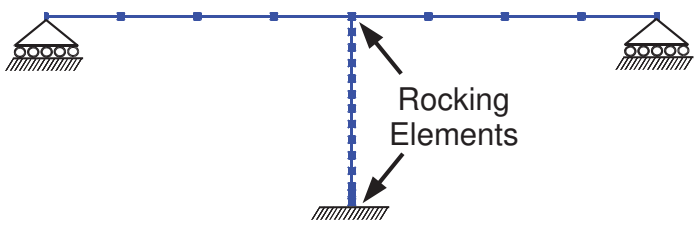

Figure 79: Single Column Bridge Configuration

The second bridge studied consists of a two columns structure. The abutment spans are of equal length and the left column is twice as high as the right column. Seismic resistance design of short columns is challenging. Indeed, a short column may undergo a brittle failure in shear. Even with a very large amount of transversal reinforcements, it may be very difficult to avoid a shear failure mode. Note that fiber elements cannot properly represent shear failure. Instead, the demand in shear observed during computation is used *a posteriori* to choose the appropriate amount of transversal steel reinforcement.

It is expected that allowing the column to rock will prevent shear failure. However, since both columns have a different aspect ratio, they have a different rocking behavior. A complicate rocking interaction will occur between these two columns due to their connection to the same girder.

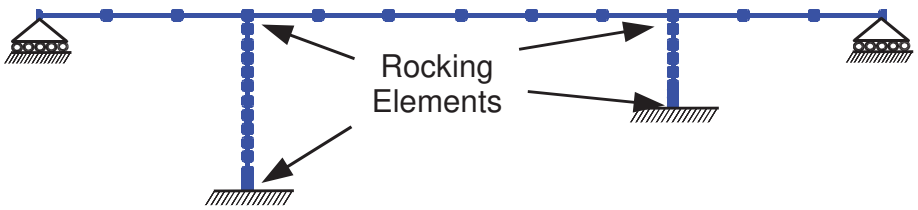

Figure 80: Two-Columns Bridge Model

Properties of both bridges are summarized in Table 8. Figure 81 depicts the design outlines. The abutment supports are simple rollers, allowing the girder to translate longitudinally. A rocking element is inserted between the columns and the footings as well as between the columns and the girder. A post-tensioning cable anchored between the girder and the footing prevents the column from overturning. Furthermore, a dissipative fuse is inserted at the base of the column connected to the footing. No fuse is installed between the top of the column and the girder.

	Single Column Bridge	Two-Columns Bridge
Column Height	$24m$	$24m$ and $12m$
Column Weight	$4,920kN$	$4,920kN$ and $2,460kN$
Girder length	$80m$	$120m$
Girder Weight	$11,772kN$	$15,696kN$
Abutment spans	$40m$	$35m$
Central span	na	$50m$

Table 8: Bridges Dimensions

Only the in-plane displacements are allowed, hence the structure can not deform laterally. The columns and the girder were modeled using corotational beam elements embedded in FEDEASLab. The geometric and material properties of the structure are presented in Table 9. The bridge properties were obtained from Ketchum et al. [18] report, which represent a typical CalTrans highway bridge. CalTrans often designs bridge columns with a circular solid section in order to optimize the concrete confinement. In this Chapter, it is proposed to use a hollow square section in order to accommodate the PT cable and the fuse. Column size and reinforcement are proposed based on experience developed in Chapter 6. The outcome of the analyses conducted in this chapter will indicate the column force design values.

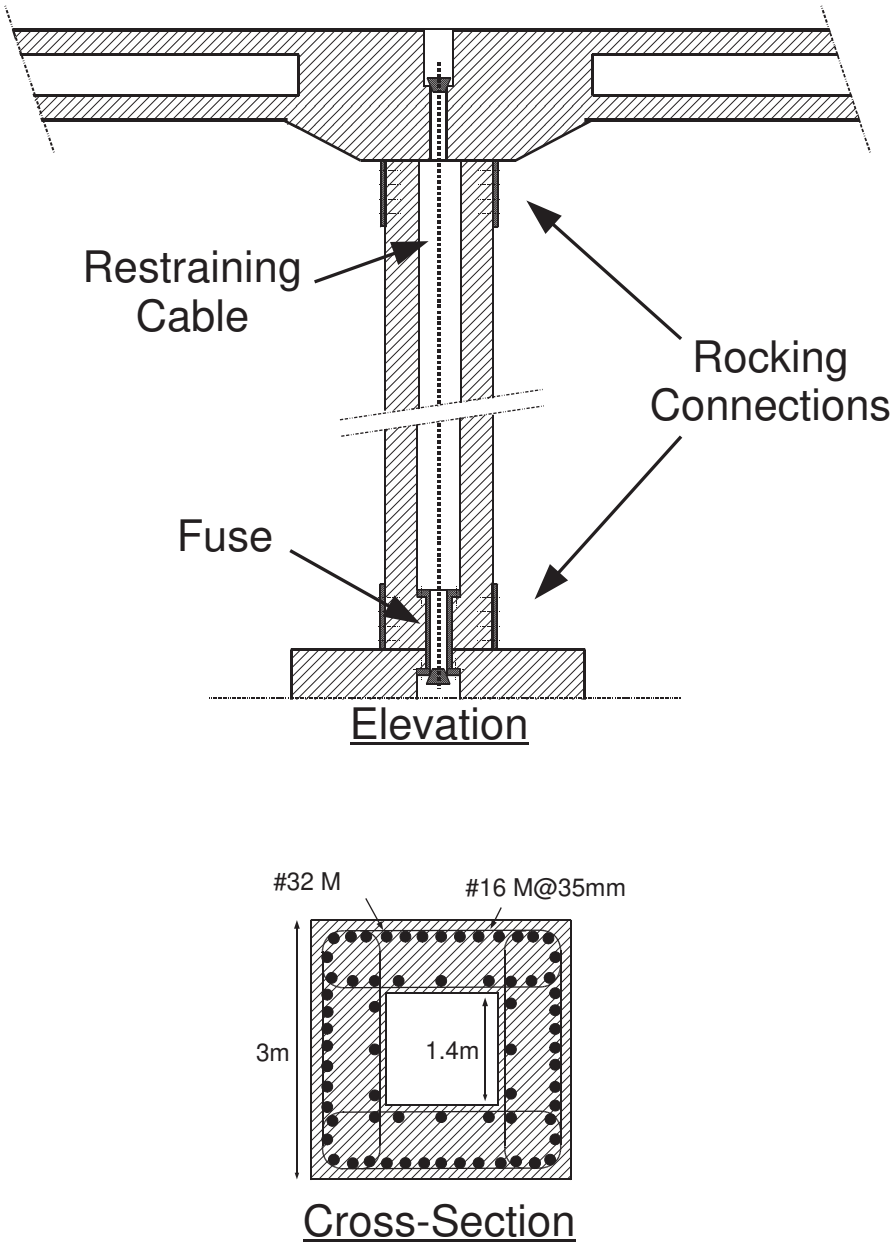

Figure 81: Drawing Outline of the Column Connections with its Footing and the Superstructure

Column	Width b	=	$3m$
	d	=	$3m$
	Wall Thickness	=	$0.8m$
	Detailed Properties in Table 10		
Girder	Young Modulus	=	$40e9N/m^2$
	Cross Section	=	$5m^2$
	I	=	$3.5m^4$
	Density	=	$2.5e3kg/m^3$
Cable	Young Modulus	=	$200GPa$
	Cross Section Area	=	$5,000mm^2$
	Prestressing force	=	$2000kN$
	Ultimate Strength f_u	=	$1800MPa$
Dissipative Fuse	Young Modulus	=	$200GPa$
	Cross Section Area A_f	=	$5,000mm^2$
	Yielding Strength f_y	=	$200MPa$
	Isotropic Hardening Modulus H_i	=	$20MPa$
Rocking Elements	Rocking Width $2R$	=	$3m$

Table 9: Bridge properties

The cable properties are chosen to meet several requirements. First, it has to allow rocking but restrain its amplitude. Secondly, it must not fail, even for a large rocking rotation. Therefore, its initial prestressing load is only 20% of the weight supported by the column. As explained in Chapter 3, a low initial prestessing force will allow the structure to rock for a low earthquake excitation, hence limit the demand on the column. Furthermore, the cable length and diameter were chosen such that the cable will not fail if the rocking rotation at the base of the tall column remains below 80% of the slenderness angle of that column.

The fuse properties are presented in Table 9. Its yielding capacity is $1,000kN$ and its hardening modulus is very low ($\frac{H_i}{E_s} = 1e-4$). The total resisting force at the base of the column (Weight and PT cable force) is equal to $12,806kN$ so the ratio between the fuse capacity and the vertical load is 8.33%. Based on the findings presented in Section 6.4, the capactiy of the fuse is sufficiently low to prevent any residual drift.

Figure 81 shows the elevation and the cross-section of the columns used for both bridges. In the numerical model, the columns are modeled with force based fiber elements developed by Neuenhofer and Filippou [25]. The concrete is represented with the hysteretic unidimensional model, commonly called Kent-Park-Scott. It was first developed by Park Kent and Sampson [26] and later enhanced by Scott, Park and Priestley [30]. In this model, the concrete confinement is taken into account to compute the ultimate compressive strength. The transversal reinforcement yield strength and its volumetric ratio are used by the material model only to represent the longitudinal concrete fiber behavior. The longitudinal steel reinforcement is modeled with a separate layer of fibers. These fibers belong to the same cross-section and it is considered that no slipping will occur between the longitudinal reinforcement and the concrete. The reinforcing steel is modeled with a conventional isotropic hardening model. The columns cross-section properties are summarized in Table 10.

Fibers layout	Concrete	=	$15 fibers$
	Longitudinal Steel Reinforcements	=	$4 fibers$
	Fiber Integration Rule	=	Midpoint
Elements layout	Geometric Description	=	Corotational
	Integration Points	=	5
	Maximum Integration Points Subdivision	=	5
	Element Integration Rule	=	*Gauss-Lobatto*
Concrete	Unconfined Compressive strength f_c	=	$30 MPa$
Longitudinal Steel	Yielding strength f_y	=	$420 MPa$
	Young Modulus E_s	=	$200 GPa$
	Isotropic Hardening H_i	=	$10 GPa$
	Outer Cross-Section area $A_s o$	=	$244 cm^2$
	Inner Cross-Section area $A_s i$	=	$147 cm^2$
Transversal Steel	Yielding strength f_y	=	$420 MPa$
	Stirrups Volumetric Ratio ρ_s	=	0.75%
	Stirrups spacing at column ends s_h	=	$35 mm$

Table 10: Column Cross-Section properties

The girder capacity is such that no plastic hinge will form even during a severe earthquake. Hence, in order to reduce the computational cost, the girder is not modeled with fiber elements but with corotational elastic beam elements whose material and geometric properties are summarized in Table 9. It is assumed that the capacity of the girder is such that the column will always yield first. Figure 82 shows the axial force behavior of the column for a monotonic loading and the moment-curvature behavior for a cyclic loading. At rest, the total resisting force on the column (Weight and PT cable force) represents 16.1% of the column's axial capacity.

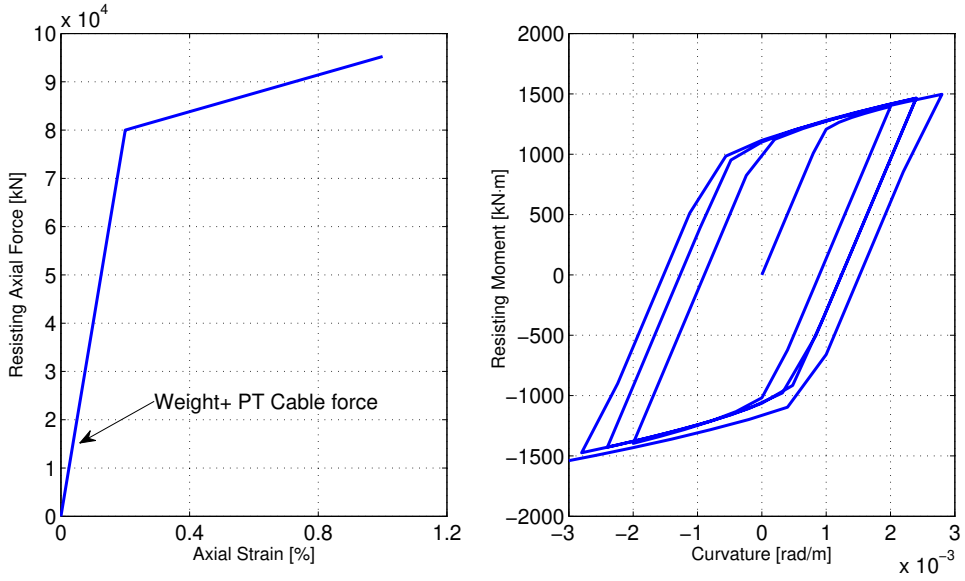

Figure 82: Bridge Column - Force vs. Strain for a monotonic loading and Moment vs. Curvature for a cyclic loading

The mass of the column and the girder are lumped at the element nodes. The density of the reinforced concrete is considered to be constant, regardless of the steel reinforcement layout. It is assumed to be $\rho_{rc} = 2500kg/m^3$. The masses of the restraining cables are neglected. The weight is computed at each node, based on the lumped mass. The service load is not considered.

A mass-proportional natural damping is modeled. Its damping ratio $\zeta = 2\%$ is computed for the first natural period of the structure. Modal analysis is conducted, assuming the rocking surfaces are closed (rocking does not occur). The time integration is performed with the HHT method [14] and a time-step division algorithm. The integration parameter is $\alpha = 1/6$. At each time step, the resisting moment is computed with a Newton-Raphson iteration scheme. The stiffness is updated after each iteration in order to achieve quadratic convergence. The smoothing parameter of the rocking elements presented in Chapter 4 is $\epsilon = 1e{-}8$ for both elements. The rocking termination is set to trigger when $\dot{\theta} < 1e{-}7 rad/sec$. Both structures are subjected to Takatori station longitudinal record of the Kobe earthquake (1995) with a magnitude of 100%.

7.2 Single Column Bridge Results

Figure 86 shows the drift ratio of the structure, equal to the girder horizontal displacement over the height of the column. The horizontal displacement is measured at the top of the column. It should be noted that the three structures undergo moderate deformations. The non-rocking structure reaches a maximum drift ratio equal to 1.13%, whereas the rocking structures without and with a fuse reach respectively 1.12% and 0.88%.

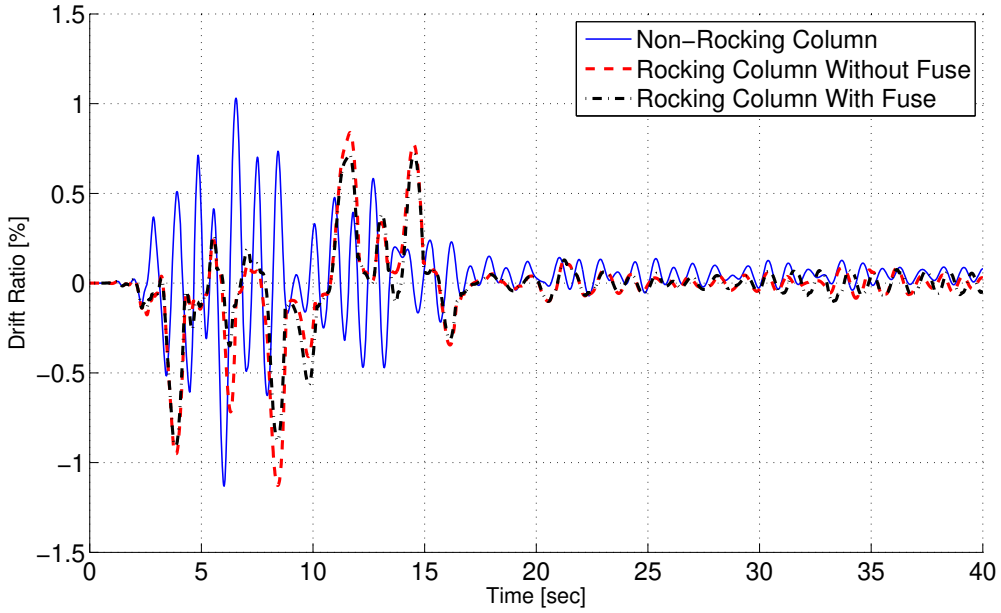

Figure 83: Structure Drift Ratio of the Single Column Bridge With Non-Rocking Column and With Rocking Column, With and Without a Dissipative Fuse - Kobe (1995)

Figure 84 shows the moment-curvature response for the non-rocking bridge. As expected, the column yielded at both ends of the column. Due to the flexural flexibility of the girder, the moment is larger at the base of the column. The maximum ductility ratio observed is 4. Therefore, the bridge resisted the earthquake, but the column is damaged. Conversely, the rocking columns remained elastic. Figure 85 shows the resisting moment observed at the column joints during the earthquake excitation. The column's resisting moment of the two structures allowed to rock (with and without the fuse) is 86% lower than the resisting moment of the non-rocking column. It should also be noted that the fuse does not change the resisting moment significantly.

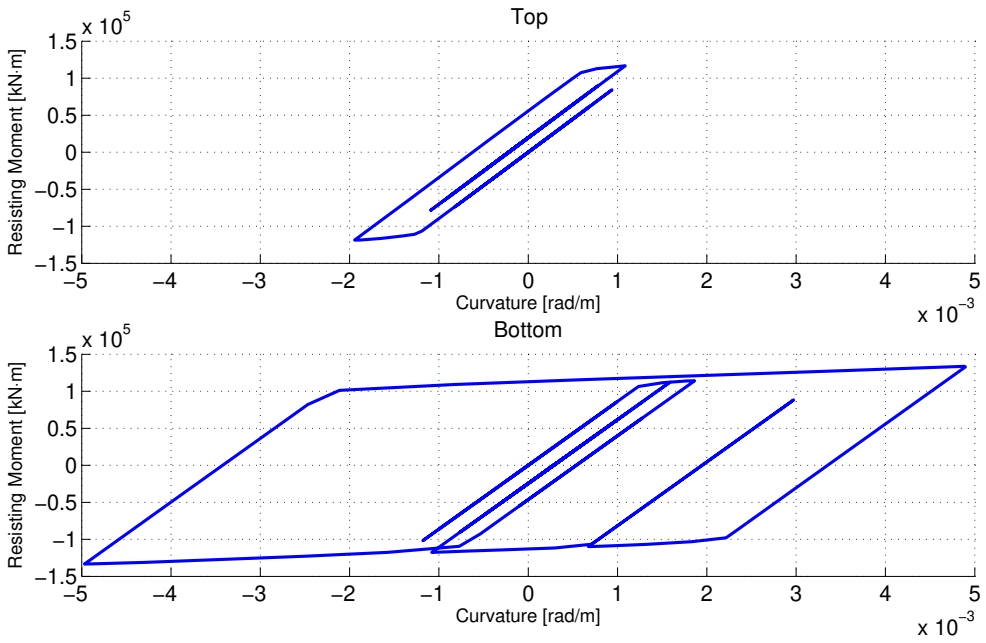

Figure 84: Moment-Curvature at the Column Joints for the Single Column Non-Rocking Bridge - Kobe (1995)

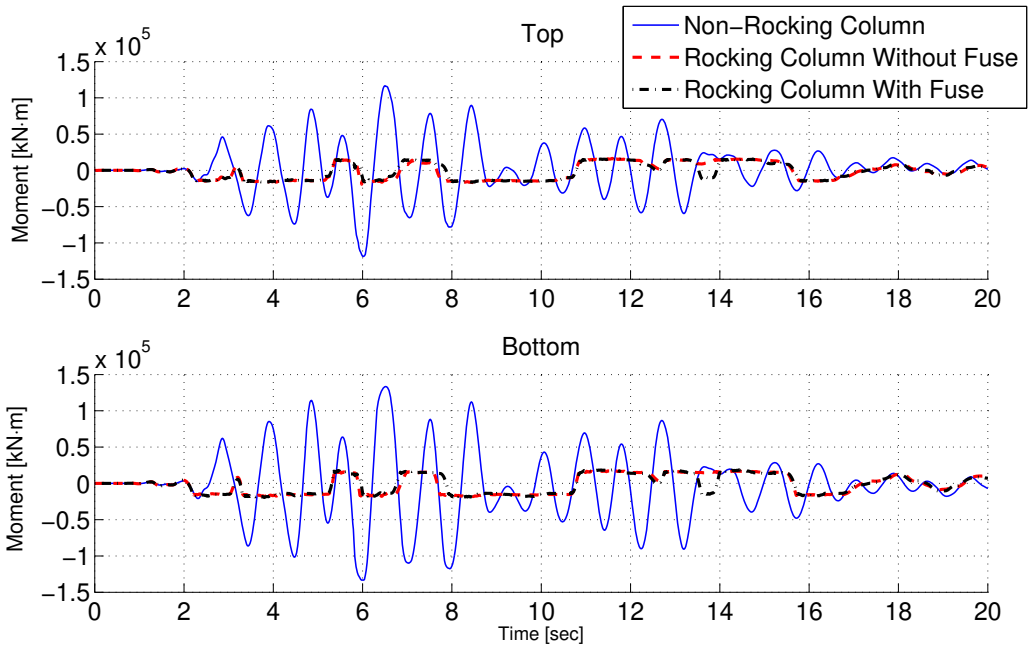

Figure 85: Resisting Moments at Column Joints of the Single Column Bridge With Non-Rocking Column and With Rocking Column, With and Without a Dissipative Fuse - Kobe (1995)

Figure 86 shows the rocking rotations at the column joints with and without a fuse. It is normalized with respect to the slenderness angle of the column $\alpha = 0.0624rad$. At both ends, the rocking rotations remain moderate. It is considered that the rocking remains stable only when $\theta_{rocking} < \alpha$ however, in this example, the cable may fail for $\theta_{rocking} > 0.8\alpha$.

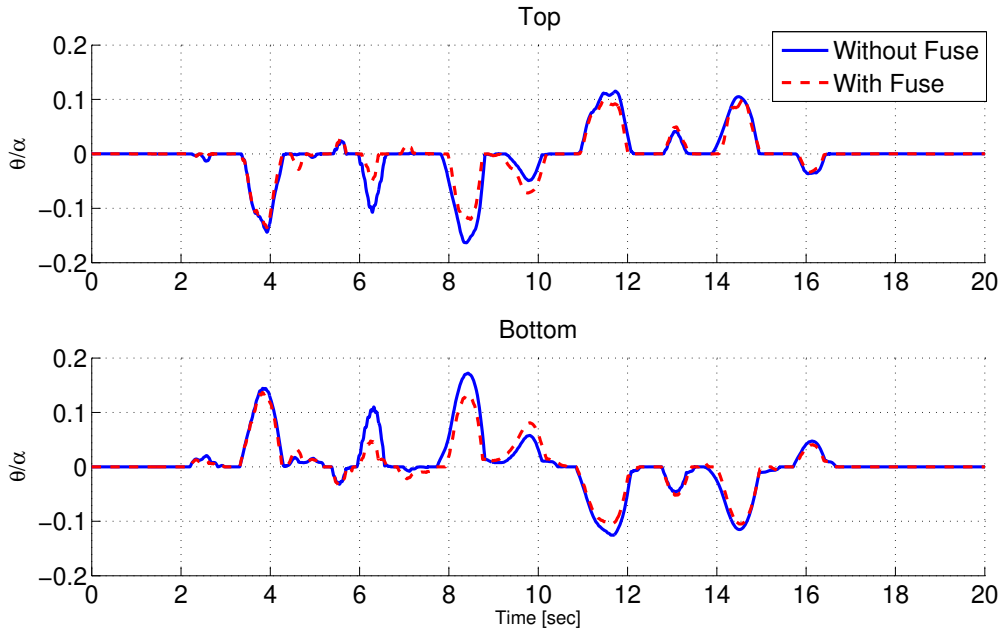

Figure 86: Rocking Rotations at Column Joints of the Single Column Bridge, With and Without a Dissipative Fuse - Kobe (1995)

In this example, the resisting moment was significantly reduced as shown in Figure 85 and the rocking rotation was limited. Hence the rocking column combined with a restraining cable proved to be a good solution to preserve stability during a large earthquake. The fuse slightly reduces the rocking rotation, but it is not essential since the drift ratio is already moderate when no fuse is used. The energy dissipation of the fuse increases with the rocking rotation. Thus, it is expected to reduce the drift ratio significantly if the rocking rotation becomes important, as shown in the example presented in Section 7.3.

The stress and the plastic strain in the fuse are shown in Figure 87. A fuse with almost no hardening was intentionally chosen to avoid residual drift (as explained in 6.4). As a consequence, the maximum plastic strain is 1.2% but there is almost no residual plastic strain inside the fuse at the end of the excitation. The weight of the structure is sufficient to reduce the plastic elongation and to recenter the column.

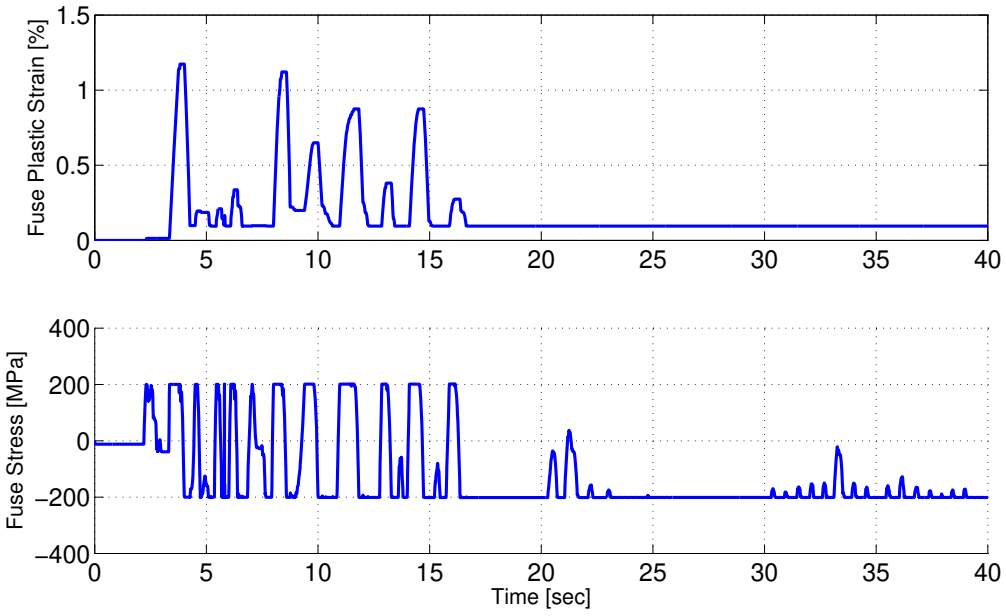

Figure 87: Fuse's Stress and Plastic Strain of the Single Column Bridge - Kobe (1995)

Figure 88 shows the stress in the restraining cable during the earthquake excitation. Despite significant increase when the column is rotating, the cable is far from exceeding its failure strength $f_u = 1,800MPa$. It was shown in Chapter 6 that cable failure must be avoided to preserve the stability of the structure. In this example, the PT cable behaves as intended. It was designed to resist rocking rotation up to 0.8α, but the maximum rocking rotation observed is only 0.18α.

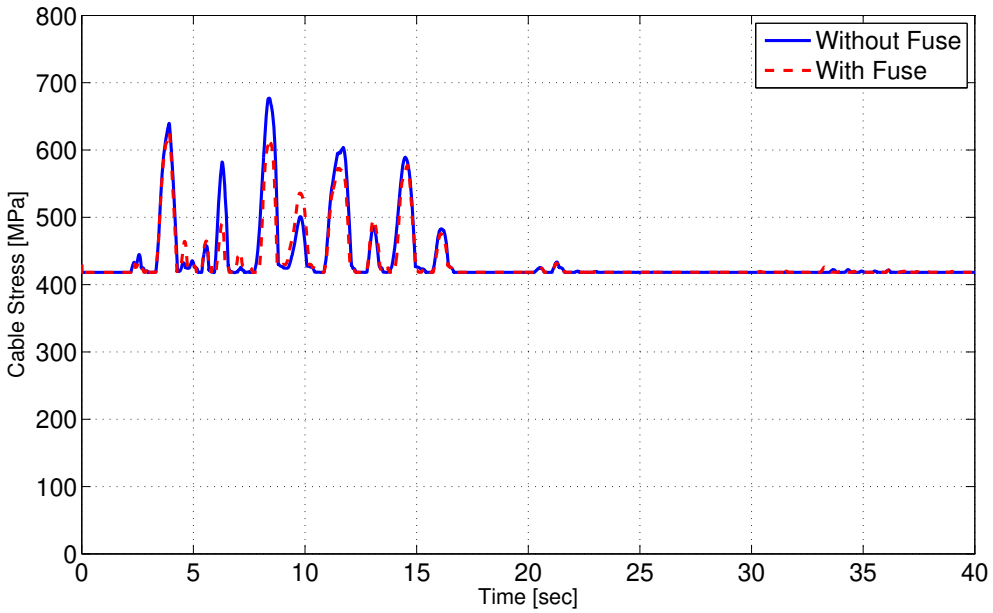

Figure 88: Restraining Cable Stress of the Single Column Bridge, With and Without Fuse - Kobe (1995)

Finally, it is proposed to study the shear demand on the foundation between the conventional bridge and the two bridges equipped with rocking columns (with and without a fuse). Figure 89 shows the horizontal reaction force at the base of the column during the earthquake excitation. The shear force is 82% less when the column is allowed to rock. This result is consistent with the reduction of the resisting moment observed in Figure 85, showing a reduction of 86%.

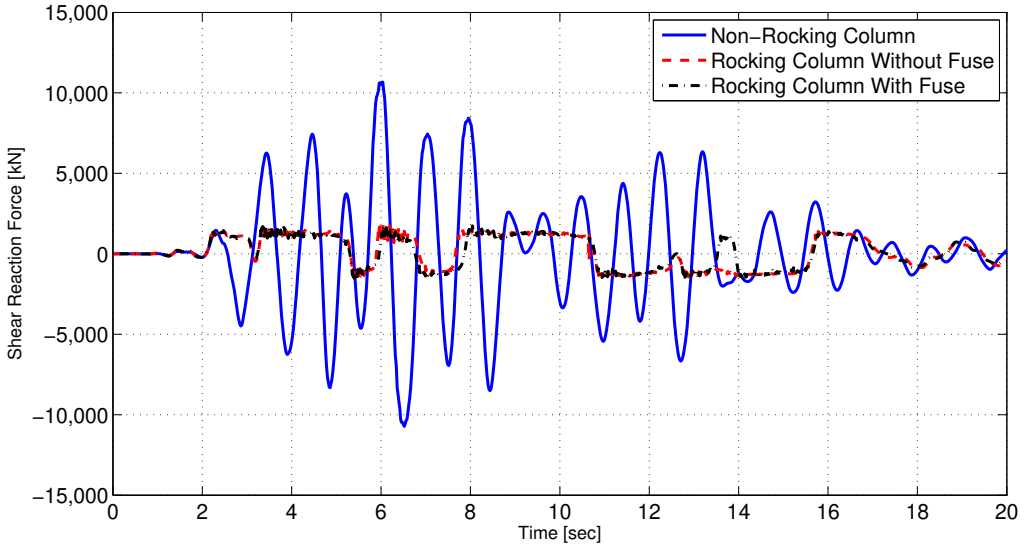

Figure 89: Shear Demand on the Footing of the Single Column Bridge - Kobe (1995)

The demand on the foundation is greatly reduced when the column is allowed to rock. This finding may help to reduce the cost of the foundation. For instance, the number of pilings can be reduced and the footing can be smaller.

7.3 Two-Columns Bridge

Columns of different heights were selected to investigate how rocking would be affected. Columns of the same height are expected to rock together however, columns of different heights may not do so. A tall column will overturn with a smaller rotation than a short column and initiation of rocking may be different since they have a different aspect ratio. But the girder is expected to force both columns to rock together. A complex interaction between the two columns will govern the rocking behavior of the structure.

The structure's drift ratio is presented in Figure 90. Note that it is computed considering that the height of the structure is the height of the short column and not the height of the tall column. The bridge with non-rocking columns has a maximum drift ratio of only 0.7%, whereas the bridge with rocking columns and without fuses has a maximum drift ratio of 2.5%. However, the bridge allowed to rock but equipped with fuses has a maximum drift ratio of only 0.75%. Thus, in this example, the fuse significantly helps to reduce drift.

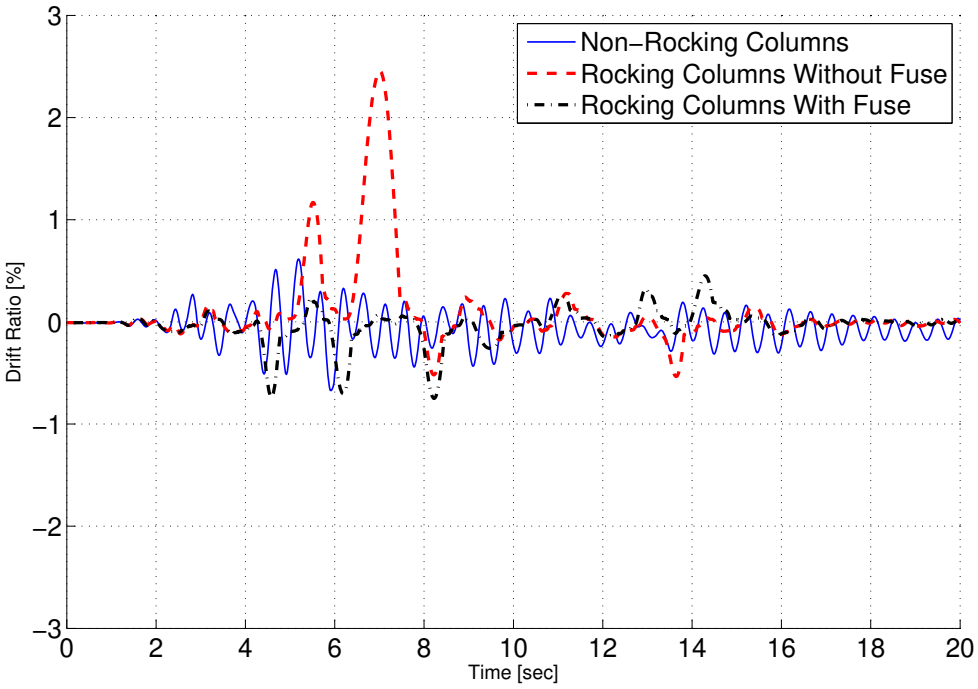

Figure 90: Structure Drift Ratio of the Two-Columns Bridge With Non-Rocking Columns and With Rocking Columns, With and Without a Dissipative Fuse - Kobe (1995)

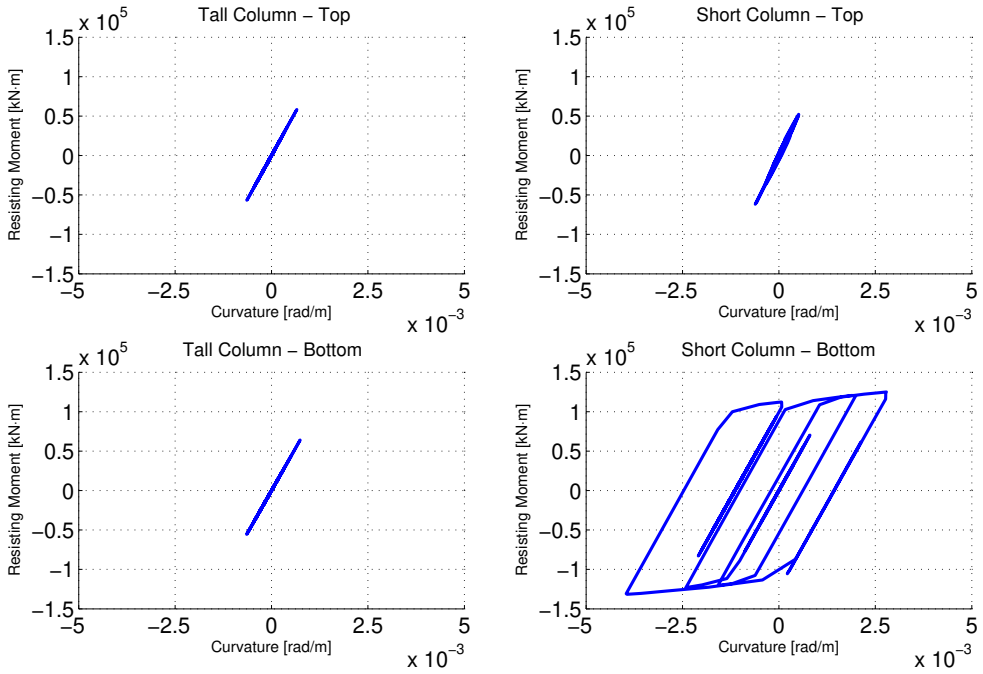

Figure 91: Moment-Curvature at the Column Joints for the Two-Column Non-Rocking Bridge - Kobe (1995)

Figure 91 shows the moment-curvature response at each column joint of the non-rocking bridge. In this example, only the short column yields, only at the base. In the previous section, it was already observed that the resisting moment was larger at the base, due to the flexural flexibility of the girder. In this example, it is more noticable since the column is shorter and the girder did not change. Furthermore, the short column is much stiffer than the tall column. Therefore, the drift ratio of the tall column remains low and the column does not yield.

The maximum ductility ratio observed is 2.6. Therefore, the bridge resisted the earthquake but the short column is damaged. Conversely, the rocking columns remained elastic. Figure 92 shows the resisting moment observed at each column joint during the earthquake excitation. Only the first $20sec$ are represented. The resisting moment at the ends of the rocking columns is significantly lower than the resisting moment at the ends of the non-rocking columns. At the base, the resisting moment is 72% lower for the tall column and 85% lower for the short column.

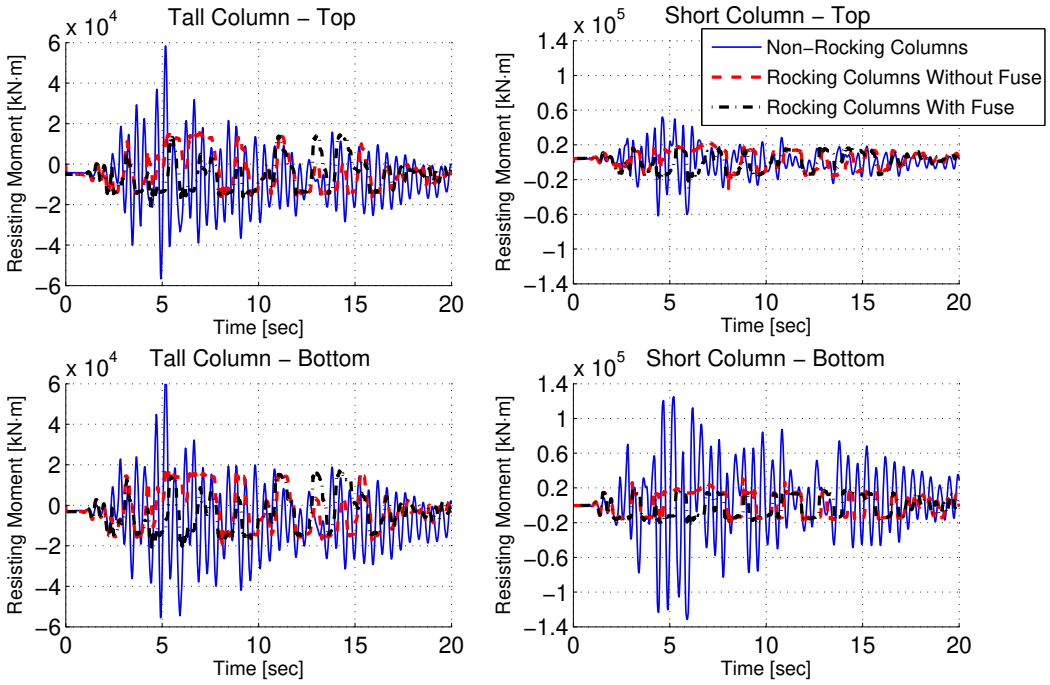

Figure 92: Resisting Moments at Column Joints of the Two-Columns Bridge With Non-Rocking Column and With Rocking Column, With and Without a Dissipative Fuse - Kobe (1995)

Figure 93 shows the rocking rotations at each rocking surface. Each rotation plot is normalized with the slenderness angle of the concerned column. Hence the two columns slenderness ratios must be distinguished they are $\alpha_{tall} = 0.0624rad$ and $\alpha_{short} = 0.124rad$. In this example, the fuses significantly reduce the rocking rotations. In fact, the maximum rocking rotations at the base of the tall column and the short column are respectively 74% and 71% smaller when fuses are used.

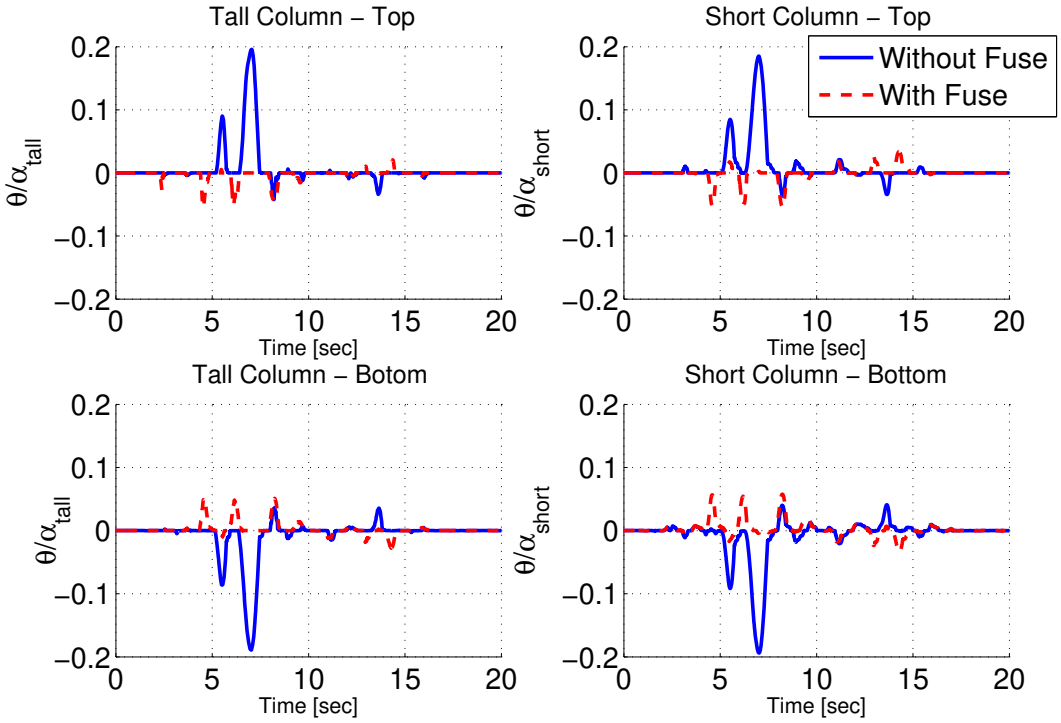

Figure 93: Rocking Rotations at Column Joints of the Two-Columns Bridge, With and Without a Dissipative Fuse - Kobe (1995)

The stress and the plastic strain in the fuses are presented in Figure 94. A fuse with almost no hardening was intentionally chosen to avoid residual drift. The maximum plastic strains are 0.35% and 0.9% but, due to the gravity load, there is almost no residual plastic strain inside the fuses at the end of the excitation. Thus, the weight of the bridge is sufficient to recenter the column.

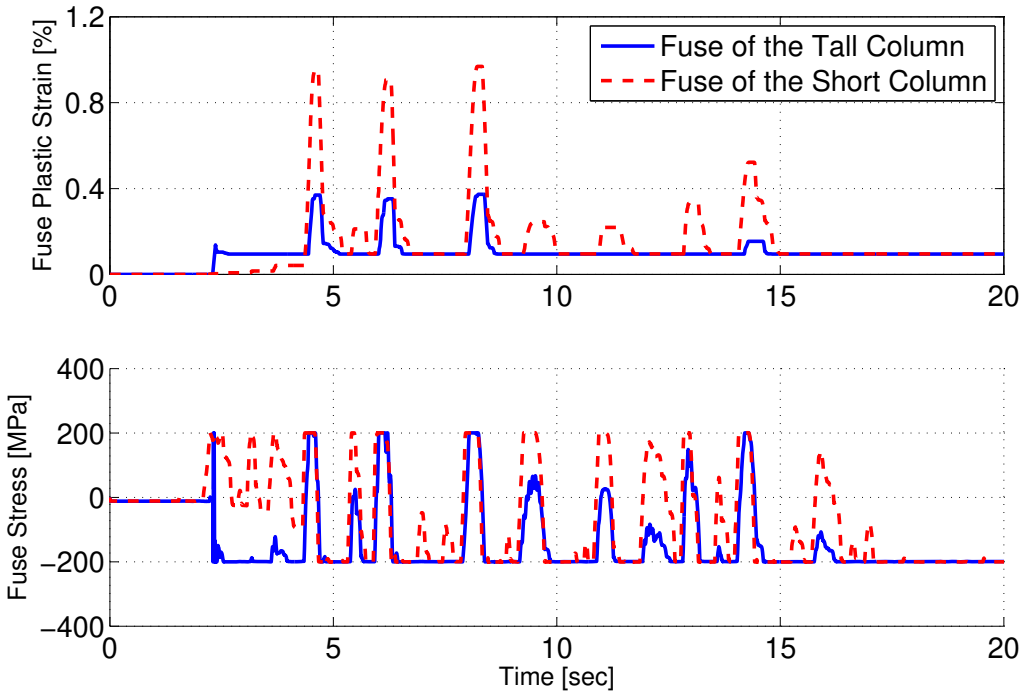

Figure 94: Fuse's Stress and Plastic Strain of the Two-Columns Bridge - Kobe (1995)

The horizontal reaction forces at the base of each column are represented in Figure 95. When the columns are allowed to rock, the shear reaction at the base of each column is 73% lower. This result is consistent with the reduction of the resisting moments observed in Figure 92 when the columns are allowed to rock. As observed in the pervious section, the use of a fuse does not change the reaction force significantly.

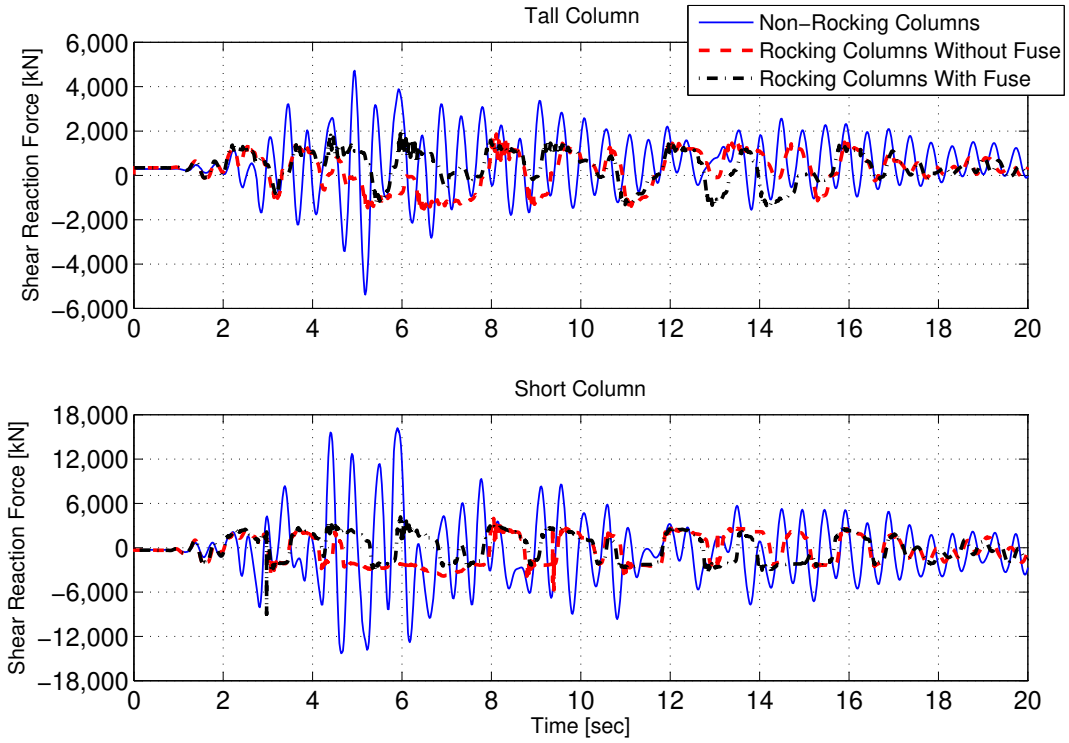

Figure 95: Shear Demand on the Footings of the Two-Columns Bridge - Kobe (1995)

7.4 Conclusion

In this chapter, the rocking element was used to assess the performance of an entire bridge structure when the columns are allowed to rock. It was chosen to compare the results with conventional monolithic bridges. Such bridges in current design philosophy can undergo significant damage at the column joints during an earthquake. Hence, in order to properly represent the permanent deformations of the columns, it was decided to use a fiber element with hysteretic models for the concrete and the longitudinal steel reinforcements.

The same bridges were allowed to rock with a restraining cable preventing overturning. The results showed that the rocking rotations remained moderate if the columns were equipped with a dissipative fuse. The bridges allowed to rock had a drift ratio of the same magnitude as the monolithic bridges that suffered from plastic hinge formation. The limitation of the rocking rotations within a controlled range was also crucial to preserve the integrity of the restraining cables. In fact, as the rocking rotations increase, the resisting forces within the cables also increase and it was shown in Chapter 6 that cable failure must be avoided.

The resisting moments at the joints of the columns were significantly reduced when the columns were allowed to rock. As a result, none of the rocking column was damaged after the earthquake. Furthermore, there was no residual drift even when fuses were used. The reduction of the resisting moment was the primary reason to study the use of rocking columns and the solution presented in this chapter proved to be very effective. It also shows that the capacity of the girder and the column footings can be reduced as shown in Figure 89 and Figure 95. In order to transfer the moment loads from the column to the girder, the bent caps are often massive in conventional earthquake resistant bridges. The use of rocking surfaces may allow to reduce their capacity. The capacity of the columns footings is also a very challenging problem. In fact, when the moment at the base of the column is very large, the foundation may be in tension. Hence it requires the use of deep concrete pilings to ensure the stability of the footing. Therefore, the use of rocking columns may allow to reduce the size of the pilings and speed up the construction.

In the first example, the fuse at the base of the column was not affecting the response significantly because the rocking rotation remained low even without a fuse but, in the second example, the rocking rotations were greatly reduced when fuses were used at the base of each column. Such device can prevent large rocking rotations and enhance the overall stability.

8 Summary and Conclusions

8.1 Summary

Current philosophy in bridge earthquake engineering is to ensure the continuity between the different parts of the structure. The columns are designed to yield and form zones (plastic hinges) where plastic deformation is expected to occur while keeping the developed resisting forces capped and under control. The remaining bridge elements are then capacity-designed to remain elastic under the forces capped by those that can be developed in the column plastic hinges.

The goal of this research is to develop a design approach that allows for a substantial reduction in the forces transmitted from the columns to the bridge elements while keeping the deformations (both maximum and residual) to the same or smaller level as the conventionally designed bridge. The design method to achieve this goal is to use segmented columns, comprised of stacked segments with dry or grouted joints post-tensioned using a cable along the longitudinal column axis. This design method enables a broad advance of accelerated bridge construction principles to regions where seismic loads are significant. This design may allow rocking motion between the segments but also between the column and the foundation, and between the column and the bent-cap. Implementation of this approach in modular and accelerated bridge construction was presented in Chapter 2. It is expected that modular designs with rocking rather than monolithic joints will greatly increase construction speed, have an earthquake performance equal to or better than conventional monolithic designs, and have significantly better repairability characteristics achieved through replacement of damaged elements rather than conventional repair and retrofit.

It is sometimes necessary to eliminate rocking at segment interfaces. For instance if rocking occurs at column's mid-height, the off-centered gravity load of the superstructure will cause buckling and lead to collapse. However, rocking can also be used to modify the seismic response of bridge structures. The mechanics and dynamics basis for this approach was presented in Chapter 3. Despite its inherent instability, it was shown that rocking behavior may be a very efficient seismic response modification mechanism for slender structures. While displacements of the rocking systems are large, the forces transmitted from the rocking elements to the rest of the structure are small. It was shown that post-tensioning greatly reduces the moments in the columns and the demands on the foundation. Despite negligible energy dissipation at the rocking surface, the motion of the rocking system was shown to attenuate and eventually disappear.

The rocking element presented in Chapter 4 is essential for modeling complex rocking

systems where rocking may occur simultaneously at several rocking surfaces, namely, between the columns and the footings, but also between the columns and the superstructure. If rocking must be prevented between two segments, the rocking element can also be used to confirm that rocking will not be triggered during the duration of the earthquake. The rocking surface finite element was developed using the augmented Lagrangian formulation, combined with an HHT integration scheme. The element behavior was verified against analytical solutions for free rocking.

The behavior of elastic rocking columns was investigated in Chapter 5. It was shown that the free rocking response of an elastic column is very similar to the response of a rigid block. However, the rocking rotations of an elastic column may suddenly stop and lead to bending oscillations.

For a very large earthquake, a column's rocking can lead to the failure of the restraining cable. It was shown in Chapter 6 that such scenario must be avoided. The cable has to remain elastic in order to preserve the initial prestressing force and prevent overturning.

At last, a model of a rocking bridge featuring the rocking element was used in Chapter 7 to investigate longitudinal direction rocking of a three-span bridge with different column lengths (i.e. aspect ratios). The element enabled computation of rocking response to an earthquake ground motion.

8.2 Conclusions

In Chapter 3, the behavior of a rigid block rocking on its base was studied. Previous studies showed that when a block is allowed to rock under earthquake excitation, the resisting moment at the base of the structure may be greatly reduced, but overturning may occur. So it was proposed to use an unbonded post-tensioning cable, in order to allow rocking but prevent overturning. This solution proved to be very effective. Actually, by adding an elastic cable, a rocking block system can be stable. Furthermore, by changing the cable's initial prestressing force, it is possible to adjust the minimum ground acceleration required to trigger rocking. However, it was shown that the cable elongation can be very large, especially for squat blocks. Hence the cable may fail.

The main purpose of the research presented in this thesis is to apply the findings made on cable restrained rocking blocks to earthquake resistant bridge design. Hence the interaction between the material deformations of the bridge and the rotations of the rocking surfaces

has to be modeled. But current literature focuses on the rocking behavior of rigid blocks, making it impossible to represent the behavior of a large deformable structure combined with rocking surfaces. Hence it was proposed to use a completely different approach; implement a zero-length rocking element. The implementation of this element was described in Chapter 4. It was shown that this element combined with a stiff beam element can match the results obtained with the rigid block model. This rocking element was essential to demonstrate the findings made in Chapters 5, 6 and 7.

This element allowed to compute the behavior of a rocking bridge structure under earthquake excitation. It helped to confirm that moderate rocking can be very beneficial. Actually, compared to a conventional monolithic structure, the base moment of the structure was greatly reduced whereas the drift ratio remained moderate. It allowed to reduce the capacity of the column's footings as well as the bent cap.

Several column configurations were investigated in Chapter 6. It was shown that when a plastic hinge forms at the base of the column, the rocking rotations are greatly reduced due to the energy dissipation. But such finding does not apply to a real structure. If a plastic hinge forms at the base of the column, it will necessarily affect the behavior of the rocking surface and compromise the integrity of the structure. Chapter 6 also revealed that cable failure can lead to overturning, hence design criteria must prevent such scenario. It was proposed to replace the cable with a tie-rod. This rod was able to yield moderately. However, it was shown that as soon as the tie-rod yielded the initial prestressing force dropped and the structure became unstable. Hence, it was concluded that the cable must remain elastic, even during a severe earthquake.

It was also proposed to use a mild-steel dissipative fuse to bound the rocking column with its footing. It allowed a cantilever column to resist a large earthquake with small rocking rotation. It was shown that if the capacity of the fuse is too high, it may prevent the column to return to its initial position. Furthermore, once the fuse yielded it may act as a spring against the weight of the structure and cause rocking to occur even for a minor ground motion. However, if the fuse is designed properly, it can help to reduce the rocking rotations and enhance the stability of the structure.

8.3 Recommendations for further research

Future work on the rocking column bridge concept should focus on the following important problems:

- Development of a 3D rocking element
- Design of the rocking surfaces
- Model the damaged rocking surface within the rocking element
- Design of rocking bridge prototypes

The rocking element presented in chapter 4 is moving in plane. The kinematic equations are significantly more complex in three dimensions [33]. In addition different shapes for the rocking surface may generate extremely different behaviors. If the rocking surface is circular, the column will no longer rock but it will roll. This phenomenon is shown in [33], for instance a soda can tilted on its side will roll on its edge, even though it seems to rock. The sign of the rotation is not determined, it will roll one way or the other depending on the perturbation applied to the support. A finite element model that intends to describe the rocking/rolling kinematics of a circular surface needs to detect these bifurcation points. Furthermore, a system analysis may involve different scenarios; for instance if two bridge columns roll, the bridge may behave very differently whether they roll in the same or in the opposite direction.

Since circular surfaces do not rock, they do not dissipate energy. Thus, a rectangular surface may be more suitable for rocking surfaces in a three dimensional space. But as shown in [34] rectangular surfaces may lead to instability. Namely, when a column tilts in both x and y directions, it may rotate on the corner of its rectangular base.

Development of a rocking/rolling three dimensional finite element is crucial to understanding the behavior of complex rocking structures with arbitrary rocking surfaces. In order to develop design guidelines, the complex instability behavior of such columns must be understood. Polygonal shape rocking surfaces with round corners may be able to rock/roll without becoming unstable. Such surfaces have not been studied yet, and further research should explain in detail their complex behavior.

Rocking surfaces are subjected to large and numerous impacts. Hence design guidelines must also pay attention to the rocking surface details. If the surface remains elastic, the shock wave will radiate and dissipate through the column. If the rocking surface undergoes permanent deformations, it may dissipate all the energy that the shock wave may propagate. So ideally a rocking surface should dissipate most of the energy induced by the shock wave, but it must withstand the gravity load during and after the earthquake excitation. Moreover, the rocking surface has to keep its sharp geometry, or the rocking kinematics may change and become unstable. Actually, if the edges of the rocking surface are damaged, the column

may roll on its foot instead of impacting from one corner to the other.

These design characteristics are very similar to ballistic shielding design requirements. Large bullet impacts are dissipated through multiple crack propagation: a matrix bonds the composite material in order to resist multiple impacts. Hence, bullet-proof windows are designed such that the crack length is maximized during impact, and an adhesive layer holds it in place such that during a second impact the crack will close and lead to new cracks.
The use of fiber reinforced concrete may have these properties. The high strength concrete can dissipate energy through crack propagation, and the fibers should be able to hold the cracked elements together. A steel jacketing may help to confine the whole surface and add strength. A prefabricated rocking surface element could be inserted in the formwork while more conventional concrete is cast.
The dissipation observed in this thesis is a lower bound. It is expected to be higher with a highly dissipative rocking surface as shown by ElGawady et al. [9].

As the rocking surface is damaged, its behavior will change. The edges of the rocking surface will loose their sharpness and the rocking radius may decrease because the impact will primarily affect the edges. It is crucial to model this localized damage because it may lead to instability, if the overturning occurs at demands smaller than predicted using a damageless model.

Rocking surface damage could be modeled as a reduction of the radius of the rocking surface. Such model shall be calibrated using a three dimensional finite element method. But it may be preferred to design the rocking surface such that the radius is not altered during a large earthquake. For instance it can be designed to resist a compressive load larger than the column capacity. Such severe criterion may be satisfied using a high strength fiber reinforced concrete and steel jacketing.

The element presented in this dissertation is unable to represent sliding. It is assumed that the friction at the base of the column is sufficient to prevent sliding from occuring. But the friction coefficient of the rocking surface is very hard to determine. When the column is not rocking, the contact with the footing is distributed over the entire surface, but when the column is rocking the contact with the footing is localized at one corner. Hence it may be preferred to design shear connectors such that no sliding can occur at the rocking interface, regardless of the friction coefficient.

Once the rocking columns are properly modeled and understood, a bridge prototype with rocking columns can be designed. It should also meet the new design solutions developed

for the next-generation of highwway bridges. Namely, the bridge prototype should be built with prefabricated modules and its behavior should be compared to that of conventionally designed bridges. A similar approach to the one developed by Dr. Ketchum for the PEER Transportation Systems Research Program can be used. The initial construction costs can be computed, taking into account the significantly reduced foundation size and number of piles needed for rocking columns. A seismic performance study can then be conducted using the PEER methodology following the pattern established in [2] to compute the likely repair costs and repair times for rocking bridges. Then a comparison between conventional and rocking bridge seismic performance of comparable bridge structures can be made to investigate and quantify the potential benefits of rocking bridges.

Bibliography

[1] East-bay bridge project http://baybridgeinfo.org/.

[2] Ady Aviram, Bozidar Stojadinovic, Gustavo J. Parra-Montesinos, and Kevin R. Mackie. Structural response and cost characterization of bridge construction using seismic performance enhancement strategies. *PEER report*, 2010/01, March 2010.

[3] CalTrans. Seismic design criteria 1.6, November 2010.

[4] Y. H. Chen, W.H. Liao, C.L. Lee, and Y.P. Wang. Seismic isolation of viaduct piers by means of a rocking mechanism. *Earthquake Engineering and Structural Dynamics*, 35:713–736, 2006.

[5] Anil K. Chopra. *Dynamics of Structures - Theory and Applications to Earthquake Engineering*. EERI.

[6] M. A. Crisfield. Non-linear finite element analysis of solids and structures. *John Wiley and Sons Ltd*, 1, 1991.

[7] DSI. Dywidag post-tensioning systems catalogue, April 2006.

[8] M.R. Eatherton, J.F. Hajjar, G.G. Deierlein, H. Krawinkler, S. Billington, and X. Ma. Controlled rocking of steel-framed buildings with replaceable energy-dissipating fuses. *14th World Conference of Earthquake Engineering*, October 2008.

[9] Mohamed A. ElGawady, Quincy Ma, John W. Butterworth, and Jason Ingham. Effects of interface material on the performance of free rocking blocks. *Earthquake Engineering and Structural Dynamics*, 40:375–392, August 2011.

[10] FEMA. Prestandard and commentary for the seismic rehabilitations of buildings. *ASCE*, 356, 2000.

[11] F. C. Filippou. Fedeaslab http://fedeaslab.berkeley.edu/, 2004.

[12] S. Gajan and B. L. Kutter. Effects of moment-to-shear ratio on combined cyclic load-displacement behavior of shallow foundations from centrifuge experiments. *Journal of Geotechnical and Geoenvironmental Engineering (ASCE)*, 135(8):1044–1055, August 2009.

[13] M. Garlock and J. Li. Steel self-centering moment frames with collector beam floor diaphragms. *Journal of Constructional Steel Research*, 64(5):526–538, 2008.

[14] Hans M. Hilber, Thomas J. R. Hughes, and Robert L. Taylor. Improved numerical dissipation for the time integration algorithms in structural dynamics. *Earthquake Engineering and Structural Dynamics*, 5:283–292, 1977.

[15] Reggie Holt. Pbes cost study: Accelerated bridge construction success stories. *FHWA report*, 2006.

[16] George W. Housner. The behavior of inverted pendulum structures during earthquakes. *Bulletin of the Seismological Society of America*, 53(2):403–417, February 1963.

[17] A. Ibrahimbegovic. Non-linear solid mechanics theoretical formulations and finite element solution methods. *Springer- Solid Mechanics and its Applications*, 2009.

[18] Mark Ketchum, Vivian Chang, and Thomas Shantz. Influence of design ground motion level on highway bridge costs. *PEER Report*, November 2004.

[19] D. Konstantinidis and N. Makris. Criteria for initiation of slide, rock and slide-rock rigid-body modes. *Joint ASME/ASCE/SES Conference on Mechanics and Materials*, June 2005.

[20] Wing-Pin Kwan and Sarah Billington. Unbonded posttensioned concrete bridge piers. i: Monotonic and cyclic analyses. *Journal of Bridge Engineering, ASCE*, 8(2):92–101, March 2003.

[21] Wing-Pin Kwan and Sarah Billington. Unbonded posttensioned concrete bridge piers. ii: Seismic analyses. *Journal of Bridge Engineering, ASCE*, 8(2):102–111, March 2003.

[22] N. Makris and D. Konstantinidis. The rocking spectrum and the limitations of practical design methodologies. *Earthquake Engineering and Structural Dynamics*, 32:265–289, 2003.

[23] Tipping Mar. Orinda city hall http://www.tippingmar.com.

[24] Eric E. Matsumoto, Michael E. Kreger, Mark C. Waggoner, and Guclu Sumen. Grouted connection tests in development of precast bent cap system. *Transportation Research Record*, 1814:55–64, 2003.

[25] A. Neuenhofer and F. C. Filippou. Evaluation of nonlinear frame finite element models. *Journal of Structural Engineering*, 123(7):958–966, 1997.

[26] R. Park, D. Kent, and R. Sampson. Reinforced concrete members with cyclic loading. *Journal of the Structural Division*, 98(7):1341–1360, July 1972.

[27] M.J.N. Priestley, R.J Evison, and A.J. Carr. Seismic isolation of viaduct piers by means of a rocking mechanism. *Bulletin of the New-Zealand National Society for Earthquake Engineering*, 11(3):141–150, 1978.

[28] I. N. Psycharis. Dynamic behavior of rocking two-block assemblies. *Earthquake Engineering and Structural Dynamics*, 19:555–575, 1990.

[29] M. L. Ralls, B. Tang, S. Bhide, B. Brecto, E. Calvert, H. Capers, D. Dorgan, E. Matsumoto, C. Napier, W. Nickas, and H. Russell. Prefabricated bridge elements and systems in japan and europe. *FHWA report*, 2005.

[30] B. D. Scott, R. Park, and M. J. N. Priestley. Stress-strain behavior of concrete confined by overlapping hoops at low and high strain rates. *ACI Journal*, 79(1):13–27, January 1982.

[31] L.F. Shampine and S. Thompson. Event location for ordinary differential equations. *Computers and Mathematics with Applications*, 39:43–54, 2000.

[32] H. Shenton. Criteria for initiation of slide, rock and slide-rock rigid-body modes. *Journal of Engineering Mechanics (ASCE)*, 122(7):690–693, 1996.

[33] M. Srinivasan and A. Ruina. Rocking and rolling: a can that appears to rock might actually roll. *In press*, 2008.

[34] T. Tobita and S. Sawada. Rotation response of a rigid body under seismic excitation. *Journal of Engineering Mechanics*, 132:375–384, April 2008.

[35] M. F. Vassiliou and N. Makris. Analysis of the rocking response of rigid blocks standing free on a seismically isolated base. *Earthquake Engineering and Structural Dynamics*, 41(177-196), February 2012.

[36] Lloyd M. Wolf and Michael D. Hyzack. Design of precast bent cap to column connections. *Concrete Bridge Conference*, 2004.

[37] J. Zhang and N. Makris. Rocking response of free-standing blocks under cycloidal pulses. *Journal of Engineering Mechanics (ASCE)*, 127(5):473–483, 2001.